DUDLEY KNOX LIBRARY
NAVAL POSTGRADUATE SCHOOL
MONTEREY, CALIFORNIA 93943-5002

NAVAL POSTGRADUATE SCHOOL
Monterey, California

THESIS

PERFORMANCE ANALYSIS OF MODIFIED M-ARY
PSK AND QAM SIGNALING SCHEMES
IN THE PRESENCE OF NOISE AND JAMMING

by

Fikret Gunes

June 1986

Thesis Advisor: D. Bukofzer

Approved for public release; distribution is unlimited.

T230603

CURITY CLASSIFICATION OF THIS PAGE

REPORT DOCUMENTATION PAGE

REPORT SECURITY CLASSIFICATION: UNCLASSIFIED	1b. RESTRICTIVE MARKINGS
SECURITY CLASSIFICATION AUTHORITY	3 DISTRIBUTION / AVAILABILITY OF REPORT: Approved for public release; distribution is unlimited.
DECLASSIFICATION / DOWNGRADING SCHEDULE	
PERFORMING ORGANIZATION REPORT NUMBER(S)	5 MONITORING ORGANIZATION REPORT NUMBER(S)
NAME OF PERFORMING ORGANIZATION: aval Postgraduate School; 6b. OFFICE SYMBOL (If applicable): 62	7a. NAME OF MONITORING ORGANIZATION: Naval Postgraduate School
ADDRESS (City, State, and ZIP Code): Monterey, CA 93943-5000	7b. ADDRESS (City, State, and ZIP Code): Monterey, CA 93943-5000
NAME OF FUNDING / SPONSORING ORGANIZATION; 8b. OFFICE SYMBOL (If applicable)	9 PROCUREMENT INSTRUMENT IDENTIFICATION NUMBER
ADDRESS (City, State, and ZIP Code)	10 SOURCE OF FUNDING NUMBERS: PROGRAM ELEMENT NO; PROJECT NO; TASK NO; WORK UNIT ACCESSION NO

TITLE (Include Security Classification)
PERFORMANCE ANALYSIS OF MODIFIED M-ARY PSK AND QAM SIGNALING SCHEMES IN THE PRESENCE OF NOISE AND JAMMING

PERSONAL AUTHOR(S)
Fikret Gunes

TYPE OF REPORT	13b TIME COVERED	14 DATE OF REPORT (Year, Month, Day)	15 PAGE COUNT
aster's Thesis	FROM _____ TO _____	1986, June	141

SUPPLEMENTARY NOTATION

COSATI CODES			18. SUBJECT TERMS (Continue on reverse if necessary and identify by block number)
FIELD	GROUP	SUB-GROUP	Digital Communication, Jamming Effect, MPSK, QAM

ABSTRACT (Continue on reverse if necessary and identify by block number)

The purpose of this thesis is to evaluate and compare the performance of certain M-ary digital modulation schemes such as MPSK, QAM and certain modifications to these which have not been considered in previous analyses. The performance of these receivers is evaluated in terms of probability of error as a function of signal to noise ratio (SNR). Design trade-offs are considered and their effect on system performance evaluated. One of the schemes considered is further evaluated in terms of its vulnerability to jamming. Using a colored Gaussian noise model, jamming effects are evaluated by determining the receiver error probability as a function of both SNR and jamming

DISTRIBUTION / AVAILABILITY OF ABSTRACT: ☑ UNCLASSIFIED/UNLIMITED ☐ SAME AS RPT ☐ DTIC USERS	21 ABSTRACT SECURITY CLASSIFICATION: Unclassified
NAME OF RESPONSIBLE INDIVIDUAL: Prof. Daniel C. Bukofzer	22b TELEPHONE (Include Area Code): (408) 646-2859; 22c. OFFICE SYMBOL: Code 62Bh

FORM 1473, 84 MAR — 83 APR edition may be used until exhausted; All other editions are obsolete — SECURITY CLASSIFICATION OF THIS PAGE

to signal ratio (JSR). An optimum jamming scheme that is derived using a maximum power constraint is presented and its effect on the performance of a 16-QAM receiver designed to operate in an additive white Gaussian noise (AWGN) only interference is evaluated.

Approved for public release; distribution is unlimited.

Performance Analysis of Modified M-ARY PSK and QAM Signaling Schemes in the Presence of Noise and Jamming

by

Fikret Gunes
LTJG., Turkish Navy
B.S., Turkish Naval Academy, 1979

Submitted in partial fulfillment of the
requirements for the degree of

MASTER OF SCIENCE IN ELECTRICAL ENGINEERING

from the

ABSTRACT

The purpose of this thesis is to evaluate and compare the performance of certain M-ary digital modulation schemes such as MPSK, QAM and certain modifications to these which have not been considered in previous analyses. The performance of these receivers is evaluated in terms of probability of error as a function of signal to noise ratio (SNR). Design trade-offs are considered and their effect on system performance evaluated. One of the schemes considered is further evaluated in terms of its vulnerability to jamming. Using a colored Gaussian noise model, jamming effects are evaluated by determining the receiver error probability as a function of both SNR and jamming to signal ratio (JSR). An optimum jamming scheme that is derived using a maximum power constraint is presented and its effect on the performance of a 16-QAM receiver designed to operate in an additive white Gaussian noise (AWGN) only interference is evaluated.

TABLE OF CONTENTS

LIST OF TABLES

LIST OF FIGURES

ACKNOWLEDGMENTS

I wish to express my appreciation to my thesis advisor Professor Daniel Bukofzer for his efforts, guidance, patience and friendship which contributed to the completion of this work. I would also like to thank Professor Jeffrey B. Knorr for his assistance. This thesis was only possible because of the loving support and typing ability of my dear wife Manolya to whom this work is dedicated.

I. INTRODUCTION

The structure and performance of digital communication receivers operating in the presence of additive white Gaussian noise is widely described in the literature [See for example Ref. 1]. Such receivers are typically designed and built to minimize the resulting error probability. Optimum receiver signal processing algorithms are obtained by application of the Maximum Aposteriori Probability (MAP) performance criterion and vector space signal representations are generally used in the receiver design procedure [Ref. 1,2].

The vector space signal representation method is introduced and applied to the well-known M-ary Phase Shift Keying (MPSK) scheme in order to obtain an optimum signal processing algorithm using a MAP criterion [Ref. 2]. After accoplishing this, the remainder of Chapter II is devoted to considering certain signal modifications to MPSK (for M=8 specifically) modulation which have not been considered in previous analyses. The resulting performance is then compared in terms of error probability to conventional MPSK schemes. The different schemes are compared in terms of their average probability of symbol error on the basis of each signal set having equal average energy. Two possible

modifications of the MPSK (for M=8) scheme are analyzed first and their performances compared to that of conventional 8-PSK modulation. Next, 8-ary modulation schemes involving combined amplitude and phase modulation are considered. The performance analysis of the modified schemes point to the complicated logic and corresponding signal processing algorithms of the optimum receiver structures. Consequently, suboptimum receiver signal processing algorithms are presented so as to simplify and reduce the complexity of the optimum schemes. The resulting degradations in performance are analyzed and discussed. Chapter II concludes with the analysis and performance of a modified QPSK modulation scheme, in which five rather than four signals can be accomodated by using the signal that is identically zero to convey information from transmitter to receiver.

All phase modulation schemes considered in Chapter II exhibit performance penalties as M increases. By utilizing a combination of multiple amplitudes and phases to transmit each of the M symbols, some of the performance penalties described above can be lessened. One example of this kind of modulation techique is the well-known M-ary Quadrature Amplitude Modulation (QAM) described in many references [Ref. 2,3,4]. In order to provide the necessary background for Chapter IV, the performance of M-ary QAM schemes for

M=16, 64 and 256 is presented in Chapter III, and the results are compared to equivalent MPSK signaling schemes.

The results on the performance of the digital communication receivers analyzed in Chapters II and III were obtained under a white Gaussian noise interference assumption. This assumption is invalid when receivers must operate in a jamming environment. In Chapter IV the vulnerability to jamming of a 16-QAM receiver designed to operate in white Gaussian interference only environment is analyzed. The jamming is modeled as a colored Gaussian noise process with an arbitrary power spectral density. A mathematical expression for the performance of the 16-QAM receiver operating in the presence of white Gaussian noise and the jamming described above is developed evaluated and compared to the performance of the same receiver operation in a white Gaussian noise interference environment only. An attempt is made to optimize the jamming interference spectrum under an overall power constraint, so as to introduce a large receiver performance penalty.

Some design trade-offs are discussed and performance comparisons are carried out. Graphical results are presented in each chapter and the performance curves are interpreted. Chapter V presents some of the major conclusions that can be derived from the analysis and the results obtained.

II. PERFORMANCE ANALYSIS OF SOME 8-ARY DIGITAL SIGNALING SCHEMES

The optimum receiver design problem involves finding a structure or signal processing algorithm that is best in a certain sense. The performance of such a structure or signal processing algorithm, defined in a manner consistent with the meaning of optimality, must be determined.

The basic M-ary receiver design problem considered in this thesis, can be stated as follows.

One of M signals $s_i(t)$ is transmitted, i=1, 2, . . . , M over a certain time interval of duration T sec. The transmission channel is modeled as an additive white Gaussian noise (AWGN) channel so that the received signal can be expressed as

$$y(t) = s_i(t) + n(t) \qquad t \in T \qquad (2.1)$$

$$i = 1, 2, \ldots, M$$

where n(t) is a sample function of the AWGN process having power spectral density (PSD) level $N_0/2$. Each signal $s_i(t)$ can be expanded in terms of an orthonormal set of functions $\{ \phi_k(t) \}$, themselves defined for $t \in T$, such that

$$s_i(t) = \sum_{k=1}^{K} S_{ik}\, \phi_k(t) \quad , \quad S_{ik} = \int_T s_i(t)\, \phi_k^*(t)\, dt \qquad (2.2)$$

It can be shown [Ref. 1] that for the signal and noise model being considered, any receiver with a reasonable optimality criterion need not process $y(t)$ as such, but can operate only on the components of $y(t)$ along the elements of the orthonormal (O.N.) set of functions $\{ \phi_k(t) \}$. That is, the receiver need only process the elements Y_k, where

$$Y_k = \int_T y(t)\, \phi_k^*(t)\, dt \quad , \quad k = 1, 2, \ldots, K$$

so that a typical receiver could incorporate the system shown in Figure 2.1.

The components of the transmitted signals $s_i(t)$ and of the received signal $y(t)$ along the elements of the O.N. set can be expressed in vectorial form as follows:

$$\underline{y} = [\, Y_1 , Y_2 , \ldots , Y_K \,]^T$$

$$\underline{s}_i = [\, S_{i1}, S_{i2}, \ldots , S_{iK} \,]^T . \qquad (2.3)$$

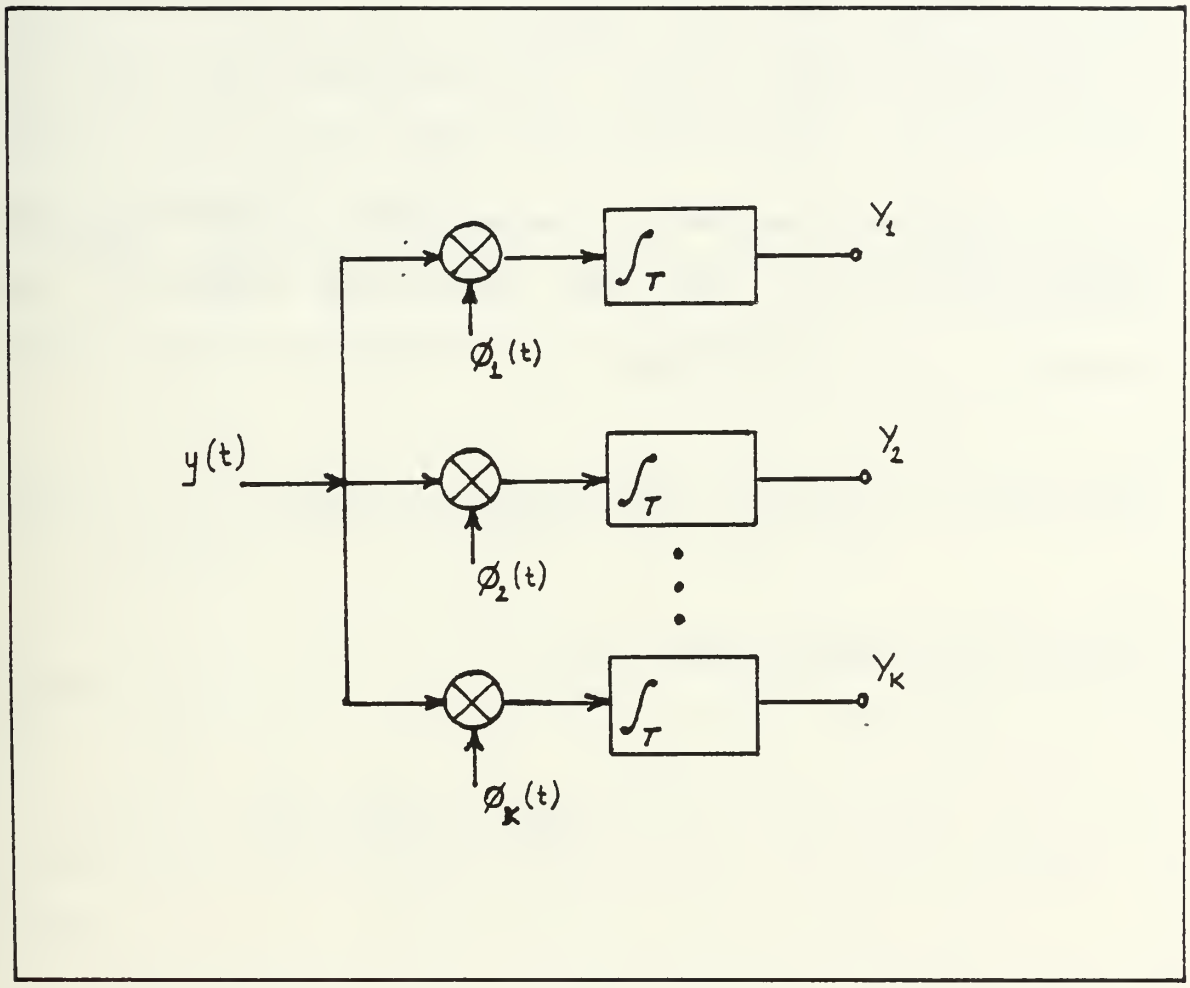

Figure 2.1. Correlator Front End Receiver Structure

The channel model allows specification of the M conditional probability density functions (p.d.f.) $f_{\underline{Y}/\underline{S}_i}(\underline{Y}/\underline{S}_i)$ $i = 1, 2, \ldots, M$. It is assumed that the priori probabilities $\{ Pr[s_i(t)] \} = \{ p_i \}$ specifying that a particular signal $s_i(t)$ is transmitted, are known for $i = 1, 2, \ldots, M$

A maximum aposteriori probability (MAP) receiver decides that $s_1(t)$ was the transmitted signal, if upon reception $y(t)$ is such that

$$Pr\{ s_1(t) / \underline{y} = \underline{Y} \} > Pr\{ s_i(t) / \underline{y} = \underline{Y} \} \qquad (2.4)$$

for all $i \neq 1$. Using Bayes rule,

$$Pr\{ s_i(t) / \underline{y} = \underline{Y} \} = \frac{f_{\underline{y}/\underline{s}_i}(\underline{Y}/\underline{S}_i) \cdot p_i}{Pr\{ \underline{y} = \underline{Y} \}} . \qquad (2.5)$$

The decision rule employed by the MAP receiver and specified by Equation 2.4 can thus be written as,

$$p_1 \, f_{\underline{y}/\underline{s}_1}(\underline{Y}/\underline{S}_1) > p_i \, f_{\underline{y}/\underline{s}_i}(\underline{Y}/\underline{S}_i) \qquad (2.6)$$

where $i = 1, 2, \ldots, M$, $i \neq 1$.

The decision rule of Equation 2.6, implies a partitioning of the entire K dimensional hyperplane into M disjoint regions, $\{ I_i \}$. Whenever the received vector $\underline{y}$ is contained in I_1, the optimum (in MAP sense) receiver decides $s_1(t)$ was transmitted. The regions $\{I_i\}$ are called optimum decision regions.

From Equations 2.1 and 2.2, if $s_i(t)$ is the transmitted signal, the kth component of $\underline{y}$ is given by

$$Y_k = \int_T [s_i(t) + n(t)] \phi_k^*(t) \, dt = S_{ik} + N_k \qquad (2.7)$$

where

$$N_k = \int_T n(t) \phi_k^*(t) \, dt \quad , \quad k = 1, 2, \ldots, K. \qquad (2.8)$$

The elements N_k, $k = 1, 2, \ldots, K$ can be conveniently used to define a noise vector $\underline{n}$, where

$$\underline{n} = [N_1, N_2, \ldots, N_K]^T. \qquad (2.9)$$

The received vector $\underline{y}$ can therefore be expressed in the form

$$\underline{y} = \underline{s}_i + \underline{n} = [\, s_{i1} + N_1,\ s_{i2} + N_2,\ \ldots,\ s_{iK} + N_K \,]$$

$$i = 1, 2, \ldots, M. \qquad (2.10)$$

Thus, the conditional probability density functions $f_{\underline{y}/\underline{s}_i}(\underline{Y}/\underline{S}_i)$ are given by

$$f_{\underline{y}/\underline{s}_i}(\underline{Y} / \underline{S}_i) = f_{\underline{n}/\underline{s}_i}(\underline{Y} - \underline{S}_i / \underline{S}_i) = f_{\underline{n}}(\underline{Y} - \underline{S}_i) \qquad (2.11)$$

where the last equality is made possible by the fact that $\underline{n}$ and $\underline{s}_i$ are statistically independent. The decision rule of Equation 2.6 therefore becomes,

$$p_1 \cdot f_{\underline{n}}(\underline{Y} - S_i) \;>\; p_i \cdot f_{\underline{n}}(\underline{Y} - \underline{S}_i) \qquad (2.12)$$

for $i = 1, 2, \ldots, M,\ i \neq 1$.

The p.d.f, $f_{\underline{n}}(\underline{N})$ can be specified by observing from the WGN assumption and Equation 2.7 that the components of $\underline{n}$ are statistically independent, zero mean, Gaussian random variables, with equal variance of $N_0 / 2$. Therefore

$$f_{\underline{n}}(\underline{N}) = \frac{1}{(2\pi \ N_0/2)^{K/2}} \exp\{ - \frac{1}{2} \frac{1}{N_0/2} \ \underline{N}^T \ \underline{N} \} \qquad (2.13)$$

where

$$\underline{N}^T \ \underline{N} = \sum_{k=1}^{K} N_k^2 = \| \underline{N} \|^2 \qquad (2.14)$$

so that

$$f_{\underline{n}}(\underline{Y} - \underline{S}_i) = \frac{1}{(2\pi \ N_0/2)^{K/2}} \exp\{- \frac{1}{2} \frac{1}{N_0/2} \| \underline{Y} - \underline{S}_i \|^2 \}. \qquad (2.15)$$

The decision rule of Equation 2.12 can be simplified by using Equation 2.15 and by eliminating the equal terms on both sides of the inequality, after taking logs. The result is given by

$$\| \underline{Y} - \underline{S}_1 \|^2 - N_0 \ \ln(p_1) < \| \underline{Y} - \underline{S}_i \|^2 - N_0 \ \ln(p_i) \qquad (2.16)$$

$$i = 1, 2, \ldots, M, \ i \neq 1.$$

Whenever all signals have equal prior probability, the optimum decision rule of Equation 2.16 states that $s_1(t)$ is decided upon as the transmitted signal if and only if $\underline{y}$ is

closer to $\underline{s}_l$ than to any other signal in Euclidean distance sense. The conditional probability of correct decision can be expressed in terms of the decision regions $\{ I_i \}$ as follows

$$\Pr\{ c / s_i(t) \} = \Pr\{ \underline{y} \text{ in } I_i / s_i(t) \}$$

$$= \int_{I_i} f_{\underline{y}/s_i}(\underline{Y} / \underline{S}_i) \, d\underline{Y}$$

$$= \int_{I_i} f_{\underline{n}}(\underline{Y} - \underline{S}_i) \, d\underline{Y} . \qquad (2.17)$$

The probability of error is therefore given by

$$\Pr\{ \varepsilon \} = 1 - \Pr\{ c \} = 1 - \sum_{i=1}^{M} \Pr\{ c / s_i(t) \} p_i . \qquad (2.18)$$

Due to the result of Equation 2.16, the optimum decision regions are obtained by defining the PERPENDICULAR hyper planes bisecting the " lines " connecting the signals. This is easily done as well as visualized when the signal set is two dimensional, i.e., K = 2.

A. M-ARY PHASE SHIFT KEYING (MPSK)

As we previously indicated, the received signal y (t) takes on the form

$$y(t) = s_i(t) + n(t) \qquad o \leqslant t \leqslant T \qquad (2.19)$$

$$i = 1, 2, \ldots, M$$

where for MPSK modulation

$$s_i(t) = (2E / T)^{1/2} \cos\left(\frac{2\pi k t}{T} + \frac{2\pi (i-1)}{M}\right) \qquad (2.20)$$

$$i = 1, 2, \ldots, M, \quad o \leqslant t \leqslant T .$$

Here n(t) is a WGN process of zero mean with power spectral density level $N_0 / 2$. Using a simple trigonometric identity we can express $s_i(t)$ in the form

$$s_i(t) = (E)^{1/2} \cos\frac{2\pi (i-1)}{M} \frac{\cos(2\pi f_0 t)}{(T/2)^{1/2}}$$

$$- (E)^{1/2} \sin\frac{2\pi (i-1)}{M} \frac{\sin(2\pi f_0 t)}{(T/2)^{1/2}} \qquad (2.21)$$

$$o \leqslant t \leqslant T .$$

Letting

$$\phi_1(t) = \frac{\cos(2\pi f_0 t)}{(T/2)^{1/2}} \quad , \quad \phi_2(t) = \frac{\sin(2\pi f_0 t)}{(T/2)^{1/2}} \qquad (2.22)$$

$$0 \leq t \leq T$$

we can see that $\phi_1(t)$ and $\phi_2(t)$ form an O.N. set, so that any signal in the set can be expressed in the form specified by Equation 2.2, with

$$S_{i1} = (E)^{1/2} \cos \frac{2\pi (i-1)}{M} \quad , \quad S_{i2} = -(E)^{1/2} \sin \frac{2\pi (i-1)}{M} \; . \qquad (2.23)$$

The signal vector and decision region I_i for the ith. signal is shown in Figure 2.2.

Due to the symmetry of the signal set, the error probability associated with the MAP decision rule can be obtained by determining $Pr\{ C / s_i(t) \}$ only. For this two-dimensional case, using the decision region shown in Figure 2.2 is obtained by application of the "Perpendicular bisector" rule. Clearly

$$Pr\{ C / s_i(t) \} = \int\int_{I_1} f_{\underline{n}}(\underline{Y} - \underline{S}) \, d\underline{Y} \; . \qquad (2.24)$$

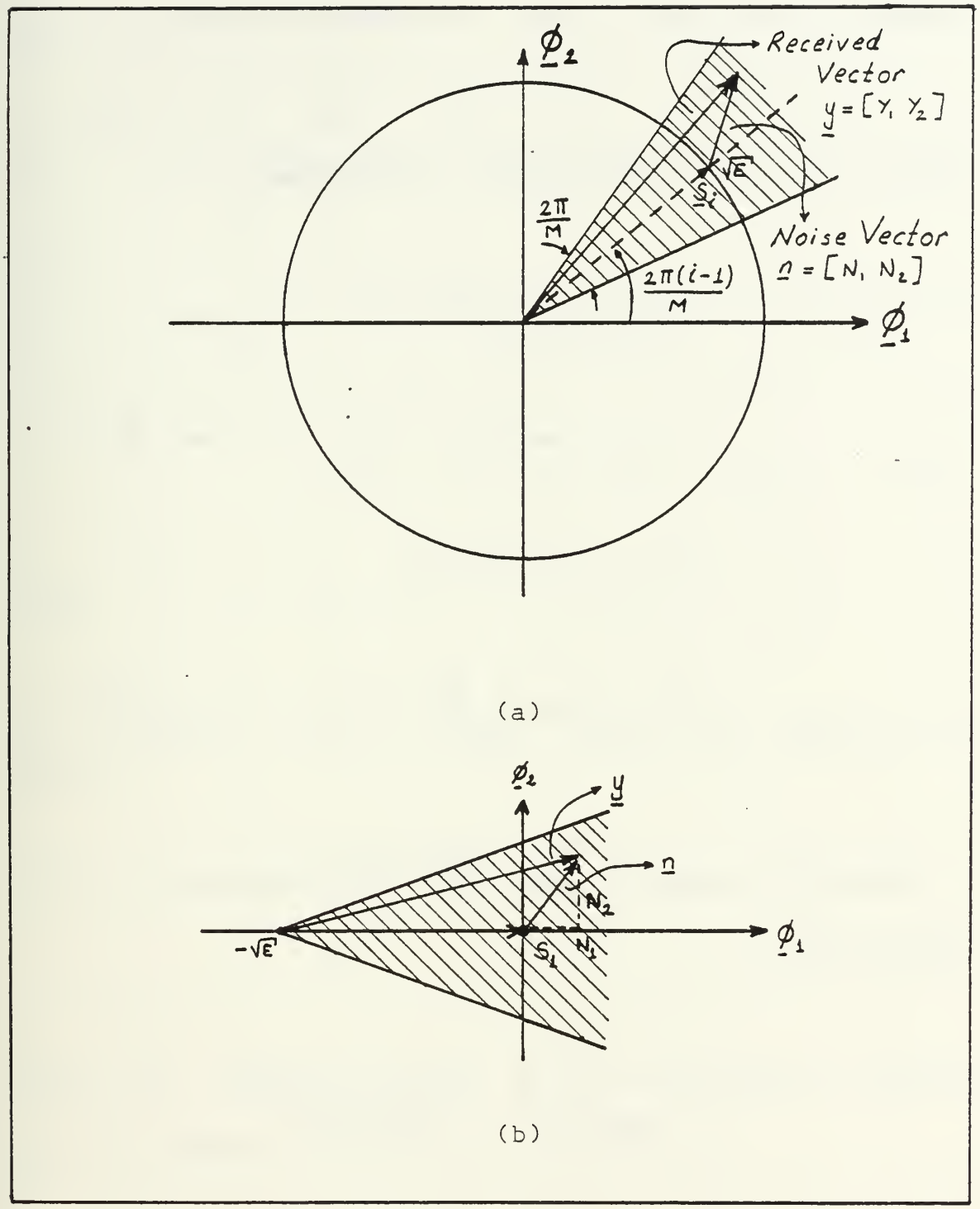

Figure 2.2. a) Signal-Space Diagram for MPSK Modulation
b) Decision Region for i th Transmitted Phase

However, from Figure 2.2(b) it is apparent that $\underline{y} \in I_1$ if $N_1 > -(E)^{1/2}$ and $-(N_1 \tan \frac{\pi}{M}) < N_2 < (N_1 \tan \frac{\pi}{M})$. Since N_1 and N_2 are statistically independent,

$$\Pr\{ C / s_1(t) \} = \Pr\{ N_1 > -(E)^{1/2} , - (N_1 \tan \frac{\pi}{M}) < N_2 < (N_1 \tan \frac{\pi}{M}) \}$$

$$= \Pr\{ N_1 > -(E)^{1/2} \} \Pr\{ - (N_1 \tan \frac{\pi}{M}) < N_2 < (N_1 \tan \frac{\pi}{M}) \}. \quad (2.25)$$

Since N_1 and N_2 are zero mean Gaussian r.v.'s of variance $N_0/2$,

$$\Pr\{ N_1 > -(E)^{1/2} \} = \int_{-(E)^{1/2}}^{\infty} \frac{1}{(2\pi N_0/2)^{1/2}} \exp\{ - n_1^2 / 2 (N_0/2) \} \, dn_1 \quad (2.26)$$

and

$$Pr\{ -(N_1 \tan \frac{\pi}{M}) < N_2 < (N_1 \tan \frac{\pi}{M})$$

$$= 2 \int_0^{n_1 \tan(\pi/M)} \frac{1}{(2\pi N_0/2)^{1/2}} \exp\{ - n_2^2 / 2(N_0/2) \} dn_2. \qquad (2.27)$$

Thus

$$Pr\{ C / s_1(t) \} = 2 \int_0^{\infty} 1/(2\pi)^{1/2} \exp[- (u - (Rd)^{1/2})^2 /2] \int_0^{u \tan(\pi/M)} 1/(2\pi)^{1/2} \exp[-v^2/2] dv\, du. \qquad (2.28)$$

Since all decision regions I_i are similar form, assuming that all signals are equally likely, we have

$$Pr\{ C \} \overset{\Delta}{=} 1/M \sum_{i=1}^{M} Pr\{ C / s_i(t) \} = Pr\{ C / s_1(t) \} \qquad (2.29)$$

so that

$$Pr\{ \varepsilon \} \overset{\Delta}{=} 1 - Pr\{ C \} = 1 - Pr\{ C / s_1(t) \}$$

or equivalently

$$Pr\{ \varepsilon \} = 1 - \int_0^{\infty} 1 / (2\pi)^{1/2} \exp [- (u - (Rd)^{1/2})^2 / 2]$$

$$[1 - 2 \text{ erfc}^*(u \tan \pi/M)] du . \qquad (2.30)$$

This expression for Pr{ε} has been extensively evaluated for values of M that are of the form, $M = 2^m$. In the sequences alternate signaling schemes will be proposed, and their performance compared to the equivalent MPSK scheme analyzed in this subsection.

B. RECTANGULAR SIGNALING SCHEME

As a possible modification of the MPSK (for M = 8) scheme, we now focus on a method which because of the signal space diagram (as shown in Figure 2.3) we have called the "Box" signaling scheme.

We can easily define energy of the signals in terms of parameter A shown in Figure 2.3. Signals $\underline{s}_2$, $\underline{s}_4$, $\underline{s}_6$, $\underline{s}_8$ have energy A^2. Signals $\underline{s}_1$, $\underline{s}_3$, $\underline{s}_5$, $\underline{s}_7$ have energy $2A^2$. The average energy of the signal set $\bar{E}$ is

$$\bar{E} = 1/8 [4 A^2 + 4 (2 A^2)] = 3A^2 / 2. \qquad (2.31)$$

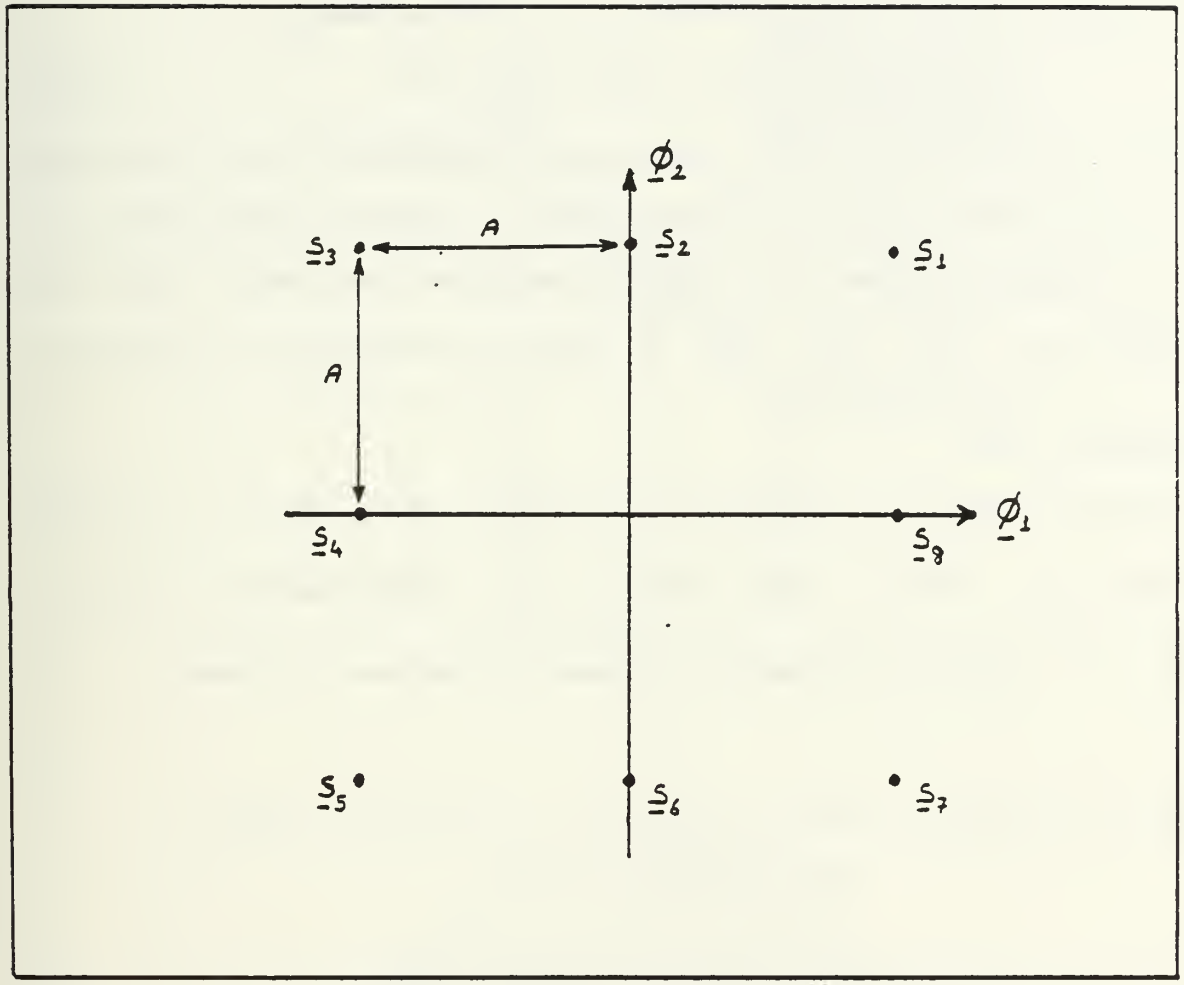

Figure 2.3. Signal-Space Diagram for Rectangular Signaling Scheme

For later comparison purposes, it is desireable to make this signal set equivalent to 8-PSK, by requiring both sets to have the same average signal energy $\bar{E}$. In order to accomplish this, since $E = \bar{E}$ for MPSK we need

$$E = \bar{E} = 3/2\ A^2 \quad \rightarrow \quad A = (2E/3)^{1/2}. \tag{2.32}$$

From Figure 2.4(a), it can be seen that there are two types of decision regions. The decision regions associated with the determination of the probability of correct decision given $\underline{s}_1$, $\underline{s}_3$, $\underline{s}_5$, and $\underline{s}_7$ were transmitted are similar. Observe that

$$Pr\{ C / s_1(t) \} = Pr\{ N_1 \geq -(A/2)\ ,\ N_2 \geq -A/2 \}. \tag{2.33}$$

Since N_1 and N_2 are statistically independent zero mean, $N_0 / 2$ variance, Gaussian random variables, we have

$$Pr\{ C / s_1(t) \} = Pr\{ N_1 \geq -(A/2) \}\ Pr\{ N_2 \geq -(A/2) \}$$

$$= [\int_{-(A/2)}^{\infty} \frac{1}{(2\pi\ (N_0/2))^{1/2}}$$

$$\exp\{-x^2/2\ (N_0/2)\}\ dx\ ]^2. \tag{2.34}$$

Let $y \overset{\Delta}{=} x\ /(N_0/2)^{1/2}$, so that from Equation 2.32.

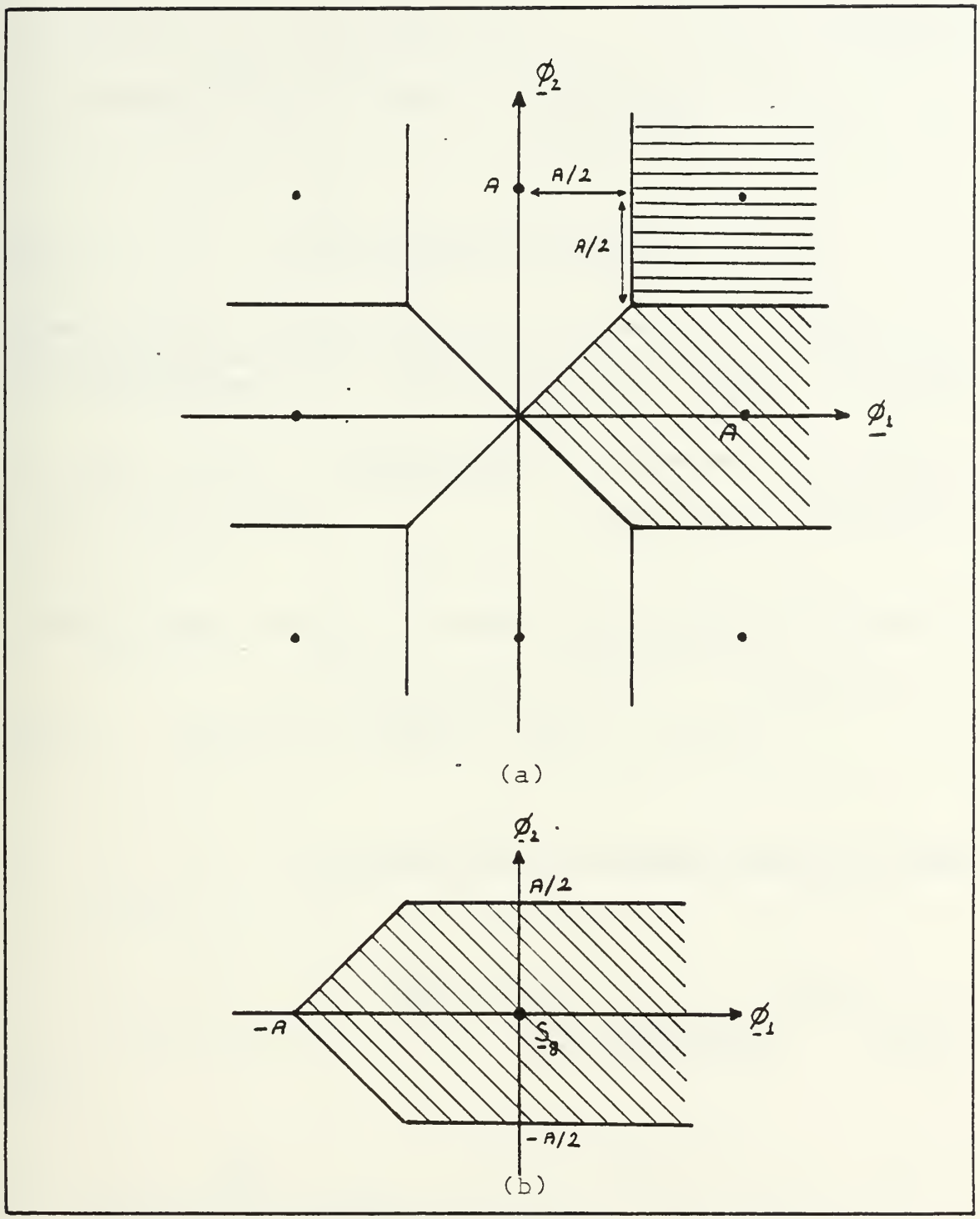

Figure 2.4. a) Decision Regions for Rectangular Signaling Scheme b) Decision Region for Signal $s_3(t)$

We obtain

$$Pr\{ C / s_1(t) \} = \left[\int_{-(E/3N_0)^{1/2}}^{\infty} 1/(2\pi)^{1/2} \; e^{-y^2/2} \; dy \right]^2$$

$$= [erfc^*(- (E/3N_0)^{1/2})]^2 \qquad (2.35)$$

The probability of making a correct decision for the second group of signals ($\underline{s}_2$, $\underline{s}_4$, $\underline{s}_6$, $\underline{s}_8$), can be determined by analysis of the decision regions shown in Figure 2.4(b). It is simple to verify that

$$Pr\{C/s_8(t)\} = Pr\{- A \leqslant N_1 \leqslant -(A/2), - (N_1 + A) \leqslant N_2 \leqslant (N_1 + A)\} +$$

$$Pr\{ N_1 \geqslant -(A/2), -(A/2) \leqslant N_2 \leqslant A/2\}. \qquad (2.36)$$

The first joint probability is given by

$$\left\{ \int_{-A}^{-(A/2)} \frac{1}{(2\pi N_0/2)^{1/2}} \; e^{-n_1^2/2} \; e^{-\frac{N_0}{2}} \right.$$

$$\left. \int_{-(n_1+A)}^{(n_1+A)} \frac{1}{(2\pi N_0/2)^{1/2}} \; e^{-n_2^2/2} \; e^{-\frac{N_0}{2}} \right\} dn_2 dn_1 =$$

$$= \int_{-(4E/3N_0)^{1/2}}^{-(E/3N_0)^{1/2}} \frac{1}{(2\pi)^{1/2}} e^{-y^2/2}$$

$$[1-2\ \mathrm{erfc}^*(y + (4E/3N_0)^{1/2}]\ dy \qquad (2.37)$$

while the second joint probability, is given by

$$\left\{ \int_{-A/2}^{\infty} \frac{1}{(2\pi N_0/2)^{1/2}} e^{-n_1^2/2(N_0/2)} \right.$$

$$\left. \int_{-A/2}^{A/2} \frac{1}{(2\pi N_0/2)^{1/2}} e^{-n_2^2/2(N_0/2)} \right\} dn_2\ dn_1 =$$

$$= \int_{-(E/3N_0)^{1/2}}^{\infty} \frac{1}{(2\pi)^{1/2}} e^{-y^2/2}\ [1 - 2\ \mathrm{erfc}^*((E/3N_0)^{1/2})]\ dy$$

$$= [1 - \mathrm{erfc}^*((E/3N_0)^{1/2})]\ [1 - 2\ \mathrm{erfc}^*((E/3N_0)^{1/2})]. \qquad (2.38)$$

Thus

$$\Pr\{C/s_B(t)\} = \left\{ \int_{-(4E/3N_0)^{1/2}}^{-(E/3N_0)^{1/2}} \frac{1}{(2\pi)^{1/2}} e^{-y^2/2} \right.$$

$$[1-2\ \mathrm{erfc}^*(y + (4E/3N_0)^{1/2}]\ dy +$$

$$+ [1 - \text{erfc}^*((E/3N_0)^{1/2})]\,[1 - 2\,\text{erfc}^*((E/3N_0)^{1/2})]\Big\}. \quad (2.39)$$

Assuming again all signals to be equally likely, we have

$$\Pr\{\varepsilon\} = 1 - \frac{1}{8}\,[4\,\Pr\{c/s_1(t)\} + 4\,\Pr\{c/s_8(t)\}]. \quad (2.40)$$

Defining

$$\frac{2E}{N_0} \triangleq Rd\ ,$$

we obtain

$$\Pr\{\varepsilon\} = 1 - \frac{1}{2}\Big\{[\,\text{erfc}^*(-(Rd/6)^{1/2})]^2 +$$

$$-(2/3\ Rd)^{1/2}\int^{-(Rd/6)^{1/2}} \frac{1}{(2\pi)^{1/2}}\, e^{-y^2/2}[1-2\text{erfc}^*(y+(2Rd/3)^{1/2})]dy$$

$$+ \text{erfc}^*(-(Rd/6)^{1/2})[\,1-2\,\text{erfc}^*((Rd/6)^{1/2}\,]\Big\}. \quad (2.41)$$

Evaluation of $\Pr\{\varepsilon\}$ as a function of Rd is carried out in the sequel, and the results compared to those for 8-PSK. It must be pointed out that the MPSK signaling scheme suffers severe performance degradations as M increases because of signal "crowding". This can be overcome by increasing $\bar{E}$, or by modifying the PSK scheme slightly to include signals other than just phase modulated signals. For instance, the 8-PSK scheme could allow for 7 phase modulated signals and 1 signal that is identically zero. This is analyzed next.

C. 8-ARY PSK WITH ONE NULL SIGNAL

We now consider the performance of a signaling scheme having a signal space arrangement as shown in Figure 2.5. Observe that the phase angle between "adjacent" signals is now greater than that encountered in 8-PSK. The average energy $\bar{E}$ of the signal set is

$$\bar{E} = \frac{1}{8} (7 A^2 + 0) = \frac{7}{8} A^2. \qquad (2.42)$$

If this signal set is to have the same average energy as that of 8-PSK (Average energy $\bar{E} = E$), we must have

$$A = (8E / 7)^{1/2}. \qquad (2.43)$$

Observe as a result of this that the non zero signals associated with the scheme under consideration have greater energy than the 8-PSK signals.

The optimum decision regions associated with the scheme under consideration are identical for the signals $\underline{s}_1$ through $\underline{s}_7$. One such decision region is shown in Figure 2.5. The decision region shown in Figure 2.6 and used for calculating $Pr\{c/s_1(t)\}$ is obtained via rotation and translation of the

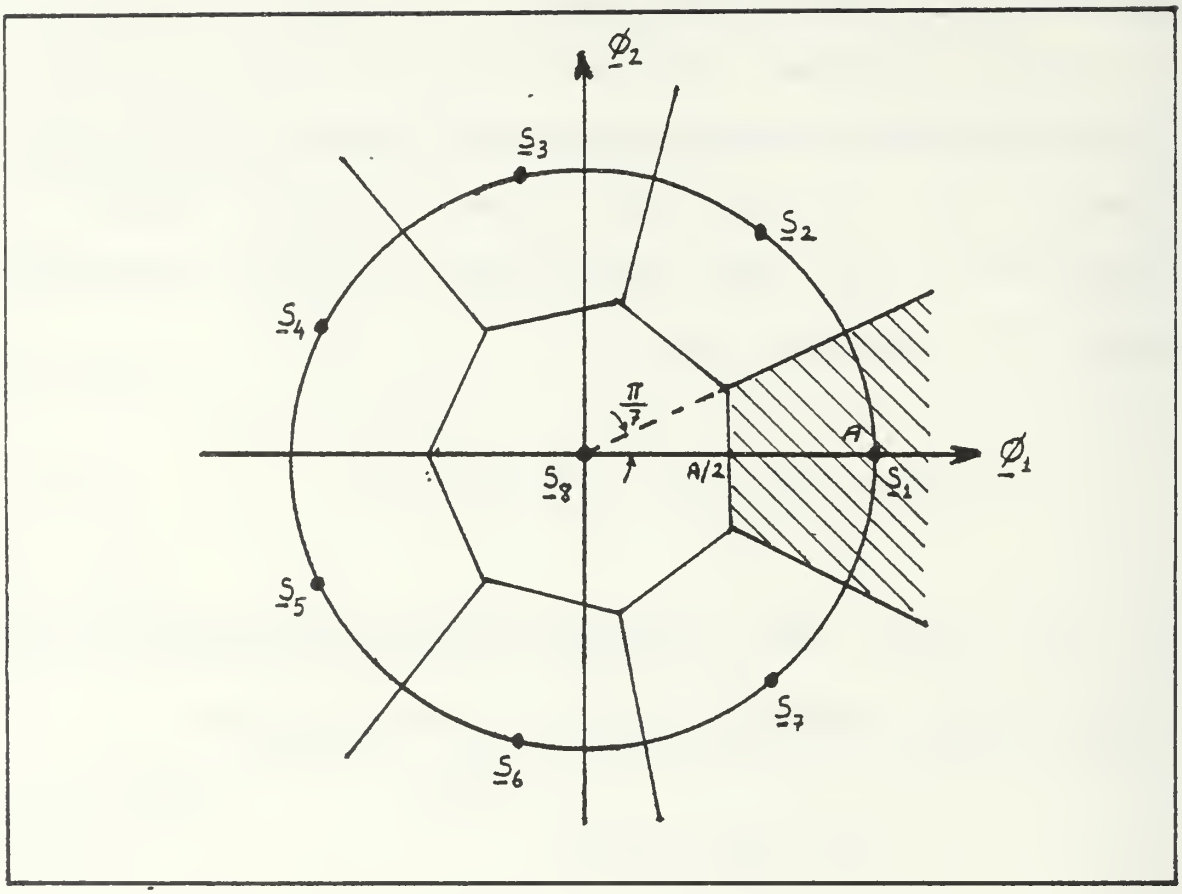

Figure 2.5. Signal-Space Diagram for (7+1) PSK Scheme

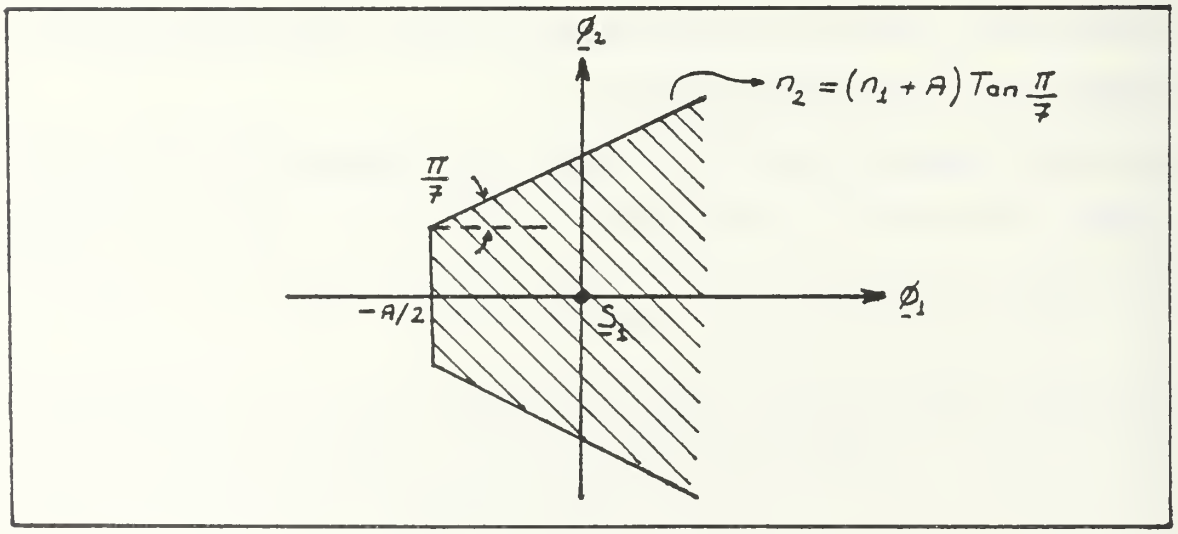

Figure 2.6. Transformed Decision Region for Calculating $Pr\{c/s_1(t)\}$

decision regions shown in Figure 2.5. It can be demonstrated that the evaluation of $Pr\{c/s_i(t)\}$ for any signal $s_i(t)$, is insensitive to such rotations and translations. From Figure 2.6 it is simple to evaluate $Pr\{c/s_1(t)\}$, since

$$Pr\{ c / s_1(t) \} = Pr\{ N_1 \geq -\frac{A}{2} ,$$

$$-(N_1 + A) \tan \frac{\pi}{7} \leq N_2 \leq (N_1 + A) \tan \frac{\pi}{7}\}. \qquad (2.44)$$

Since N_1 and N_2 are statistically independent, zero mean, $N_0/2$ variance, Gaussian random variables, we obtain

$$Pr\{c/s_1(t)\} = \int_{-A/2}^{\infty} \frac{1}{(2\pi N_0/2)^{1/2}} e^{-n_1^2/2 (N_0/2)}$$

$$\int_{-(n_1+A)\tan(\pi/7)}^{(n_1+A)\tan(\pi/7)} \frac{1}{(2\pi N_0/2)^{1/2}} e^{-n_2^2/2(N_0/2)} dn_2 dn_1 . \qquad (2.45)$$

Through the change of variables

$$\frac{n_1}{(N_0/2)^{1/2}} \triangleq y \quad , \quad \frac{n_2}{(N_0/2)^{1/2}} \triangleq x$$

we have

$$Pr\{c/s_1(t)\} = \int_{-A/2\ (N_0/2)^{1/2}}^{\infty} \frac{1}{(2\pi)^{1/2}} e^{-y^2/2}$$

$$\left[1-2\ \text{erfc}^*\left(\left(y + \frac{A}{(N_0/2)^{1/2}}\right) \tan\frac{\pi}{7}\right)\right] dy. \quad (2.46)$$

Finally, $Pr\{ c/s_8(t) \}$ can be obtained by evaluating the probability that the noise vector $\underline{n}$ is contained in the region diagrammed in Figure 2.7. Due to the symmetry of the problem, this can be obtained by multiplying fourteen times the probability that $\underline{n}$ is contained in the shaded triangle.

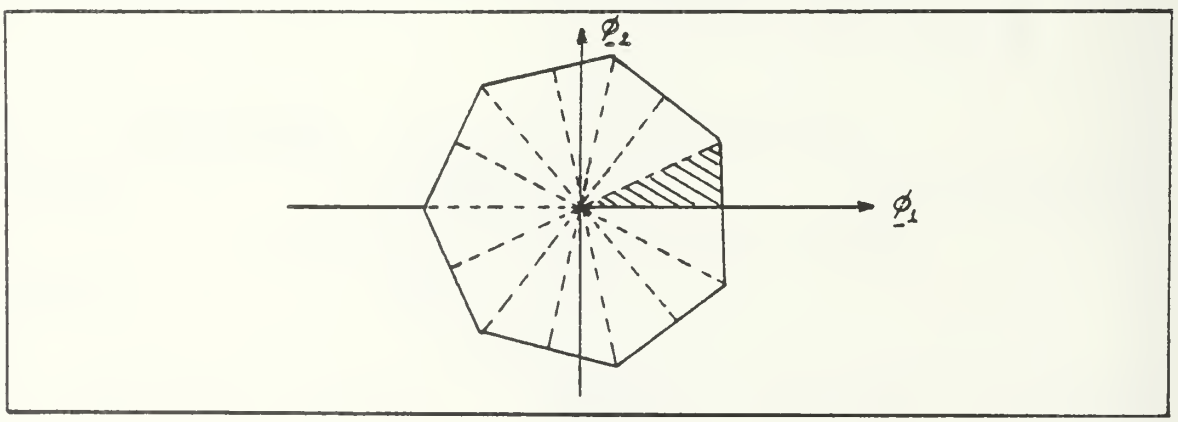

Figure 2.7. Transformed Decision Region for Calculating $Pr\{c/s_8(t)\}$

Thus,

$$Pr\{c/s_8(t)\} = 14\ Pr\{\ 0 \leqslant N_1 \leqslant A/2\ ,\ 0 \leqslant N_2 \leqslant N_1 \tan\ (\pi/7)$$

$$= 14\Bigg\{ \int_0^{A/2} \frac{1}{(2\pi\ N_0/2)^{1/2}}\ e^{-n_1^2/2\ (N_0/2)} \int_0^{n_1 \tan\frac{\pi}{7}} \frac{1}{(2\pi\ N_0/2)^{1/2}}\ e^{-n_2^2/2(N_0/2)^{1/2}} \Bigg\} dn_2\ dn_1$$

$$= 14\Bigg\{ \int_0^{A/2\ (N_0/2)^{1/2}} \frac{1}{(2\pi)^{1/2}}\ e^{-y^2/2} \Big[\ \frac{1}{2} - \text{erfc}^*(y \tan\frac{\pi}{7})\ \Big] \Bigg\} dy \qquad (2.47)$$

From Equation 2.30, we have

$$Pr\{\ c\ \} = \frac{1}{8}\ [\ 7\ Pr\{c/s_1(t)\} + Pr\{c/s_8(t)\}] \qquad (2.48)$$

In order to express the probability of error in terms of Rd, the signal to noise ratio, Equation 2.43 can be used in conjunction with Equation 2.46, Equation 2.47 and Equation 2.48, so that

$$\Pr\{\varepsilon\} = 1 - \frac{7}{8}\left\{ \int_{-(2Rd/7)^{1/2}}^{\infty} \frac{1}{(2\pi)^{1/2}} e^{-y^2/2} \right.$$

$$[1-2\ \mathrm{erfc}^*((y + (8Rd/7)^{1/2})\ \tan\ \pi/7)]\ dy$$

$$+ \int_{0}^{(2Rd/7)^{1/2}} \frac{1}{(2\pi)^{1/2}} e^{-y^2/2}$$

$$\left. [\ 1\ -\ 2\ \mathrm{erfc}^*(\ y\ \tan\ \frac{\pi}{7}\ )]\ dy \right\} \qquad (2.49)$$

where $Rd = 2\ E\ /\ N_0$.

These mathematical results given by Equation 2.30 for MPSK, Equation 2.41 for the "box" signaling scheme and Equation 2.49 for the modified 8 PSK are now used to graphically display the performance of the MAP receivers when the channel interference can be modeled as AWGN. The results on probability of error are shown in Figure 2.8 and graphs as a function of signal to noise ratio (Rd). The graphs show that 8 PSK tends to perform worse than the other two schemes considered. However, this must be weighed against the fact that the more complicated and dissimilar decision regions associated with the modified signaling schemes necessitates more complicated decision logic in the receiver implementation.

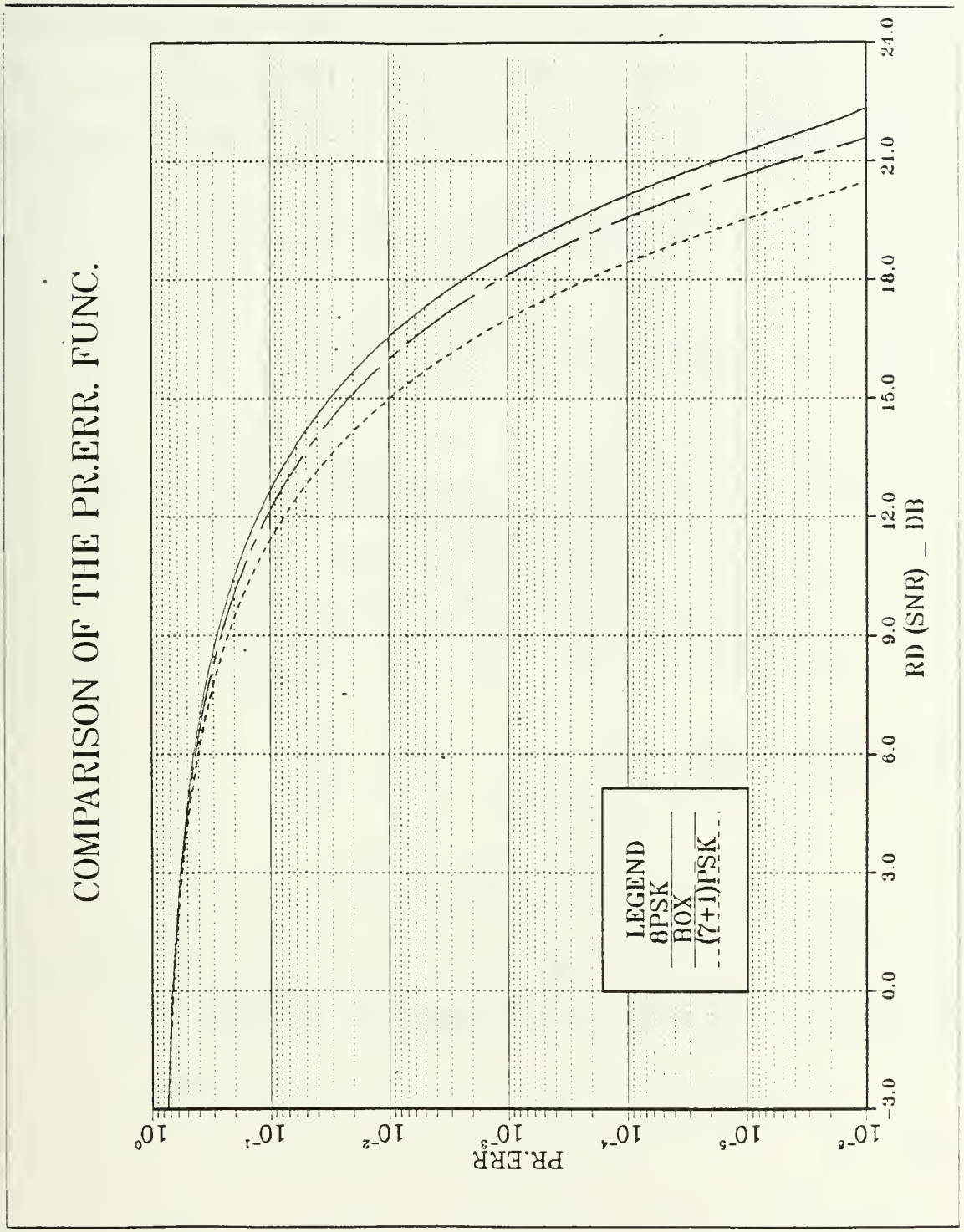

Figure 2.8. Comparison of Pr{ε} Performance for 8-PSK, Box, and (7+1) PSK Signaling Schemes

D. MULTI AMPLITUDE MPSK MODULATION SYSTEMS

Consider a situation in which the signal space diagram of an eight equiprobable signal set is as diagrammed in Figure 2.9. In this arrangement signals $\underline{s}_1$, $\underline{s}_3$, $\underline{s}_5$, $\underline{s}_7$ have energy R_1^2 and signals $\underline{s}_2$, $\underline{s}_4$, $\underline{s}_6$, $\underline{s}_8$ have energy R_2^2. The average energy $\bar{E}$ of the signal set is given by

$$\bar{E} = \frac{1}{8} \left(4 R_1^2 + 4 R_2^2 \right) = \frac{1}{2} \left(R_1^2 + R_2^2 \right)$$

If we let, $R_2 = R_1 + \varepsilon$ and require that $E = \bar{E}$, then

$$E = R_1^2 + R_1 \varepsilon + \frac{\varepsilon^2}{2}$$

This implies that

$$R_1 = \frac{-\varepsilon \pm \left(4E - \varepsilon^2 \right)^{1/2}}{2} \qquad (2.50)$$

Since R_1 must be real and non-negative, we must have

$$4E - \varepsilon^2 \geq 0 \quad \rightarrow \quad \varepsilon \leq 2(E)^{1/2}$$

and

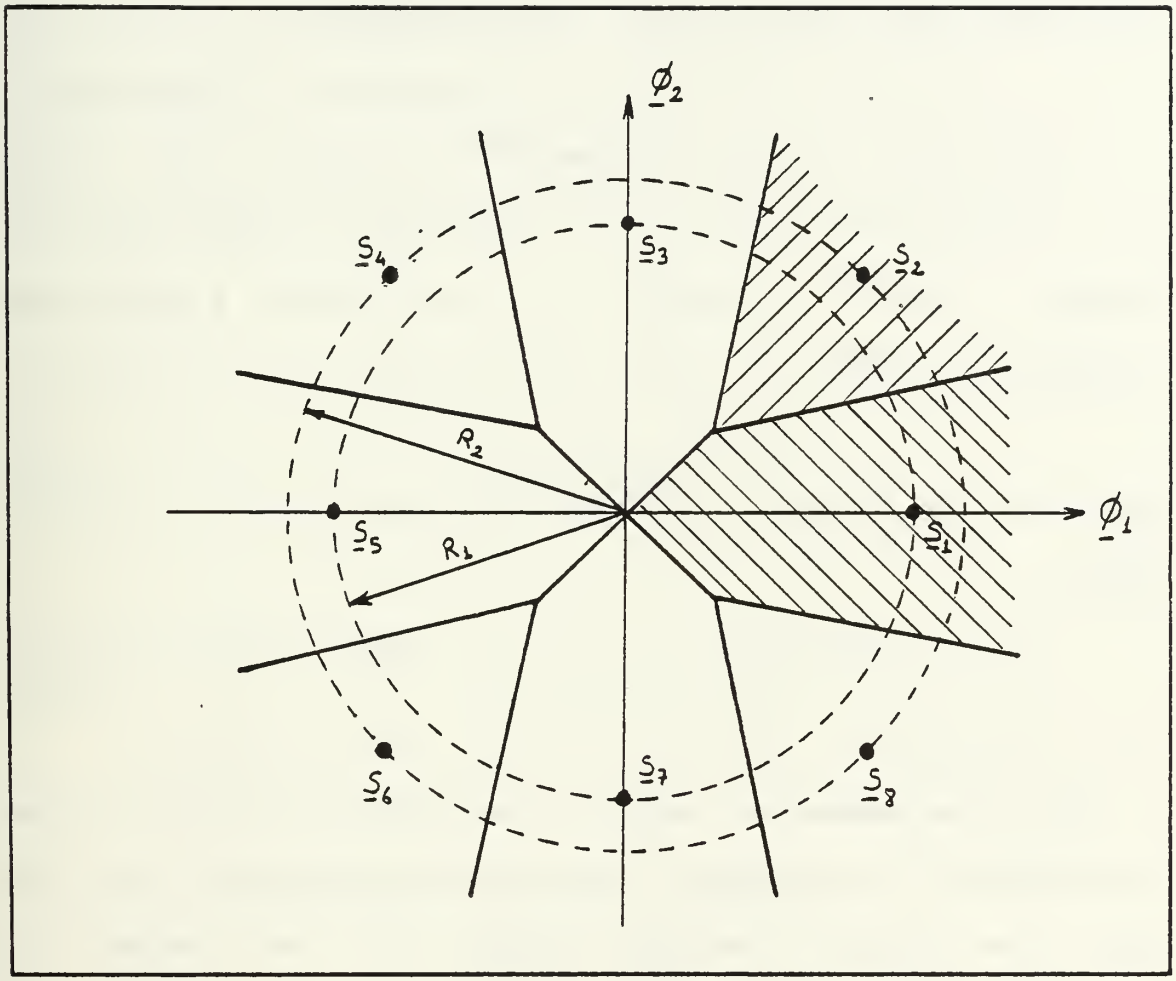

Figure 2.9. Signal-Space Diagram and Optimum Decision Regions for Multi Amplitude MPSK Modulation Systems

$$-\varepsilon + (4E - \varepsilon^2)^{1/2} \geq 0 \quad \rightarrow \quad \varepsilon \leq (2E)^{1/2}.$$

Therefore ε is constrained to the interval

$$0 \leq \varepsilon \leq (2E)^{1/2} \tag{2.51}$$

since $(2E)^{1/2} < 2(E)^{1/2}$. If we define a normalized variable ε', where

$$\varepsilon' \stackrel{\Delta}{=} \frac{\varepsilon}{(2E)^{1/2}} \tag{2.52}$$

then

$$0 \leq \varepsilon' \leq 1. \tag{2.53}$$

The performance of this signaling scheme is now considered. The analysis is somewhat complicated by the fact that the optimum decision regions are odd shaped and dependent on the parameter ε'.

Now we can focus on performance. The probability of correct decision associated with the transmission of signals $\underline{s}_1$, $\underline{s}_3$, $\underline{s}_5$, $\underline{s}_7$ is first considered. Because the corresponding decision regions are similar, only one case need be considered.

1. Derivation of Probability of Correct Decision Given That $\underline{s}_i$ Was Transmitted.

The decision region for determining the probability of correct reception given that $\underline{s}_1$, $\underline{s}_3$, $\underline{s}_5$, $\underline{s}_7$ were trasmitted is illustrated in Figure 2.10.

The probability of making a correct decision, given that $s_i(t)$ was transmitted, $Pr\{c/s_i(t)\}$, is given by

$$Pr\{c/s_i(t)\} = Pr\{-R_i \leq N_i \leq f\ ,\ -(N_i + R_i) \leq N_2 \leq (N_i + R_i)\} +$$

$$Pr\{N_i > f,\ -[(N_i - f)\tan(45-\beta)+a] \leq N_2 \leq [(N_i - f)\tan(45-\beta)+a]\} \qquad (2.54)$$

where $f = -R_i + a$. When $R_i > a$, f is negative.

Since N_i and N_2 are statistically independent, zero mean, $N_0/2$ variance Gaussian random variables, the first of the two joint probabilities above becomes,

$$\left\{\int_{-R_i}^{f} \frac{1}{(2\pi\ N_0/2)^{1/2}}\ e^{-n_i^2/2(N_0/2)} \right.$$

$$\left. \int_{-(n_i+R_i)}^{n_i+R_i} \frac{1}{(2\pi\ N_0/2)^{1/2}}\ e^{-n_2^2/2(N_0/2)}\ dn_2\ dn_i \right\} =$$

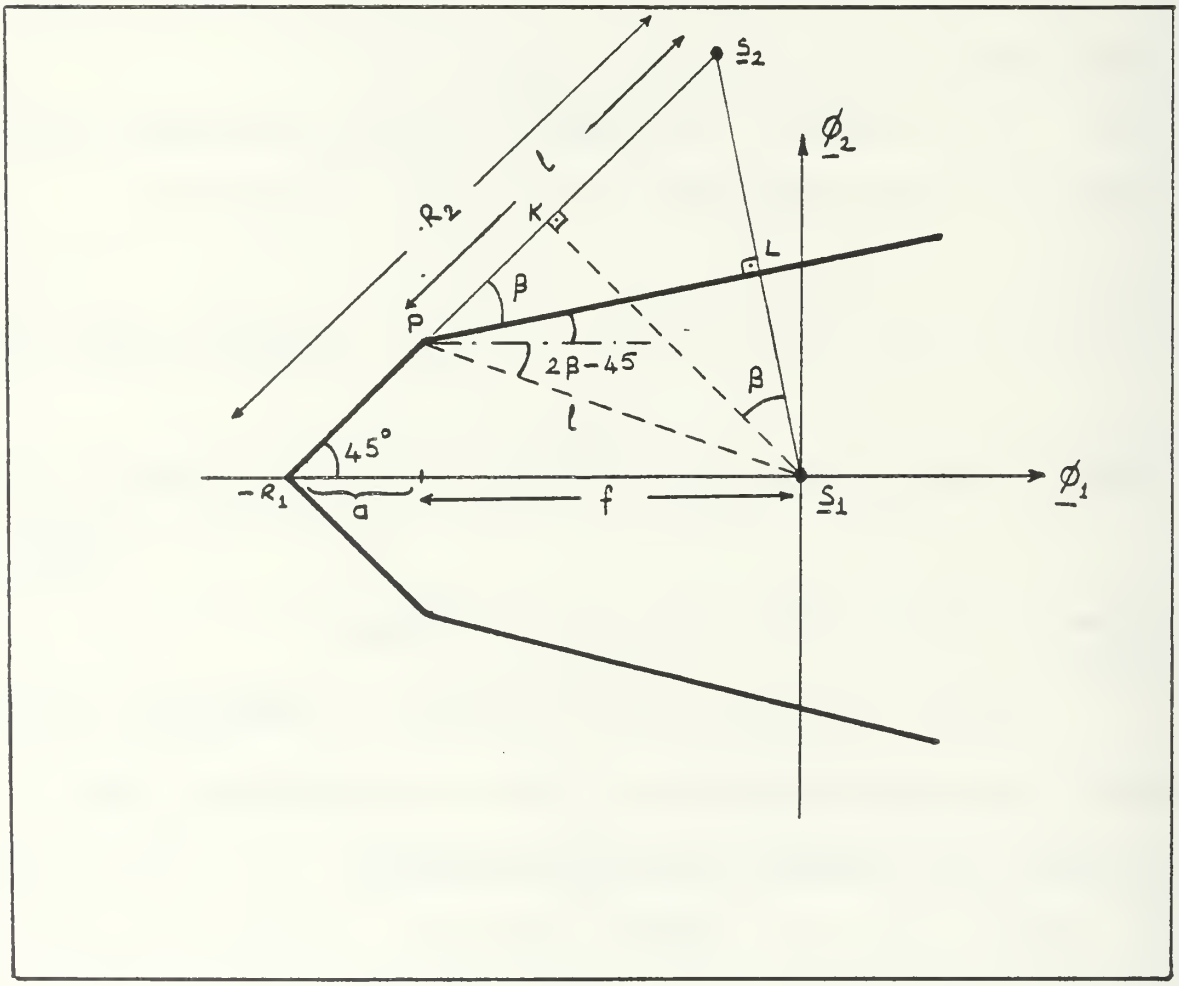

Figure 2.10. Transformed Decision Region for Calculating $Pr\{c/s_1(t)\}$

$$= \left\{ \int_{-R_1/(N_0/2)^{1/2}}^{f/(N_0/2)^{1/2}} \frac{1}{(2\pi)^{1/2}} e^{-y^2/2} \right.$$

$$\left. [1-2\ \mathrm{erfc}^*(y + \frac{R_1}{(N_0/2)^{1/2}})] \right\} dy \qquad (2.55)$$

and the second of the two joint probabilities above becomes

$$\left\{ \int_f^{\infty} \frac{1}{(2\pi\ N_0 2)^{1/2}} e^{-n_1^2/2(N_0/2)} \right.$$

$$\int_{-[(n_1-f)\tan(45-\beta)+a]}^{[(n_1-f)\tan(45-\beta)+a]} \frac{1}{(2\pi\ N_0/2)^{1/2}}$$

$$\left. e^{-n_2^2/2(N_0/2)} \right\} dn_2 dn_1 =$$

$$= \int_{f/(N_0/2)^{1/2}}^{\infty} \frac{1}{(2\pi)^{1/2}} e^{-y^2/2}$$

$$[\ 1-2\ \mathrm{erfc}^*((y - \frac{f}{(N_0/2)^{1/2}})\ \tan(45-\beta) + \frac{a}{(N_0/2)^{1/2}})]\ dy$$

(2.56)

In order to be able to express probability of error necessary to correctly identify the parameters in Equations 2.55 and 2.56. From Equation 2.51, we have

$$R_1 = \frac{(-\varepsilon + (4E - \varepsilon^2)^{1/2})}{2}$$

and defining the signal to noise ratio Rd, by $Rd = (2E/N_0)^{1/2}$ we have

$$D \overset{\Delta}{=} \frac{R_1}{(N_0/2)^{1/2}} = (-\varepsilon' + (2-\varepsilon'^2)^{1/2}) (RD/2)^{1/2}. \qquad (2.57)$$

The angle of β can be defined in terms of ε'. In Figure 2.10,

$$\overline{KS_2} = \overline{KS_1} \tan\beta$$

$$\overline{R_1S_2} - \overline{R_1K} = \overline{KS_1} \tan\beta$$

$$R_2 - R_1 \cos 45 = R_1 \cos 45 \tan\beta$$

$$\tan\beta = (2)^{1/2} \frac{R_2}{R_1} - 1 \qquad (2.58)$$

so that

$$\tan\beta = (2)^{1/2} \left(\frac{R_1 + \varepsilon}{R_1} \right) - 1 = (2)^{1/2} \left(1 + \frac{\varepsilon}{R_1} \right) - 1.$$

From Equation 2.51, $\tan\beta$ now becomes

$$\tan\beta = (2)^{1/2} \left(\frac{\varepsilon' + (2-\varepsilon')^{1/2}}{-\varepsilon' + (2-\varepsilon'^{2})^{1/2}} \right) - 1 . \qquad (2.59)$$

Looking at Figure 2.10, the triangle defined by vertices PS_1K has angle of $KPS_1 = 2\beta$ so that

$$\sin 2\beta = \frac{\overline{KS_1}}{\overline{PS_1}} = \frac{R_1 \cos 45}{1}$$

or

$$1 = \frac{R_1}{(2)^{1/2} \sin(2\beta)} .$$

Using the trigonometric identity,

$$\sin(2\beta) = \frac{2\tan\beta}{1 + \tan^2\beta}$$

we have

$$l = \frac{R_i}{(2)^{1/2}} \left(\frac{1 + \tan^2\beta}{2\tan\beta} \right) \qquad (2.60)$$

and

$$L \overset{\Delta}{=} \frac{l}{(N_0/2)^{1/2}} = D \left(\frac{1 + \tan^2\beta}{2(2)^{1/2}\tan\beta} \right). \qquad (2.61)$$

Since

$$a = l \sin (2\beta - 45)$$

and

$$A \overset{\Delta}{=} \frac{a}{(N_0/2)^{1/2}} = L \sin (2\beta - 45) \qquad (2.62)$$

we obtain,

$$F \overset{\Delta}{=} \frac{f}{(N_0/2)^{1/2}} = \frac{-R_i + a}{(N_0/2)^{1/2}} = -D + A. \qquad (2.63)$$

It is now possible to put $Pr\{ c/s_i(t)\}$ in simpler form, namely

$$Pr\{c/s_i(t)\} = \int_{-D}^{F} \frac{1}{(2\pi)^{1/2}} e^{-y^2/2} [1-2\ erfc^*(y+D)]\ dy +$$

$$\int_{F}^{\infty} \frac{1}{(2\pi)^{1/2}} e^{-y^2/2} [1-2\ erfc^*((y-F)\tan(45-\beta)+A)]dy. \qquad (2.64)$$

2. Derivation of Probability of Correct Decision Given That S_2 Was Transmitted.

The decision region for determining the probability of correct reception, given that $\underline{s}_2$, $\underline{s}_4$, $\underline{s}_6$, $\underline{s}_8$ were transmitted, is illustrated in Figure 2.11.

The probability of making a correct decision, given that $s_2(t)$ was transmitted, $Pr\{ c/s_2(t)\}$, is given by

$$Pr\{c/s_2(t)\} = Pr\{ N_1 \geq -1,\ -(N_1+1)\tan\beta \leq N_2 \leq (N_1+1)\tan\beta \}$$

$$= \int_{-1}^{\infty} \frac{1}{(2\pi N_0/2)^{1/2}} e^{-n_1^2/2} \int_{-(n_1+1)\tan\beta}^{(n_1+1)\tan\beta} \frac{1}{(2\pi N_0/2)^{1/2}} e^{-n_2^2/2} dn_2\, dn_1$$

$$= \int_{-L}^{\infty} \frac{1}{(2\pi)^{1/2}} [\ 1-2\ \mathrm{erfc}^*((y+L)\tan\beta\ )]\ dy \qquad (2.65)$$

where L is defined by Equation 2.61.

It is now necessary to return to Figure 2.9 and investigate how the decision regions change as a function of changes in ε'. As can be seen when ε' increases, R_1 becomes

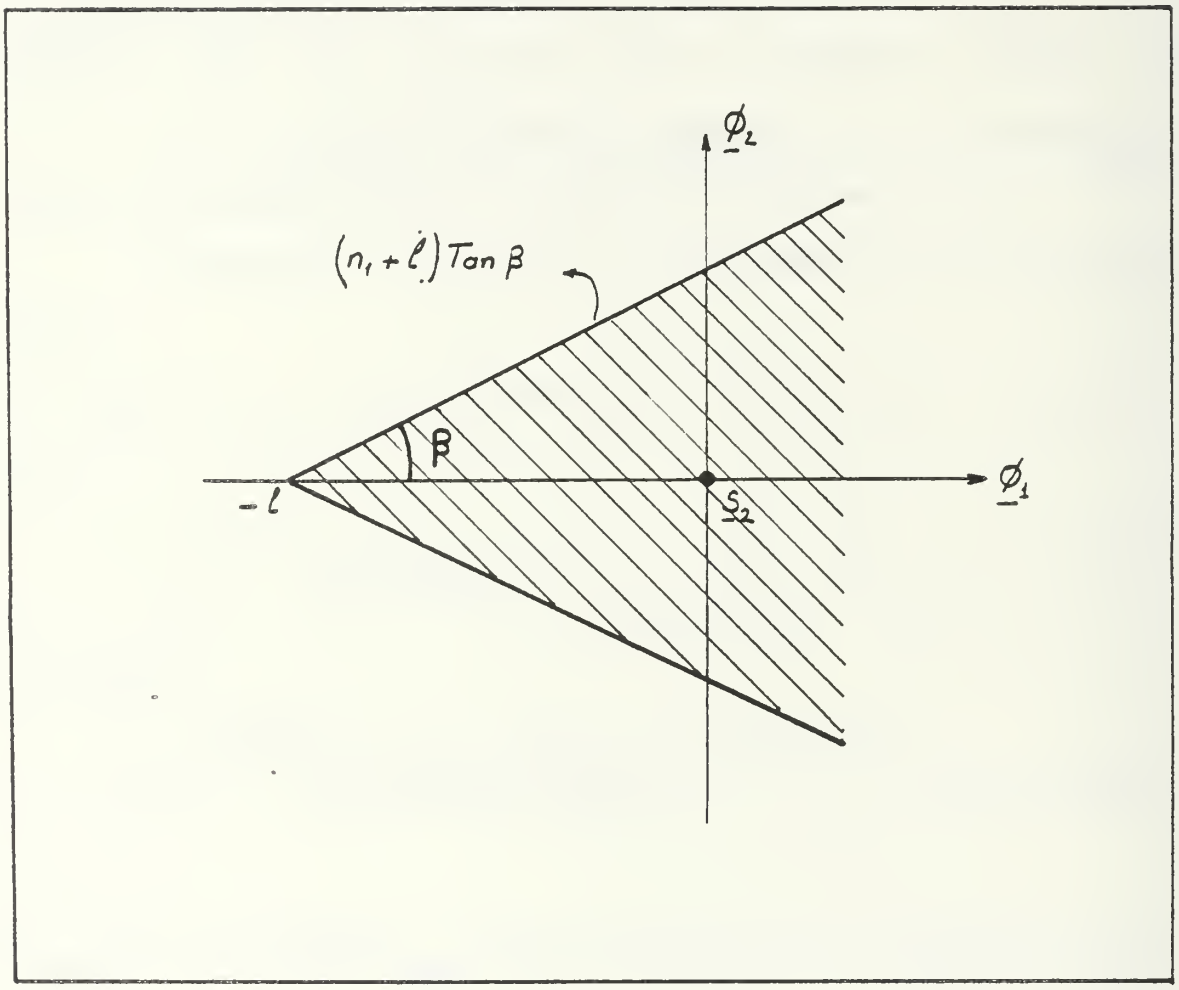

Figure 2.11. Transformed Decision Region for Calculating $Pr\{c/s_2(t)\}$

smaller, while R_2 and β become larger. If we focus on the special case where $R_2 = (2)^{1/2} R_1$. We have from Equation 2.58

$$\tan \beta = 1 \quad \rightarrow \quad \beta = 45^0$$

and

$$L = \frac{R_1}{(2)^{1/2}} = \frac{R_2}{2} \tag{2.66}$$

where the second equality in Equation 2.66 is due to our assumption that $\frac{R_2}{R_1} = (2)^{1/2}$. Furthermore, this assumption implies that ε' satisfies

$$\varepsilon' (1 + (2)^{1/2}) = (2 - \varepsilon'^2)^{1/2} ((2)^{1/2} - 1)$$

or equivalently

$$\varepsilon' = .2391 \tag{2.67}$$

due to the fact that $R_2 = R_1 + \varepsilon$ and R_1 is given by Equation 2.51. It can be seen without a great deal of difficulty that this special case results in a signal constellation of the form analyzed in Section B, and labeled "Rectangular" signaling scheme.

If ε' is allowed to continue to increase, β exceeds 45^0, and the decision regions change to the form shown in

Figure 2.12. This figure illustrates just one quadrant of Figure 2.9, for $\beta > 45^0$. In Figure 2.9, observe that

$$b = \frac{a}{\tan(\beta - 45)}$$

and using the trigonometric identity

$$\tan(\beta - 45) = \frac{\tan\beta - 1}{1 + \tan\beta}$$

we have,

$$B \triangleq \frac{b}{(N_0/2)^{1/2}} = A\left(\frac{1 + \tan\beta}{\tan\beta - 1}\right) \qquad (2.68)$$

where A is defined by Equation 2.62. The shaded area in Figure 2.12 shows the optimum decision region for signal $\underline{s}_i$. When $\underline{s}_i$ is shifted to the origin Equation 2.64 can be modified to account for the different decision region of Figure 2.12. The probability of correct decision for $\underline{s}_i$, $Pr\{c/s_i(t)\}$ is given now by

$$Pr\{c/s_i(t)\} = \int_{-D}^{F} \frac{1}{(2\pi)^{1/2}} e^{-y^2/2} [1-2\ \text{erfc}^*(y+D)]\, dy +$$

$$\int_{F}^{F+B} \frac{1}{(2\pi)^{1/2}} e^{-y^2/2} [1-2\ \text{erfc}^*((y-F)\tan(45-\beta)+A)]\, dy. \qquad (2.69)$$

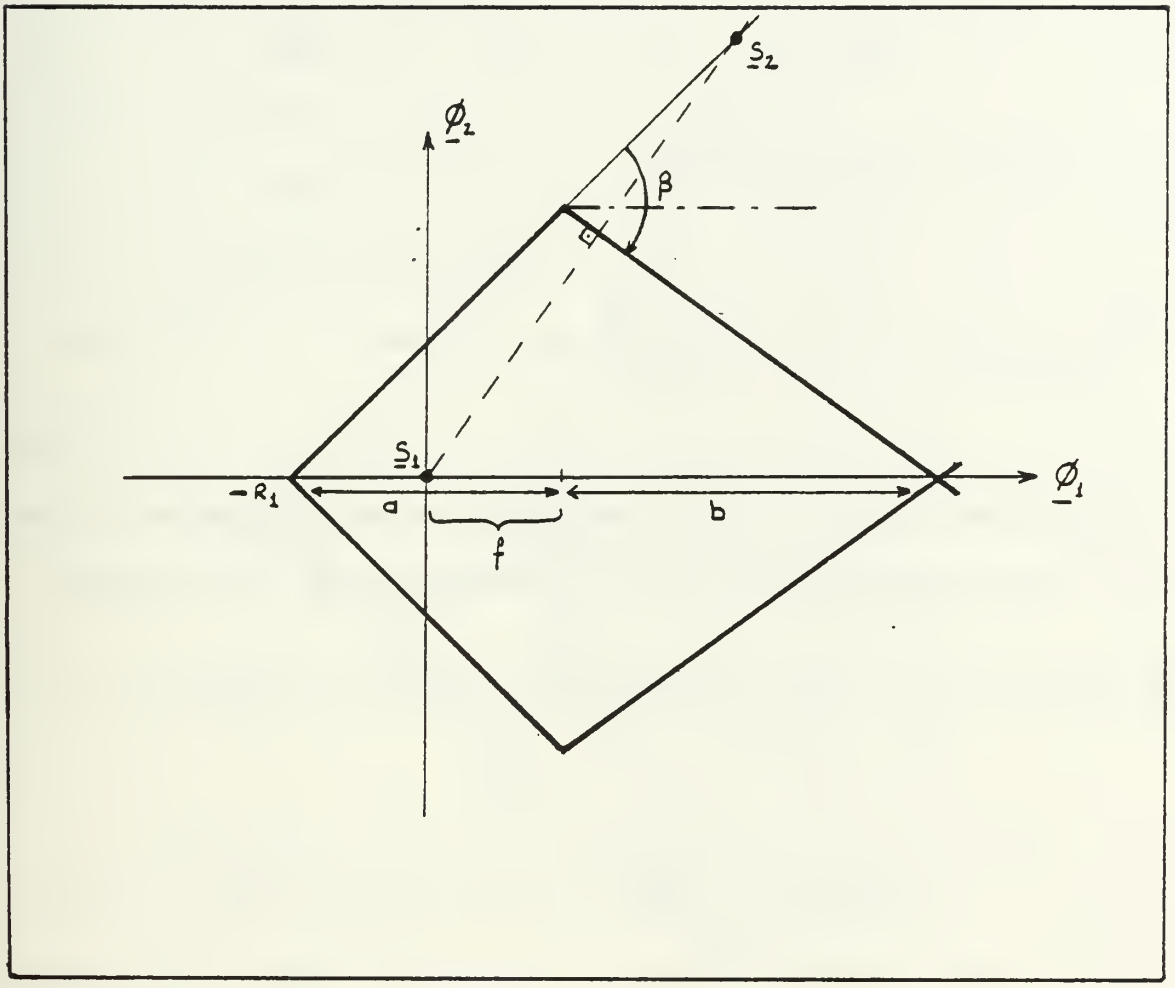

Figure 2.12. Transformed Decision Region for Calculating $Pr\{c/s_1(t)\}$ ($45^0 < \beta < 90^0$)

For $\beta > 45$, the decision region for signal $\underline{s}_2$ must also be modified and reanalyzed. In Figure 2.13 this situation is depicted, where

$$v = -1 + ((a)^2 + (b)^2)^{1/2} \cos\beta$$

Using Equation 2.62 and Equation 2.68, we have

$$V \overset{\Delta}{=} \frac{v}{(N_0/2)^{1/2}} = -L + \frac{A}{(\tan\beta - 1)} (2(\tan^2\beta + 1))^{1/2} \cos\beta \qquad (2.70)$$

The probability of making a correct decision, given $s_2(t)$ was transmitted, given by Equation 2.65 now becomes,

$$Pr\{c/s_1(t)\} = \int_{-L}^{V} \frac{1}{(2\pi)^{1/2}} e^{-y^2/2} [1-2\ erfc^*(y+L)\tan\beta\ ]\ dy +$$

$$\int_{V}^{\infty} \frac{1}{(2\pi)^{1/2}} e^{-y^2/2} [1-2\ erfc^*(y+D+\varepsilon'(2\ Rd)^{1/2})]\ dy. \qquad (2.71)$$

The derived conditional proabilities of correct decision, denoted by $Pr\{c/s_1(t)\}$ and $Pr\{c/s_2(t)\}$, are now used to obtain the overall probability of error assuming all

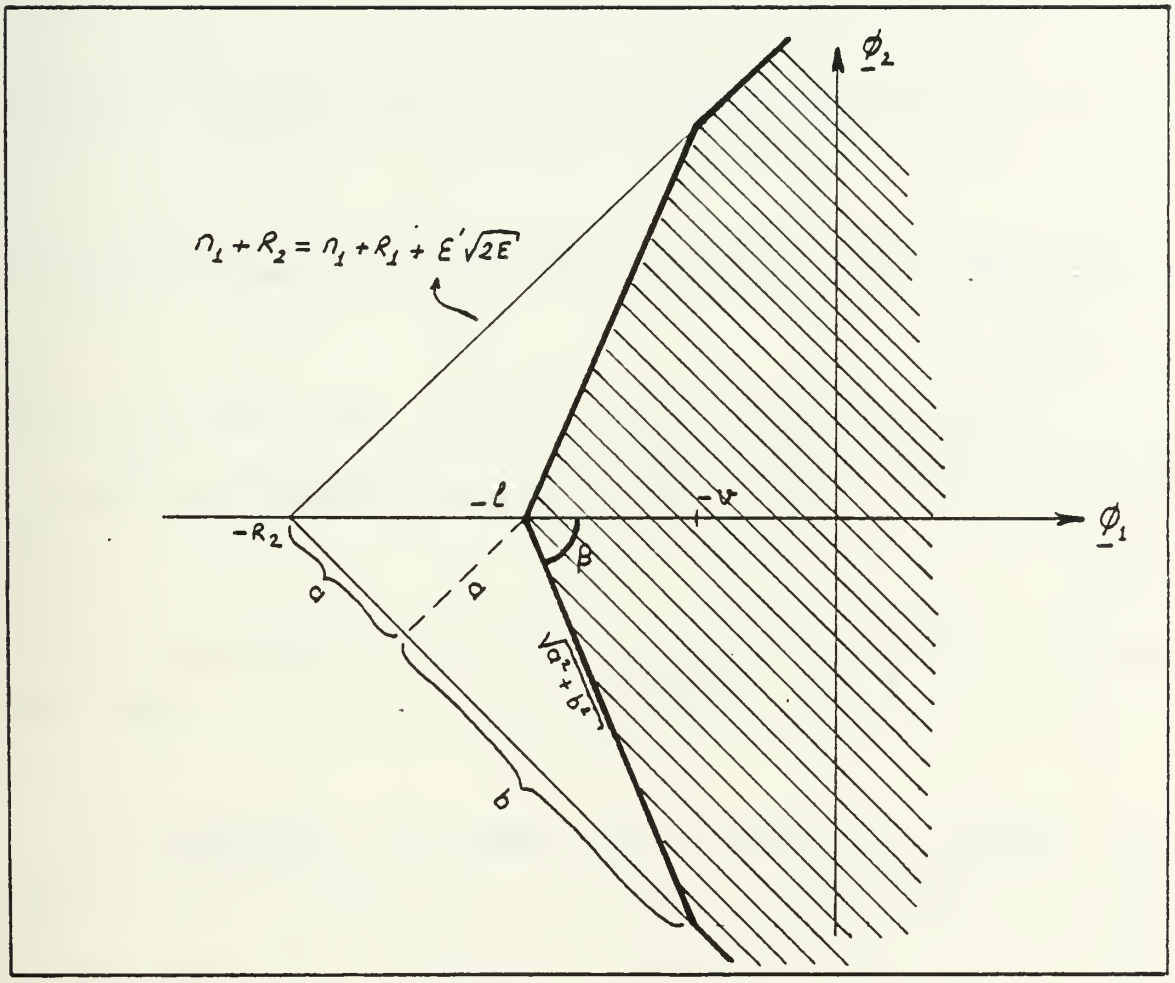

Figure 2.13. Transformed Decision Region for Calculating $Pr\{c/s_2(t)\}$ ($45^0 < \beta < 90^0$)

signals are equally likely to be transmitted. Thus

$$Pr\{\varepsilon\} \overset{\Delta}{=} 1 - Pr\{ c \}$$

$$= 1 - \frac{1}{2} [Pr\{c/s_1(t)\} + Pr\{c/s_2(t)\}] \qquad (2.72)$$

which takes on two forms depending on whether, $\beta < 45^0$ or $\beta > 45^0$.

Using Equations 2.64, 2.65, 2.69, and 2.71 in Equation 2.72, we obtain $Pr\{\varepsilon\}$ as a function of ε and Rd,

$$Pr\{\varepsilon\} = 1 - 0.5 \left\{ \int_{-D}^{F} \frac{1}{(2\pi)^{1/2}} e^{-y^2/2} [1-2\ erfc*(y+D)]\, dy + \right.$$

$$\int_{F}^{\infty} \frac{1}{(2\pi)^{1/2}} e^{-y^2/2} [1-2\ erfc*((y-F)\tan(45-\beta)+A)]dy$$

$$\left. \int_{-L}^{\infty} \frac{1}{(2\pi)^{1/2}} e^{-y^2/2} [1-2\ erfc*((y+L)\tan\beta\ )]\, dy \right\} \qquad (2.73)$$

for $\varepsilon \leq .2391$ ($\beta \leq 45$),

and

$$Pr\{\varepsilon\} = 1 - 0.5\left\{ \int_{-D}^{F} \frac{1}{(2\pi)^{1/2}} e^{-y^2/2} \left[1-2\ erfc^*(y+D)\right]dy + \right.$$

$$\int_{F}^{F+B} \frac{1}{(2\pi)^{1/2}} e^{-y^2/2} \left[1-2\ erfc^*((y-F)\tan(45-\beta)+A)\right]dy +$$

$$\int_{-L}^{V} \frac{1}{(2\pi)^{1/2}} e^{-y^2/2} \left[1-2\ erfc^*(y+L)\tan\beta\ \right] dy +$$

$$\left. \int_{V}^{\infty} \frac{1}{(2\pi)^{1/2}} e^{-y^2/2} \left[1-2\ erfc^*(y+D+\varepsilon'(2\ Rd)^{1/2}\ \right] dy \right\} \qquad (2.74)$$

for $.2391 < \varepsilon' < 1.$ $(45^0 < \beta < 90^0)$.

Equation 2.73 has been plotted in Figure 2.14 showing the probability of error versus signal to noise ratio (Rd) for different values of ε'. If ε' is equal to zero we have $R_1 = R_2$, so that Equation 2.73 yields the same performance curve previously evaluated for 8-PSK. When ε' is allowed to increase up to the value of 0.2391, the probability of error decreases for a fixed value of Rd. As mentioned earlier for ε'=0.2391 we have the "box" signal constellation and the performance curves substantiate this

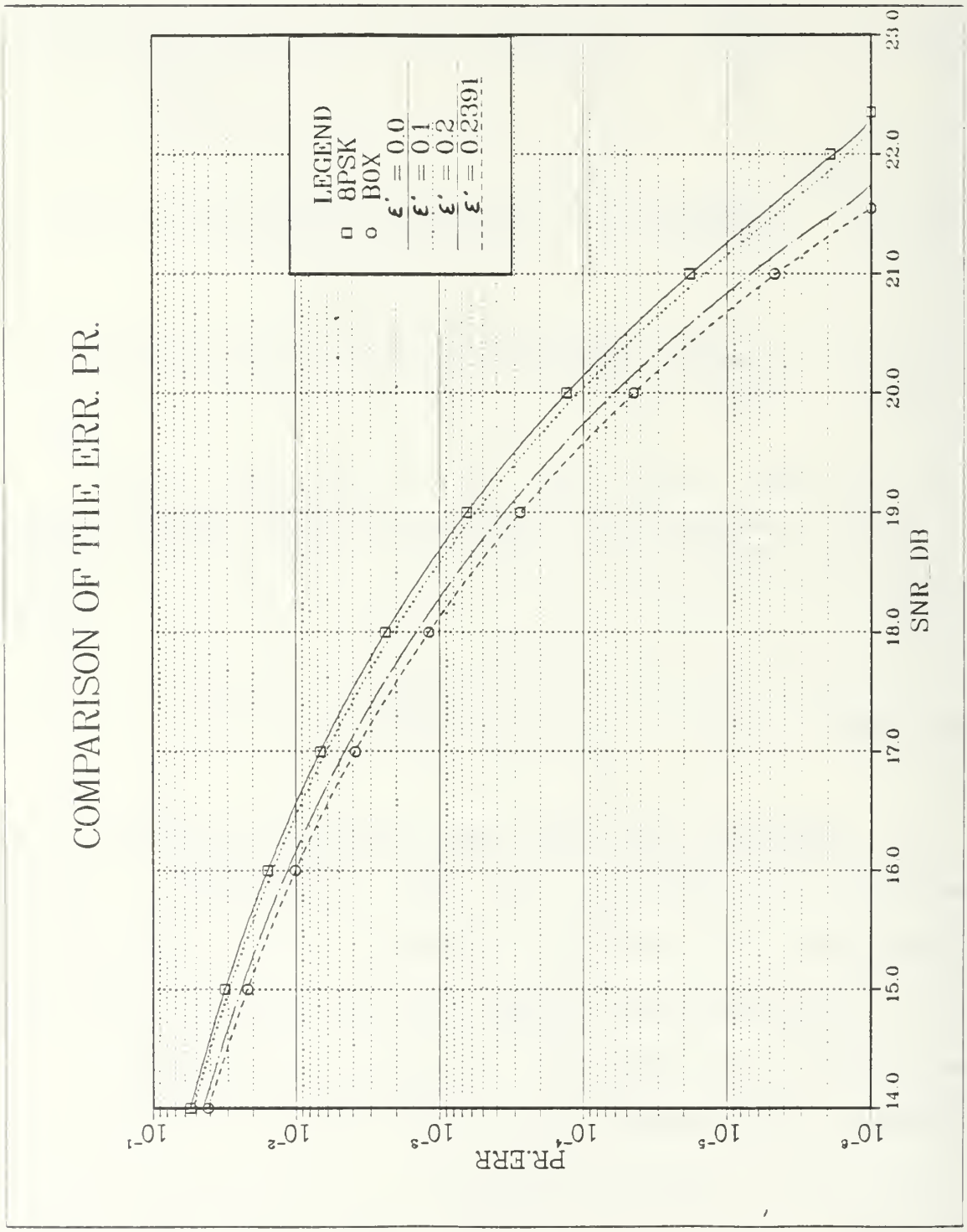

Figure 2.14. Comparison of Pr{ε} Performance for Multi Amplitude MPSK Modulation ($0 \leq \varepsilon' \leq 0.2391$)

result. If ε' continues to increase, better system performance is observed up to the value of abaut $\varepsilon'=0.4$. It has been observed that $Pr\{\varepsilon\}$ start to increase for fixed values of Rd as ε' increases beyond the value of 0.4. We can observe the behavior of $Pr\{\varepsilon\}$ as a function of ε' and Rd in Figure 2.15. It is not surprising that there is an increasing deterioration of performance as $\varepsilon' \rightarrow 1$. With increasing ε', four out of the eight signals "collapse" to the origin while the remaining four signals achieve their maximum energy. With four signals being essentially equal (of zero amplitude) one must expect that these signals cannot be discriminated at the receiver so we must expect a high error probability under these circumstances.

E. MODIFIED MULTI AMPLITUDE MPSK SYSTEMS.

The analysis carried out in section D of this chapter, demonstrated that, the optimum decision regions were complicated and difficult to implement in logic. Therefore in this section, modifications to the optimum decision regions analyzed in section D will be presented in order to obtain simpler decision regions that would vetimately result in similar logic implementations. Obviously performance will be degraded since the simpler decision regions are no longer optimum.

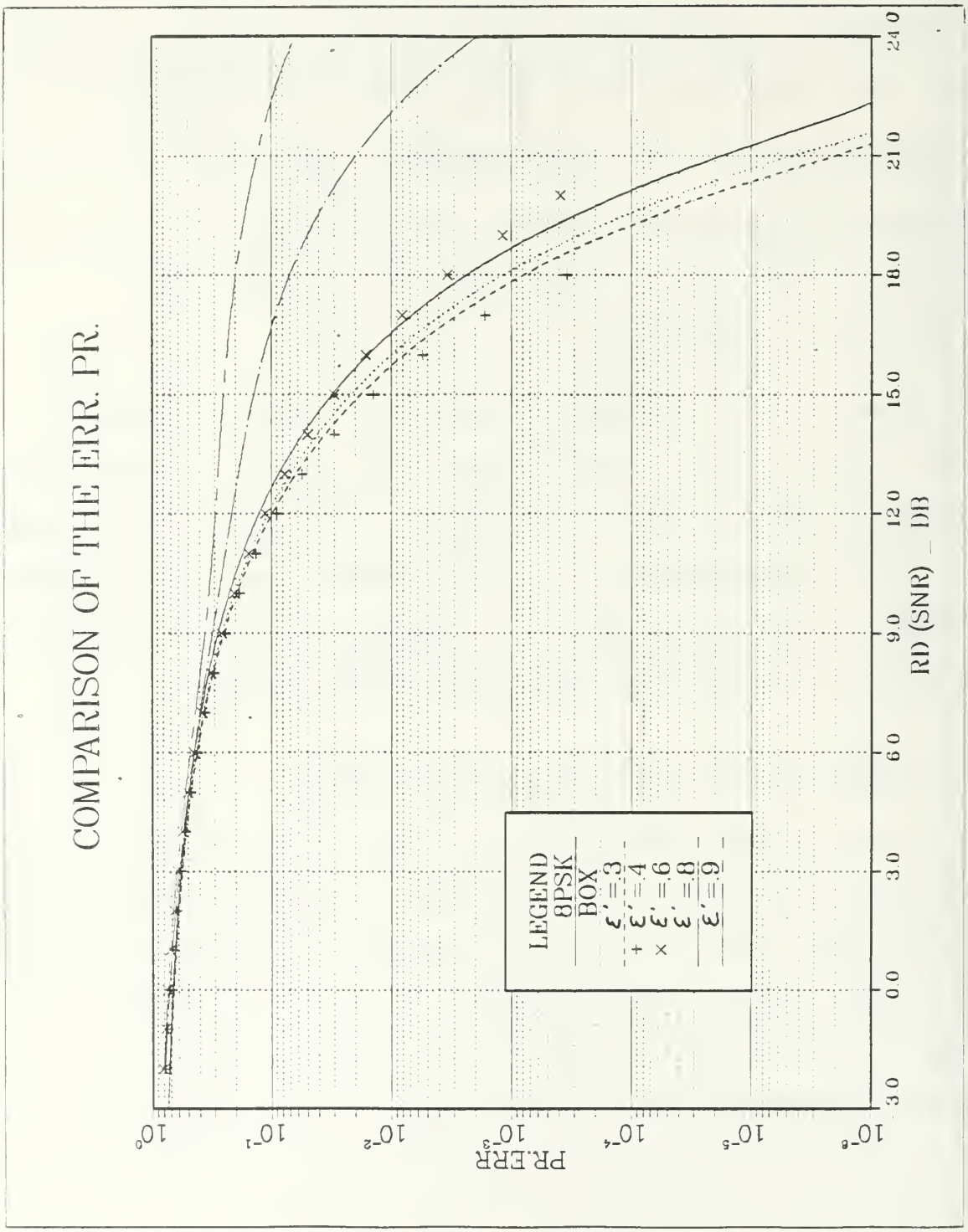

Figure 2.15. Comparison of Pr{ε} Performance for Multi Amplitude MPSK Modulation ($0.3 \leq \varepsilon' \leq 0.9$)

1. Modification 1

The decision regions of the signal constellation illustrated in Figure 2.9 are modified as illustrated in Figure 2.16. Observe that all signals are recovered by simple phase measurement without regard to their energy. The parameter $D \triangleq \frac{R_1}{(N_0/2)^{1/2}}$ has been expressed in terms of signal to noise ratio and the parameter $\varepsilon' \triangleq \frac{\varepsilon}{(2E)^{1/2}}$ in the previous section. Recall from Equation 2.57 that

$$D \triangleq \frac{R_1}{(N_0/2)^{1/2}} = (- \varepsilon' + (2 - \varepsilon'^2)^{1/2})(Rd/2)^{1/2} .$$

The region associated with the determination of $Pr\{ c/s_1(t)\}$ is shown in Figure 2.17(a). The probability of correct decision given that $s_1(t)$ was transmitted can be expressed with the aid of Figure 2.17(a) as

$$Pr\{c/s_1(t)\} = Pr\{N_1 \geq -R_1 , -(N_1+R_1)\tan\frac{\pi}{8} \leq N_2 \leq (N_1+R_1)\tan\frac{\pi}{8}\}$$

$$= 2 \left\{ \int_{-R_1}^{\infty} \frac{1}{(2\pi N_0/2)^{1/2}} e^{-n_1^2/2 (N_0/2)} \right.$$

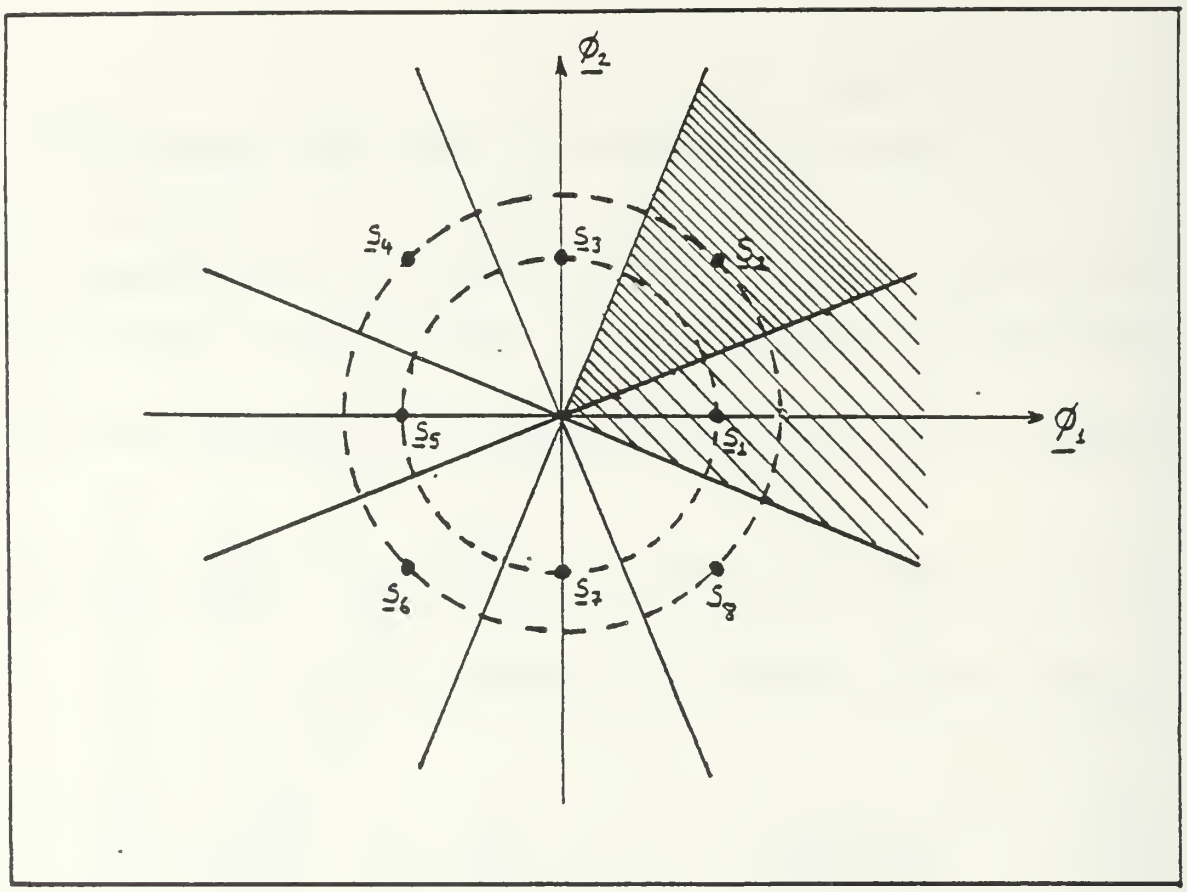

Figure 2.16. Signal-Space Diagram and Decision Region for MOD.1

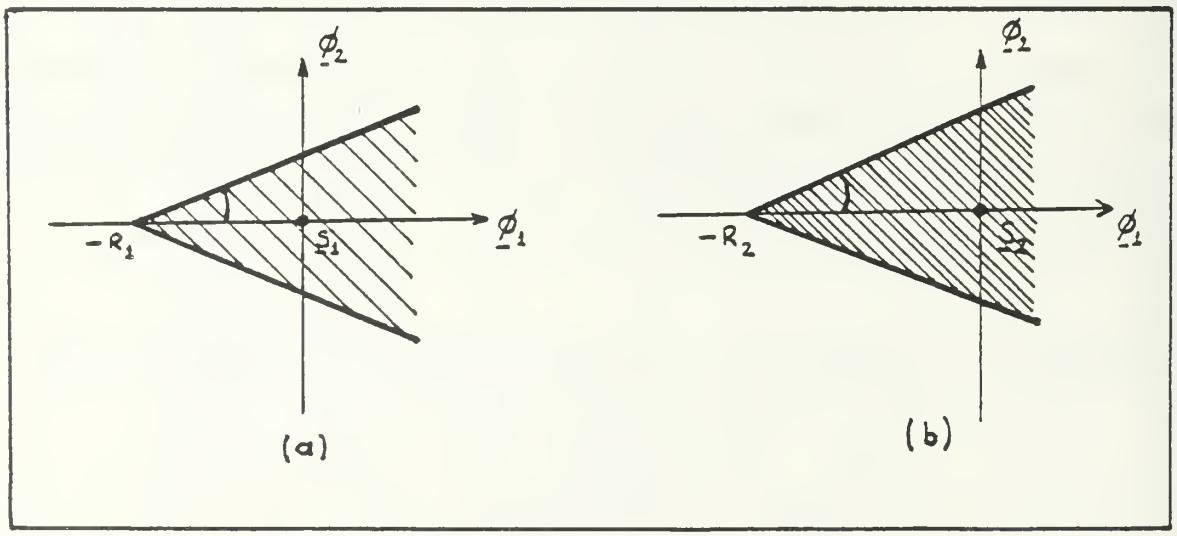

Figure 2.17. Transformed Decision Regions for MOD.1

$$\left. \int_{0}^{(n_1+R_1)\tan\frac{\pi}{8}} \frac{1}{(2\pi N_0/2)^{1/2}} e^{-n_2^2/2(N_0/2)} \right\} dn_2 dn_1 .$$

(2.75)

By using appropriate change of variables of integration we obtain

$$\Pr\{c/s_1(t)\} = \int_{-D}^{\infty} \frac{1}{(2\pi)^{1/2}} e^{-y^2/2} \left[1-2\ \mathrm{erfc}^*\left((y+D)\tan\frac{\pi}{8}\right)\right] dy.$$

(2.76)

From Figure 2.17(b), the probability of making a correct decision given that $s_2(t)$ was transmitted is similar to $\Pr\{ c/s_1(t) \}$, except that R_1 must be replaced by R_2, where

$$R_2 = R_1 + \varepsilon .$$

Let

$$H \overset{\Delta}{=} \frac{R_2}{(N_0/2)^{1/2}}$$

so that in terms of signal to noise ratio and ε', we have

$$H \overset{\Delta}{=} \frac{R_2}{(N_0/2)^{1/2}} = (\varepsilon' + (2 - \varepsilon'^2)^{1/2}) (Rd/2)^{1/2} \qquad (2.77)$$

and $\Pr\{ c/s_2(t)\}$ is

$$\Pr\{c/s_2(t)\} = \int_{-H}^{\infty} \frac{1}{(2\pi)^{1/2}} e^{-y^2/2} \left[1-2\ \mathrm{erfc}^*\left((y+H)\tan\frac{\pi}{8}\right)\right] dy.$$

(2.78)

From the symmetry of the decision regions and assuming all signals to be equally likely, we have

$$Pr\{c\} = \frac{1}{2}\left[Pr\{c/s_i(t)\} + Pr\{c/s_i(t)\} \right] \qquad (2.79)$$

so that

$$Pr\{\varepsilon\} = 1 - \frac{1}{2}\left\{ \int_{-D}^{\infty} \frac{1}{(2\pi)^{1/2}} e^{-y^2/2} \left[1-2\,erfc^*(y+D)\tan\frac{\pi}{8}\right] dy \right.$$

$$\left. + \int_{-H}^{\infty} \frac{1}{(2\pi)^{1/2}} e^{-y^2/2} \left[1-2\,erfc^*(y+H)\tan\frac{\pi}{8}\right] dy \right\}. \qquad (2.80)$$

The performance of this receiver is plotted in Figure 2.18 in terms of the probability of error versus Rd(SNR) for various values of ε'. For $\varepsilon'=0$, $R_1 = R_2$ and the resulting performance is equal to that of the 8-PSK receiver, as expected. However we can observe that $Pr\{\varepsilon\}$ increases for fixed values of Rd as ε' increases. This is partly due to the fact that the decision regions are not modified as ε' changes. Furthermore, as $\varepsilon' \to 1$, four out eight signals once again cluster around the origin resulting in very poor performance.

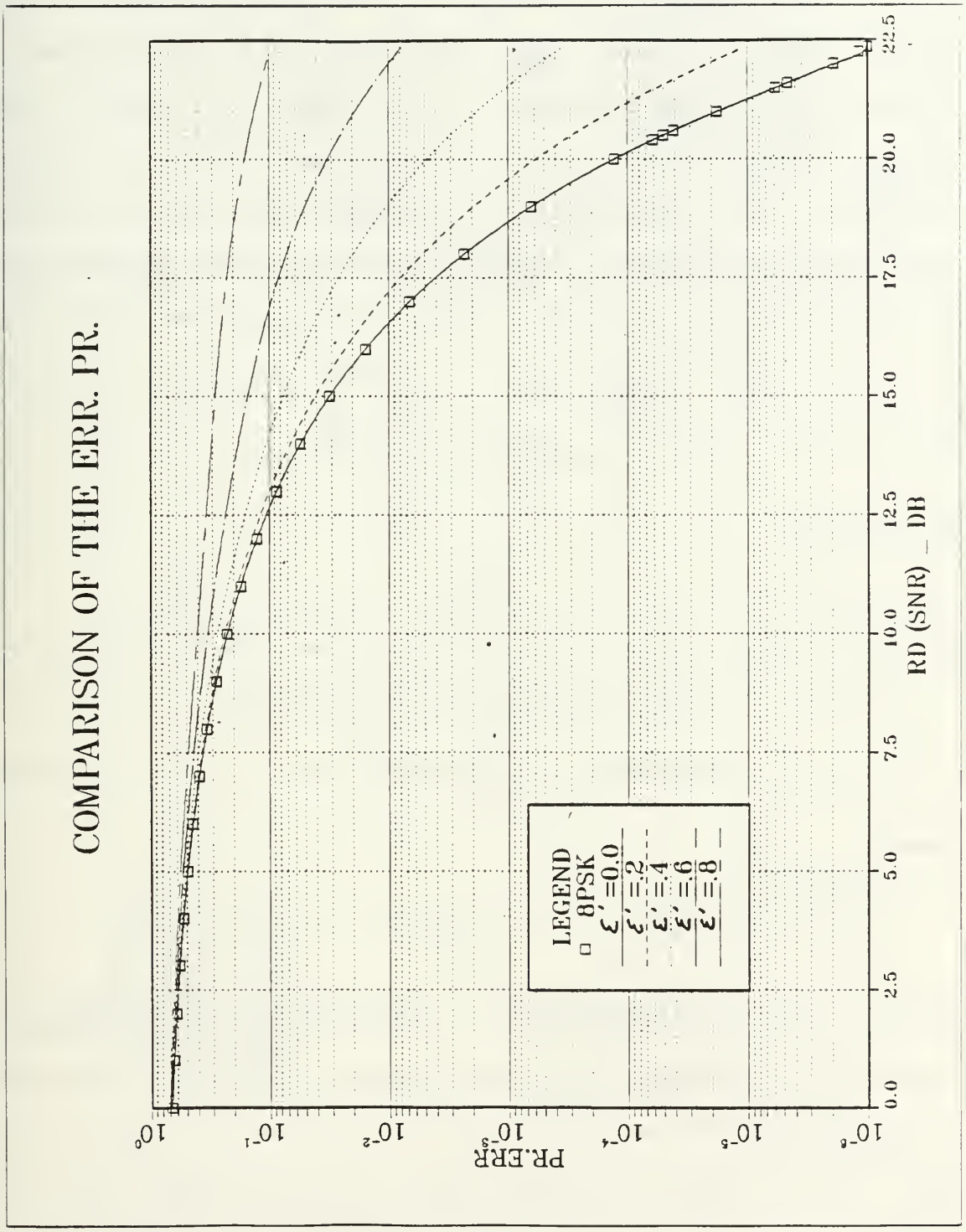

Figure 2.18. Comparision of Pr{ε} Performance for Multi Amplitude MPSK Systems MOD.1

2. Modification 2.

The decision regions of the signal constellation illustrated in Figure 2.9 are modified as illustrated in Figure 2.19. The parameter Δ controls the size of the decision regions to some extent and can be set as a design parameter to be optimized for minimum probability of error. The decision regions can be redrawn in order to determine The probability of making correct decisions given that $s_1(t)$ or $s_2(t)$ were transmitted. This is illustated in Figure 2.20. From Figure 2.20(a) we can determine $Pr\{c/s_2(t)\}$ by evaluating

$$Pr\{c/s_2(t)\} = Pr\{ N_1 \geq -\Delta \frac{R_2}{(2)^{1/2}} , N_2 \geq -\Delta \frac{R_2}{(2)^{1/2}} \}$$

$$= [erfc^*(-\Delta \frac{H}{(2)^{1/2}})]^2 \qquad (2.81)$$

where

$$H = \frac{R_2}{(N_0/2)^{1/2}} .$$

Referring back to Equation 2.40 and the discussion preceding that equation, we can expect a similar result here for $Pr\{c/s_1(t)\}$. Comparing Figure 2.20(b) with Figure 2.4(b) the similarities are obvious while the differences are only the parameters, A, R_1, etc. Thus,

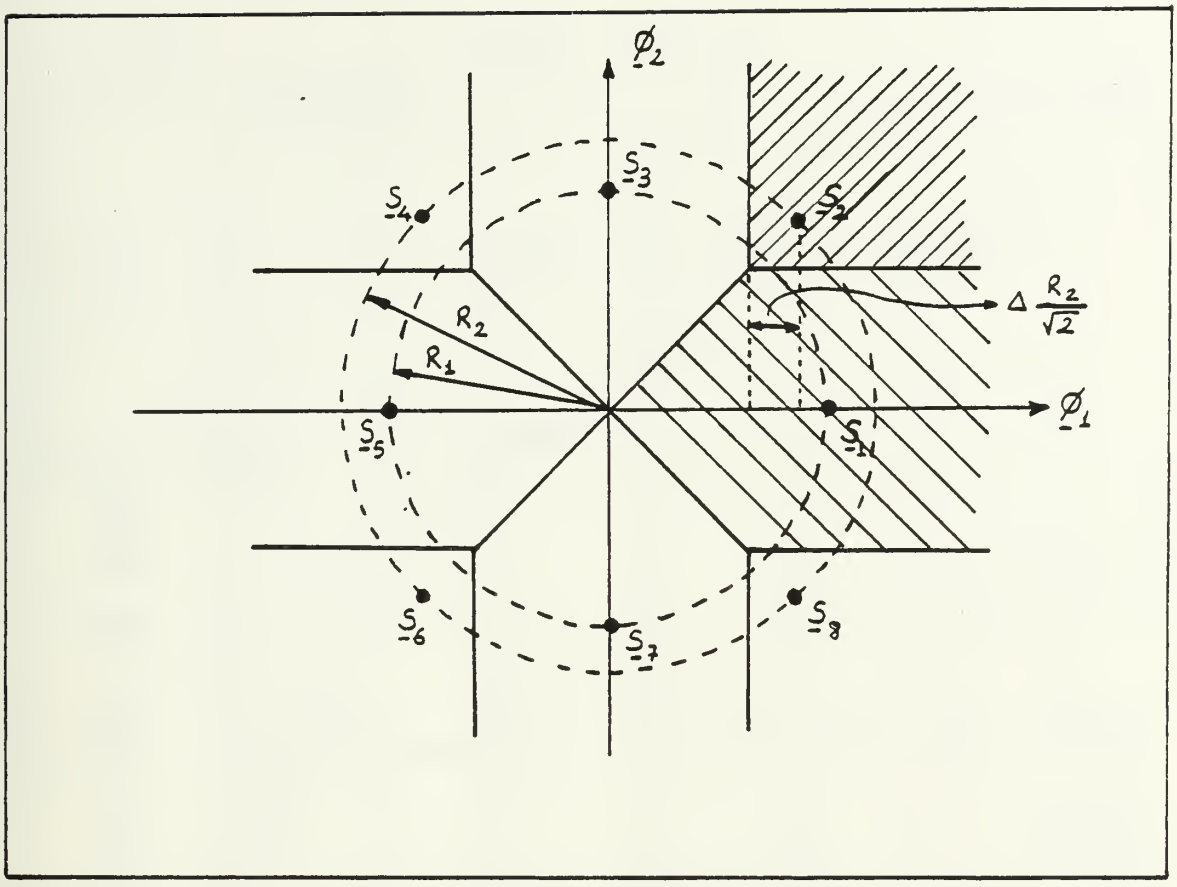

Figure 2.19. Signal-Space Diagram and Decision Regions for Multi Amplitude MPSK MOD.2

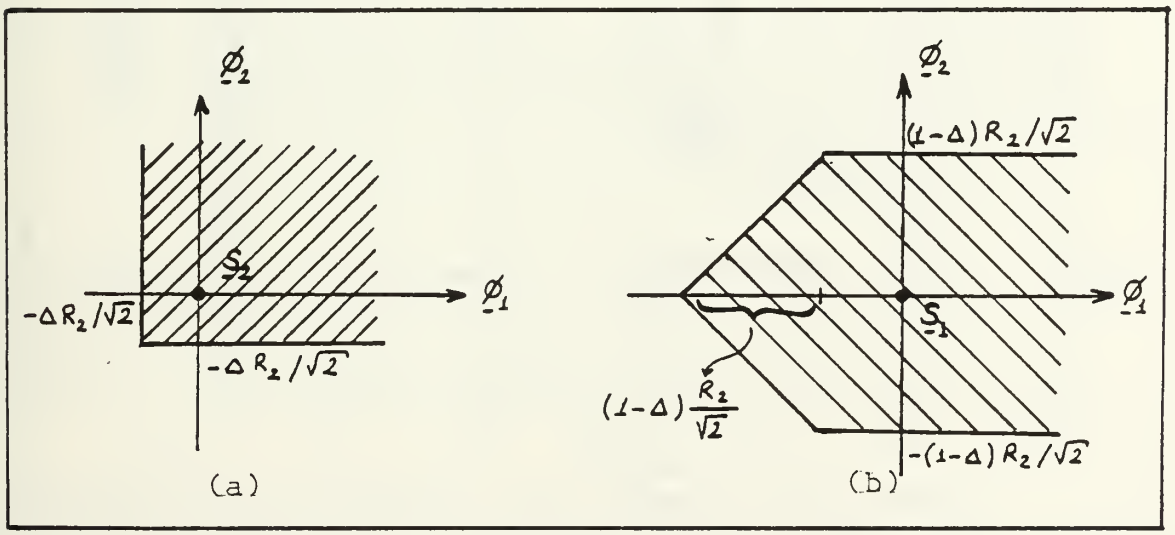

Figure 2.20. Transformed Decision Regions for MOD.2

$$\Pr\{c/s_i(t)\} = \int_{-D}^{-D+(1-\Delta)\frac{H}{(2)^{1/2}}} \frac{1}{(2\pi)^{1/2}} e^{-y^2/2}$$

$$[1-2\ \mathrm{erfc}^*(y+D)]\,dy + \mathrm{erfc}^*\left(-D + (1-\Delta)\frac{H}{(2)^{1/2}}\right)$$

$$\left[1-2\ \mathrm{erfc}^*\left((1-\Delta)\frac{H}{(2)^{1/2}}\right)\right] \qquad (2.82)$$

and finally

$$\Pr\{c\} = \frac{1}{8}\left[4\ \Pr\{c/s_2(t)\} + 4\ \Pr\{c/s_1(t)\}\right] \qquad (2.83)$$

so that

$$\Pr\{\varepsilon\} = 1 - \frac{1}{2}\left\{\left[\mathrm{erfc}^*\left(-\Delta\frac{H}{(2)^{1/2}}\right)\right]^2 + \int_{-D}^{-D+(1-\Delta)(H/(2)^{1/2})} \frac{1}{(2\pi)^{1/2}} e^{-y^2/2}\,[1-2\ \mathrm{erfc}^*(y+D)]\,dy + \mathrm{erfc}^*\left(-D+(1-\Delta)\frac{H}{(2)^{1/2}}\right)\left[1-2\ \mathrm{erfc}^*\left((1-\Delta)\frac{H}{(2)^{1/2}}\right)\right]\right\}. \qquad (2.84)$$

Figures 2.21 through 2.27 illustrate the performance of the receiver as the parameter Δ changes for various

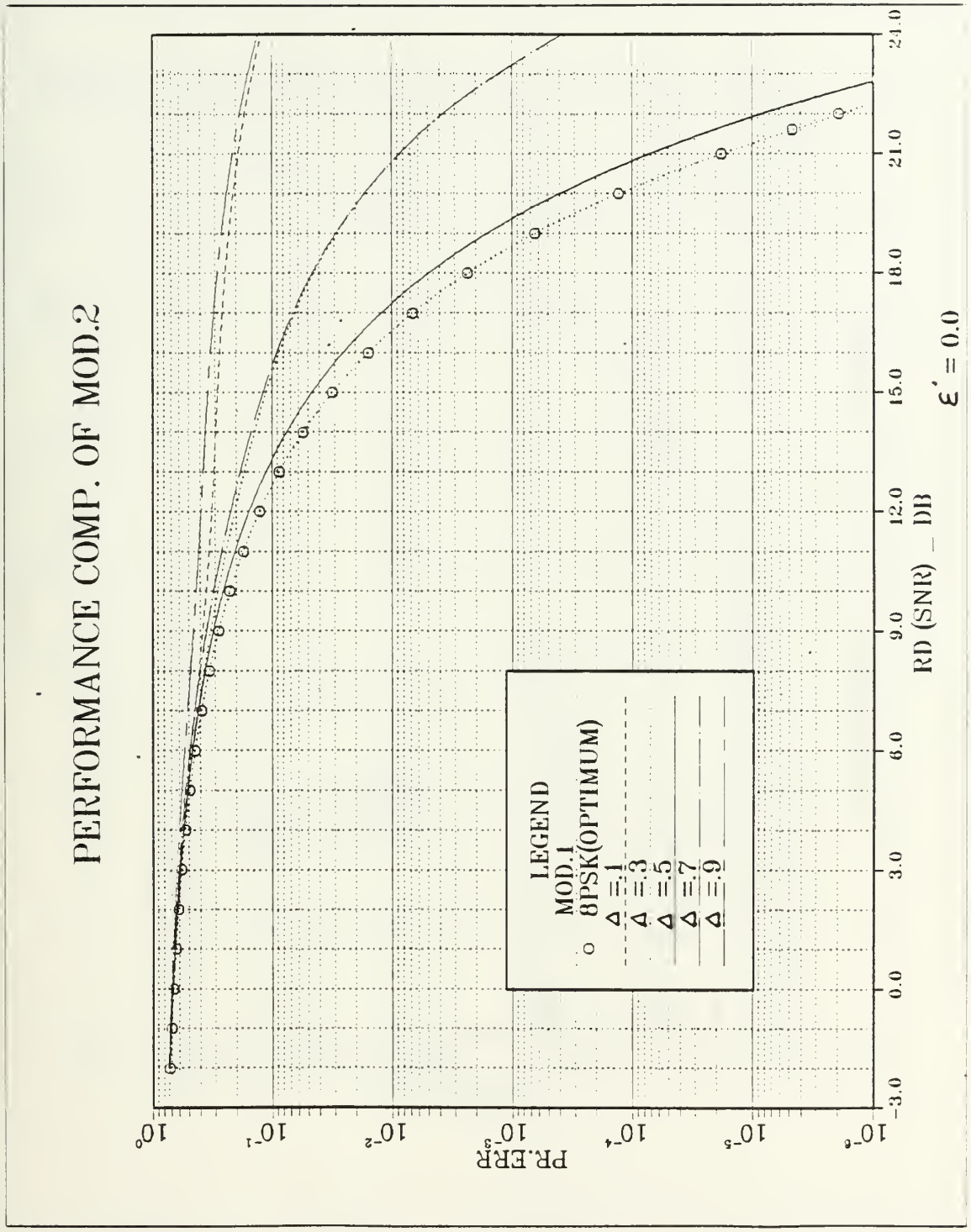

Figure 2.21. Comparison of Pr{ε} Performance for MOD.2 ($\varepsilon' = 0.0$)

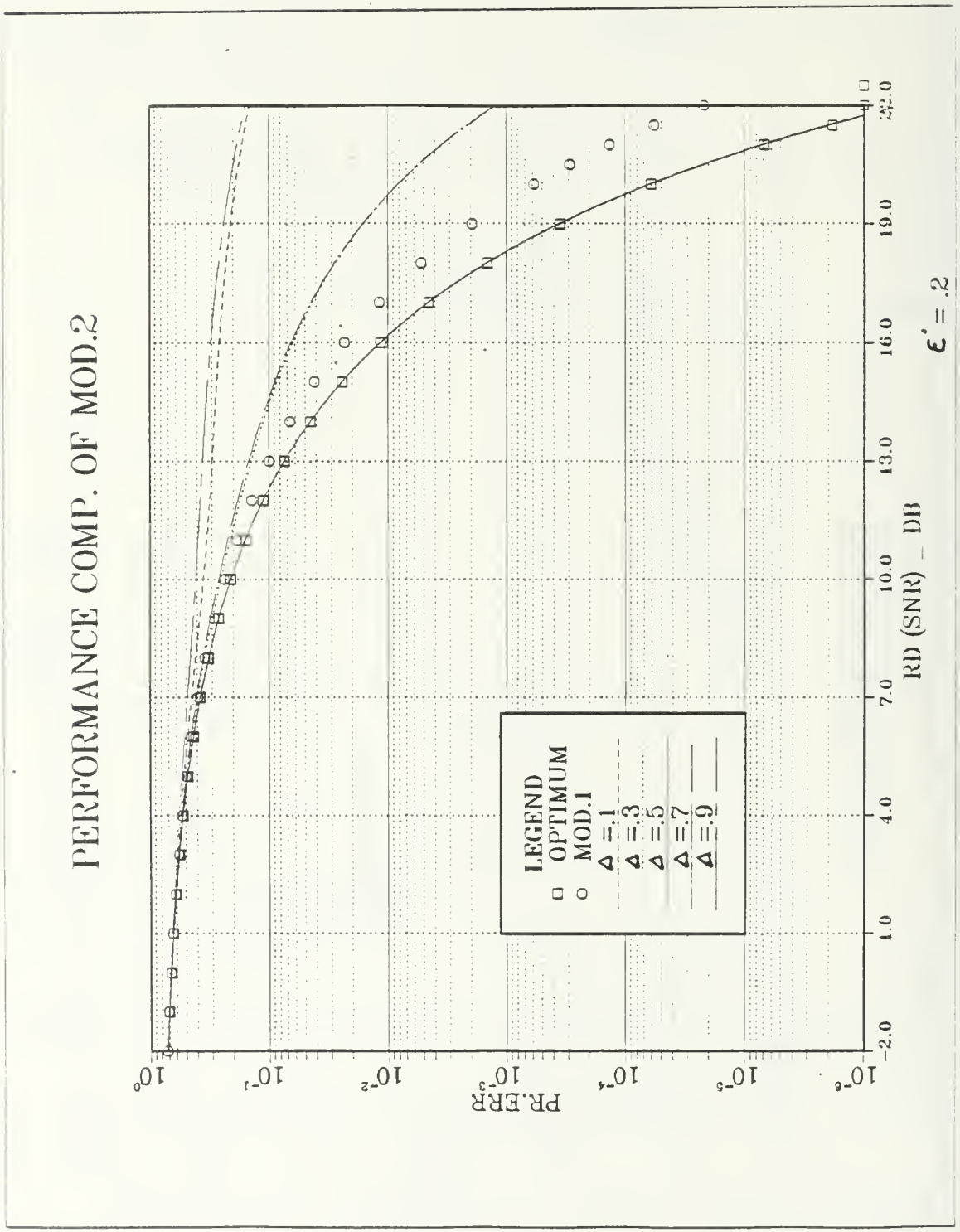

Figure 2.22. Comparison of Pr{ε} Performance for MOD.2 (ε' = 0.2)

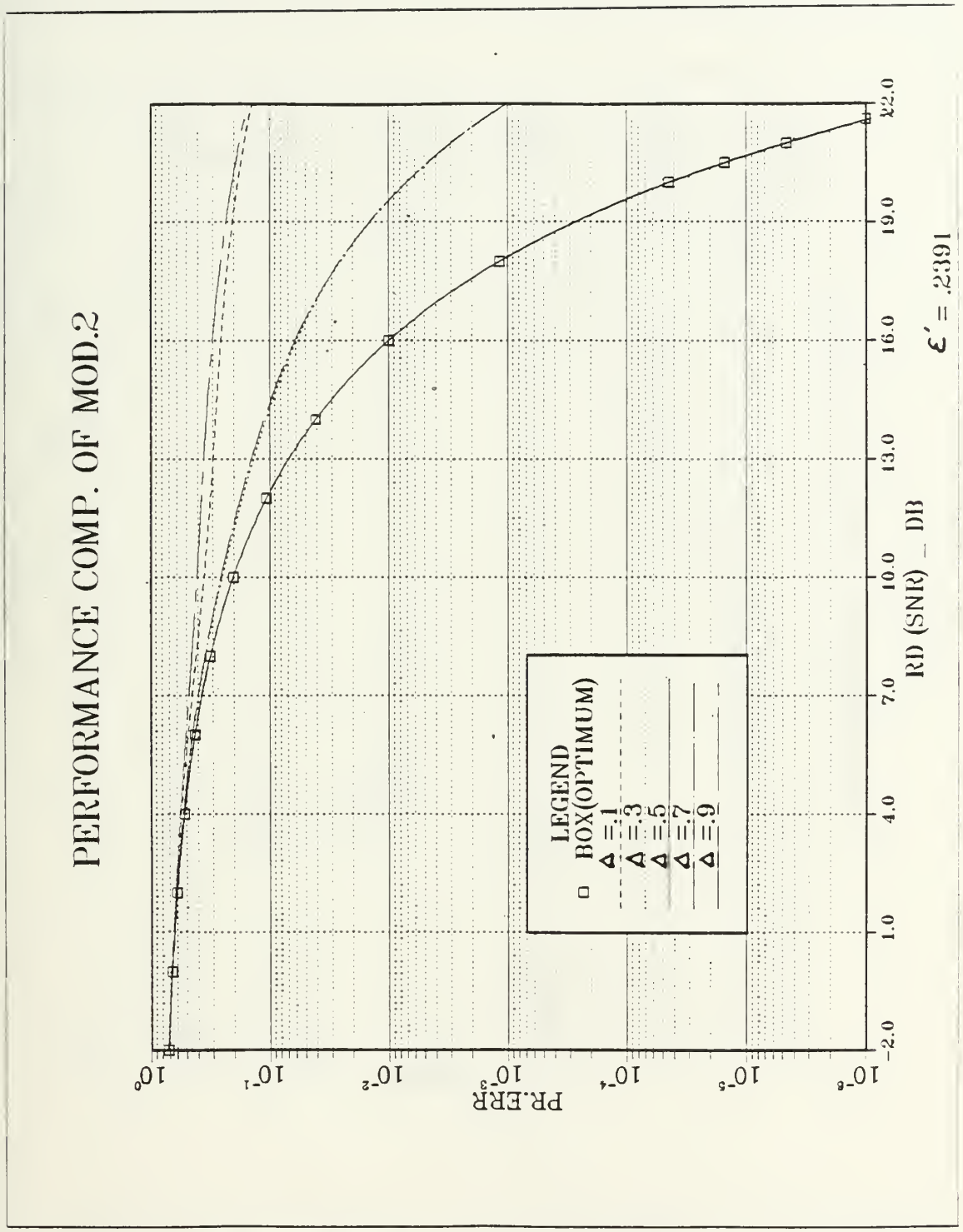

Figure 2.23. Comparison of Pr{ε} Performance for MOD.2 (ε' = 0.2391)

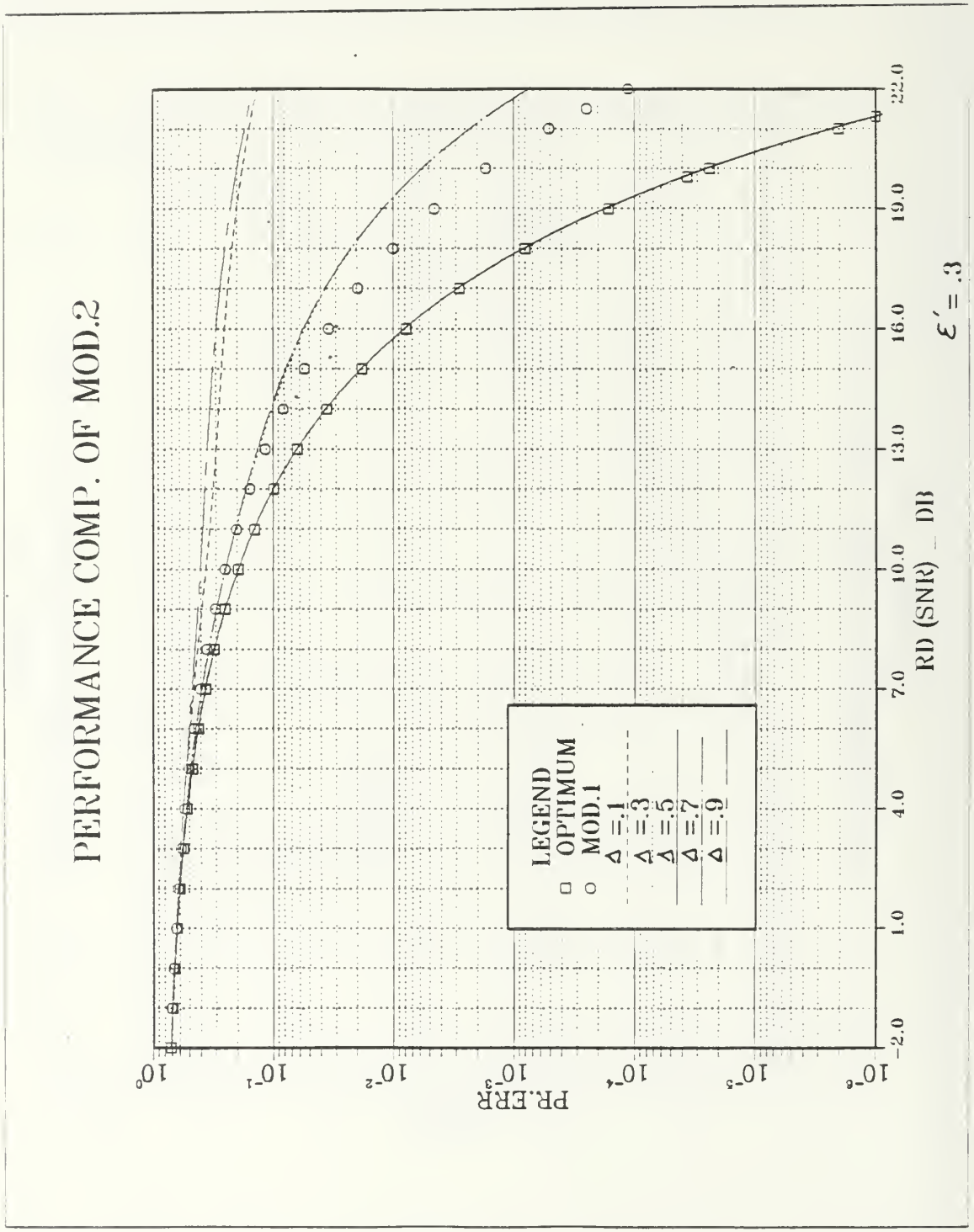

Figure 2.24. Comparison of Pr{ε} Performance for MOD.2 (ε′ = 0.3)

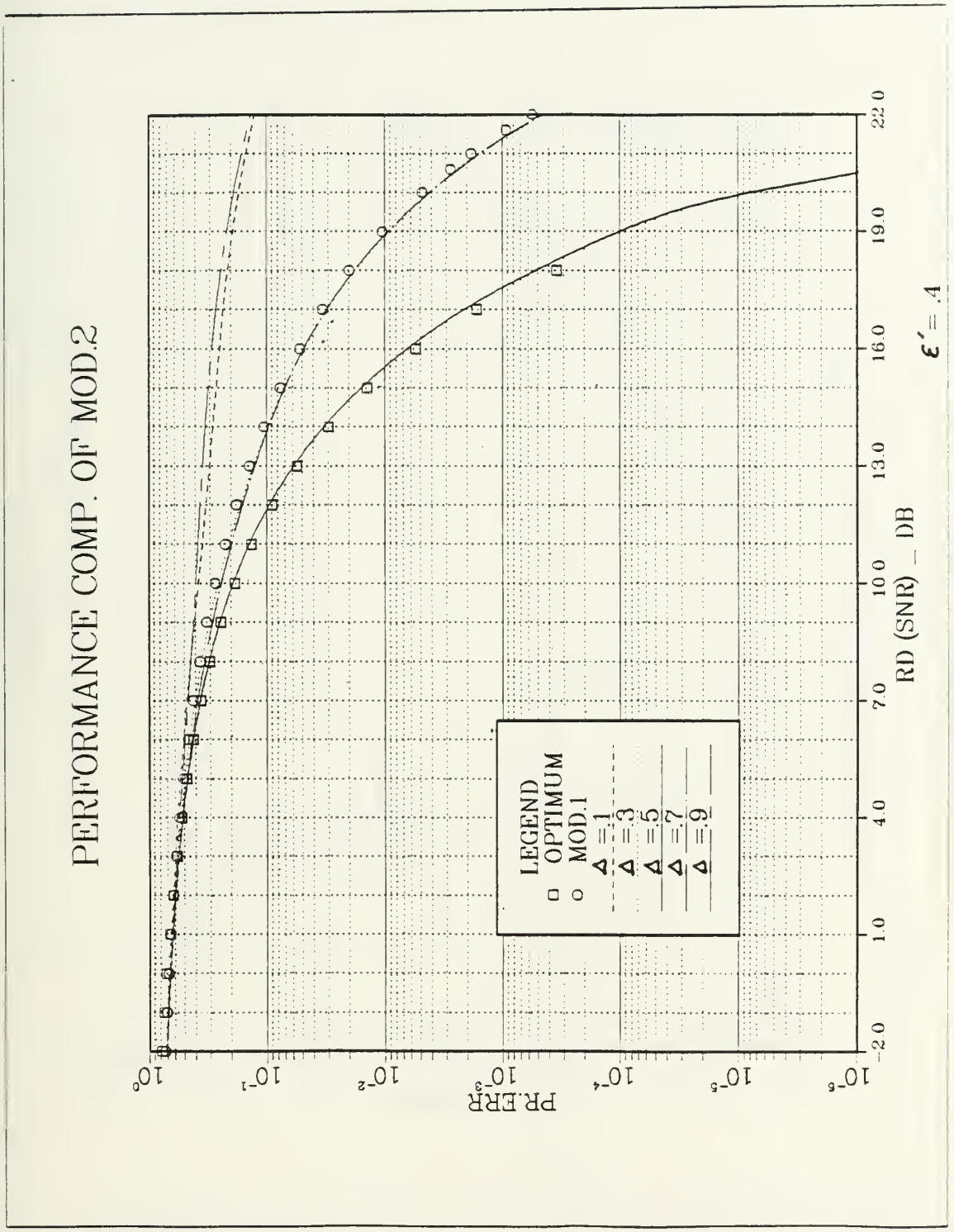

Figure 2.25. Comparison of Pr{ε} Performance for MOD.2 ($\varepsilon' = 0.4$)

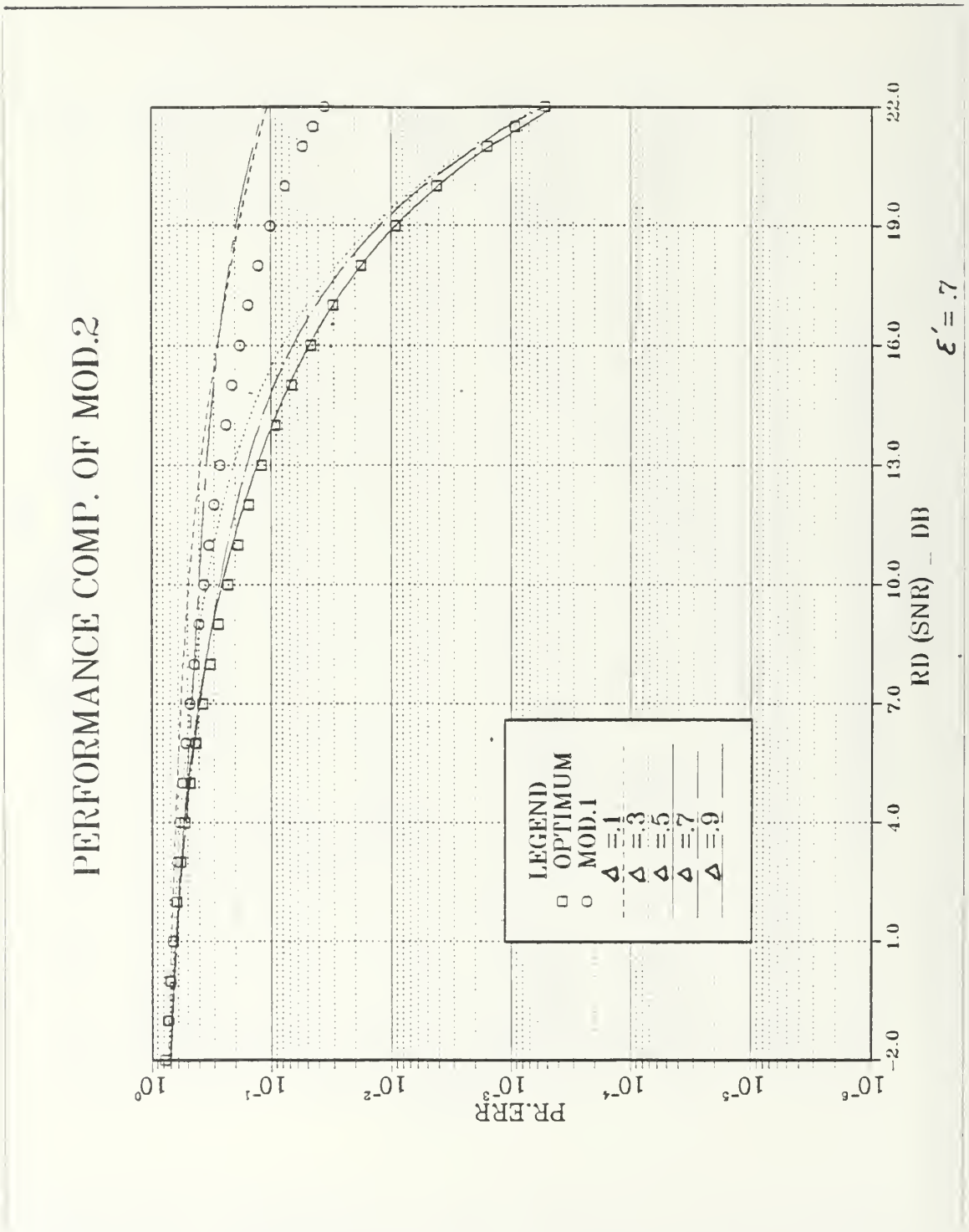

Figure 2.26. Comparison of Pr(ε) Performance for MOD.2 (ε′ = 0.7)

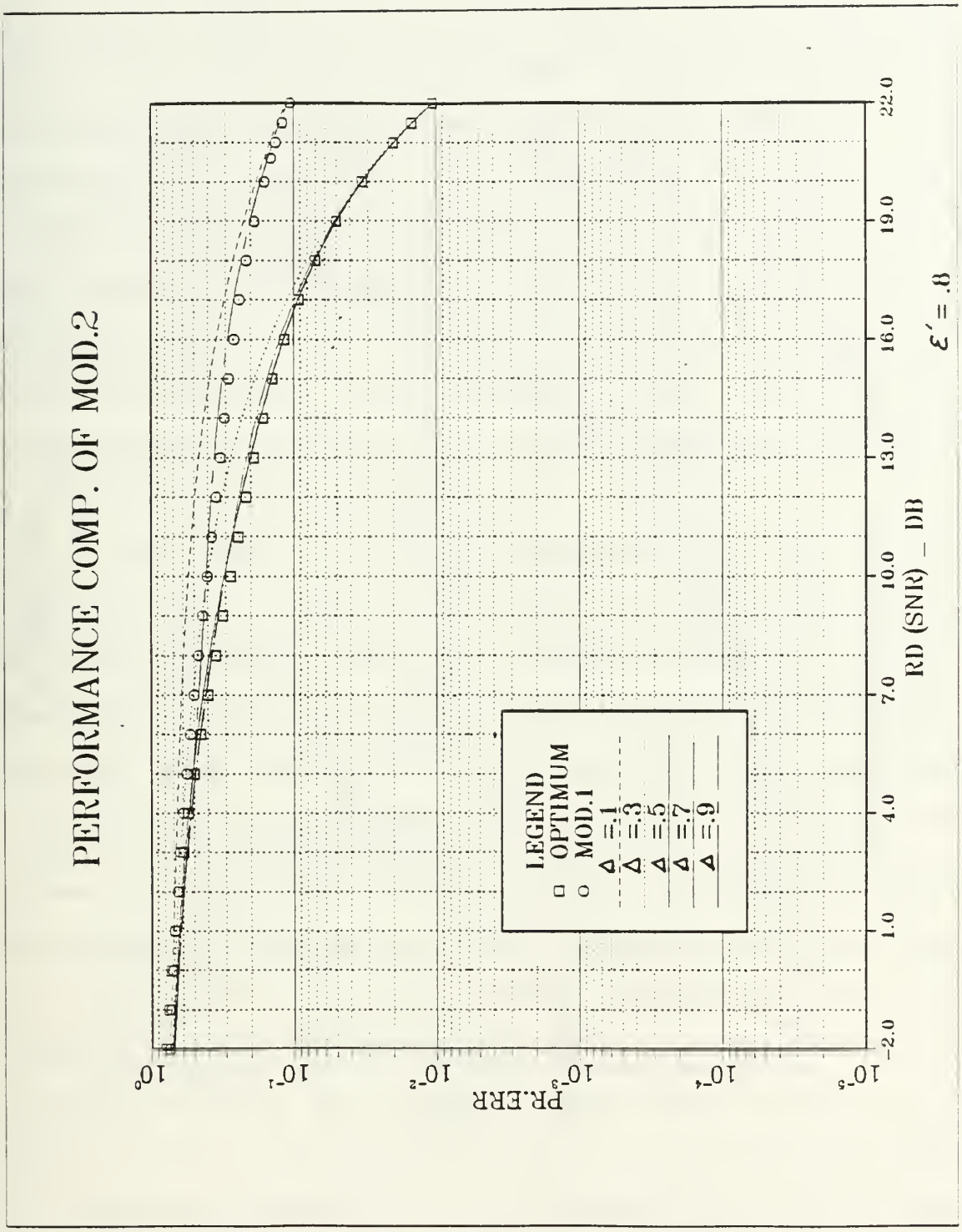

Figure 2.27. Comparison of Pr(ε) Performance for MOD.2 (ε′ = 0.8)

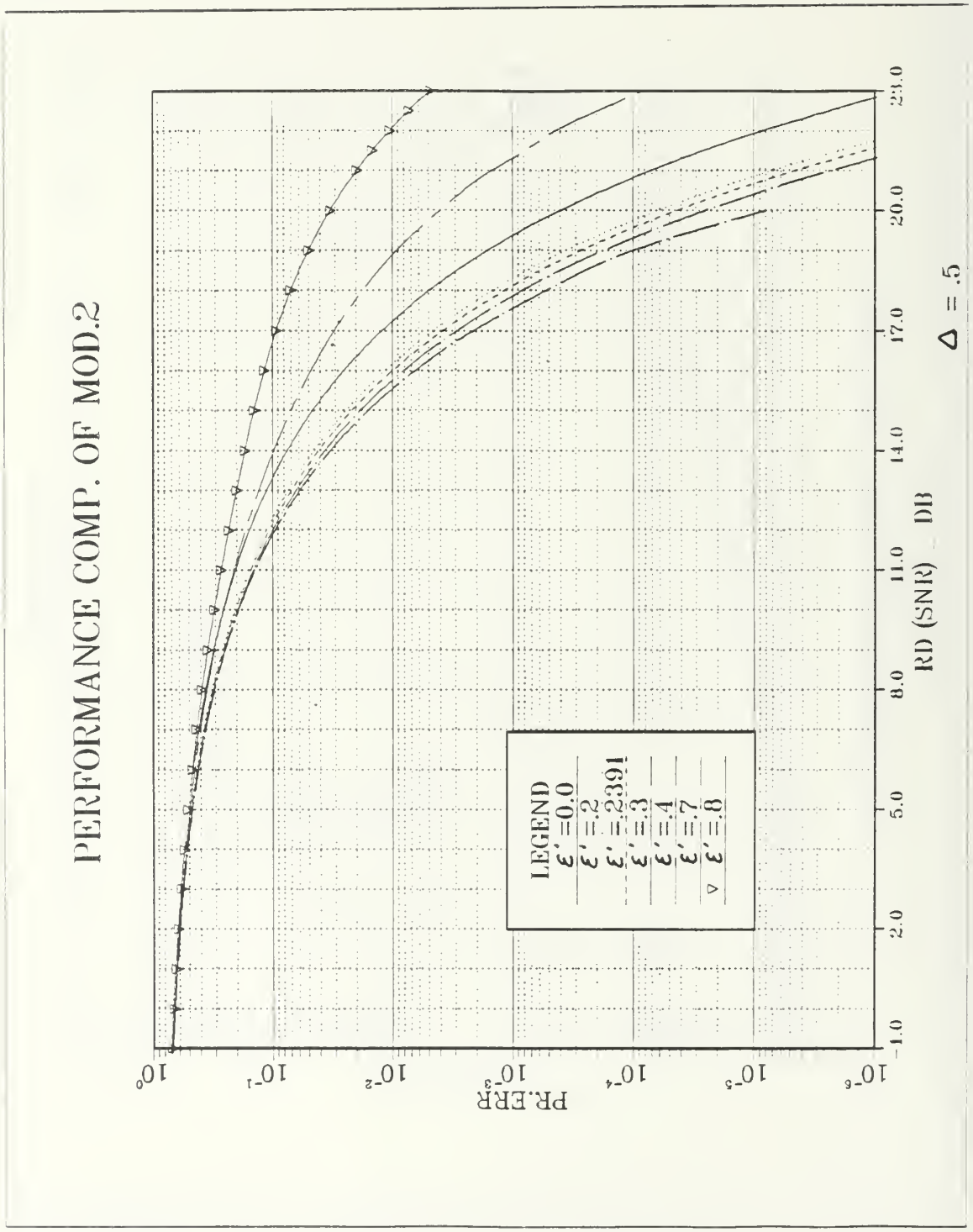

Figure 2.28. Comparison of Pr{ε} Performance for MOD.2 (Δ = 0.5)

values of the parameter ε' and Rd. Setting Δ = .5 when ε' = .2391 results in a performance similar to that encountered for the so called "Box" signal set. This can be confirmed by observing the plots in Figure 2.23. For purposes of comparison, the performance of the optimum receivers discussed in Section D is plotted along side the performance of the modified receiver discussed in the previous section, as shown in Figures 2.21 to 2.27. The results demonstrate that the suboptimum receiver using simple decision regions based on phase measurements exhibits a significant loss in performance.

For the modification discussed in this section however, when Δ takes on the value of 0.5, the performance of the (suboptimum) receiver is almost identical to that of the optimum receiver. Figure 2.21 shows that the suboptimum receiver with rectangular decision regions (for Δ=0.5 and ε'=0.0) requires 0.5 dB more SNR than the conventional 8-PSK scheme in order to achieve an error probability of 10^{-6}. The suboptimum receiver utilizing the decision regions shown in Figure 2.16, exhibits better performance than the suboptimum receiver utilizing the decision regions shown in Figure 2.19 when $\Delta \neq 0.5$ for values of ε' up to ε'= 0.4. Figure 2.25 illustrates that when ε'= 0.4, the performance of suboptimum receiver utilizing the decision regions shown in Figure 2.16 is almost identical to that of the suboptimum

receiver utilizing the decision regions shown in Figure 2.19 for Δ=0.3 and 0.7. The former suboptimum receiver exhibits degraded performance in comparison to that of the latter suboptimum receiver for Δ=0.3 and 0.7 as ε' increases beyond the value of 0.4 as can be verified from Figures 2.26 and 2.27. It can be observed from Figure 2.27 that for ε'=.8 the performance of the receiver analyzed in this section is approximately similar to that of the optimum receiver for Δ = 0.3, 0.5, and 0.7. Figure 2.28 presents plots of Pr{ε} for various values of ε' when Δ = 0.5.

F. PERFORMANCE ANALYSIS OF QPSK AND (4+1)PSK.

In this section, a modification of the well-known QPSK signaling scheme is presented and its performance evaluated. Figure 2.29 shows the signal-space diagram of the QPSK scheme, and the optimum decision regions. Evaluation of $Pr\{c/s_1(t)\}$ can be accomplished by analyzing Figure 2.29 and observing that

$$Pr\{c/s_1(t)\} = Pr\{ N_1 \geq -(E/2)^{1/2} \ , \ N_2 \geq -(E/2)^{1/2} \}$$

$$= \left[\int_{-(E/2)^{1/2}}^{\infty} \frac{1}{(2\pi)^{1/2}} e^{-y^2/2} \right]^2 dy$$

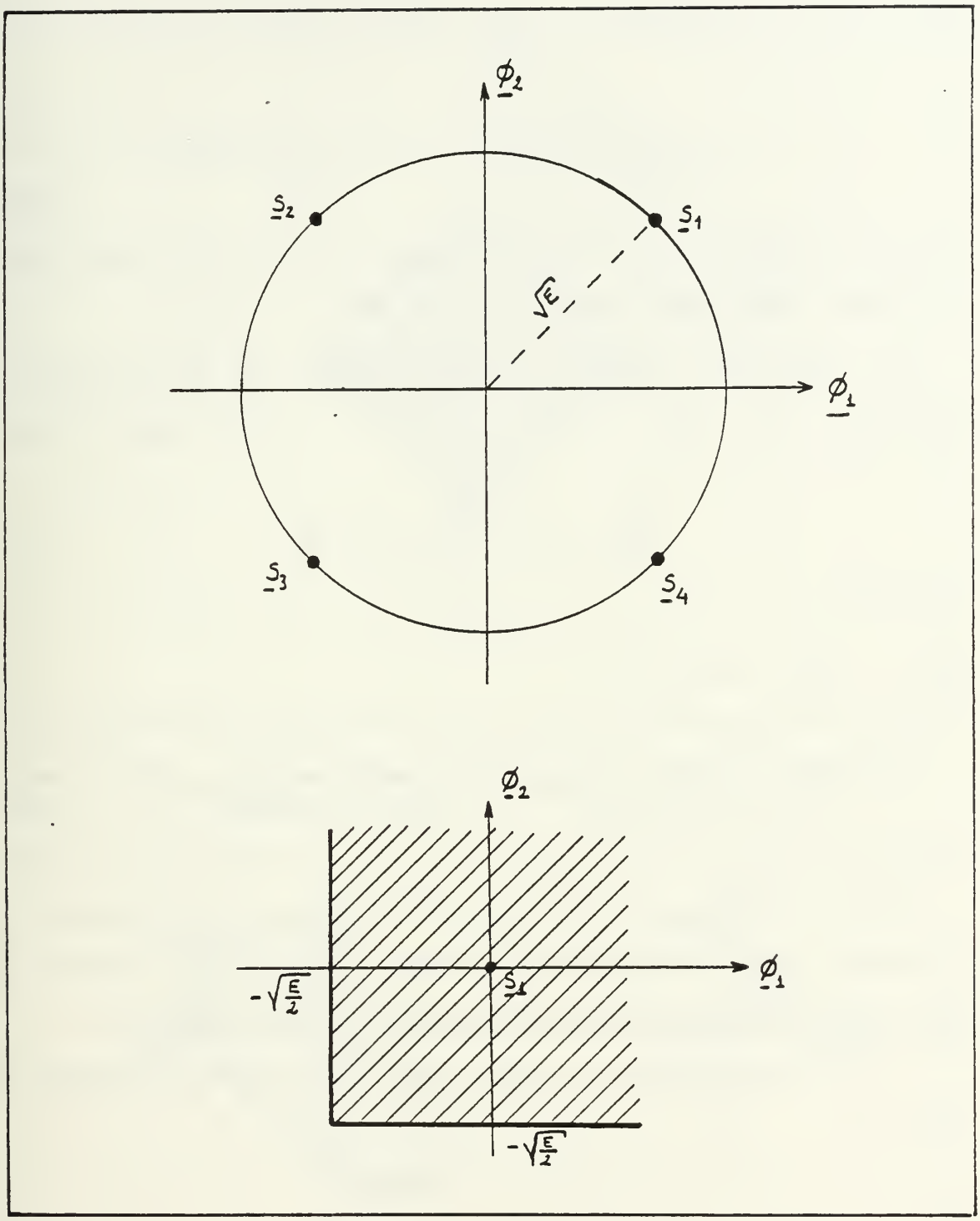

Figure 2.29. Signal-Space Diagram and Decision Regions for QPSK Modulation

$$= [\ \mathrm{erfc}^*(-(Rd / 2)^{1/2})\ ]^2$$

$$= 1-2\ \mathrm{erfc}^*((Rd/2)^{1/2}) + [\ \mathrm{erfc}^*(Rd/2)^{1/2}\ ]^2 \qquad (2.85)$$

in which several appropriate variable changes have been used to obtain the final form of $Pr\{c/s_1(t)\}$.

As noticed earlier, the symmetry of the decision regions, and equal prior probability of each signal result in

$$Pr\{ c \} = Pr\{ c / s_1(t) \}$$

so that

$$Pr\{ \varepsilon \} \overset{\Delta}{=} 1 - Pr\{ c \}$$

$$= 2\ \mathrm{erfc}^*((Rd/2)^{1/2}) - [\ \mathrm{erfc}^*((Rd/2)^{1/2})]^2 \qquad (2.86)$$

Now, a modification to the QPSK scheme is introduced by allowing the presence of one more signal at the center of the signal space diagram, as shown in Figure 2.30.

The average energy of the signal set can be expressed as follows

$$E = \frac{1}{5}\ [\ 4\ R^2 + 0\ ] = \frac{4R^2}{5} \qquad (2.87)$$

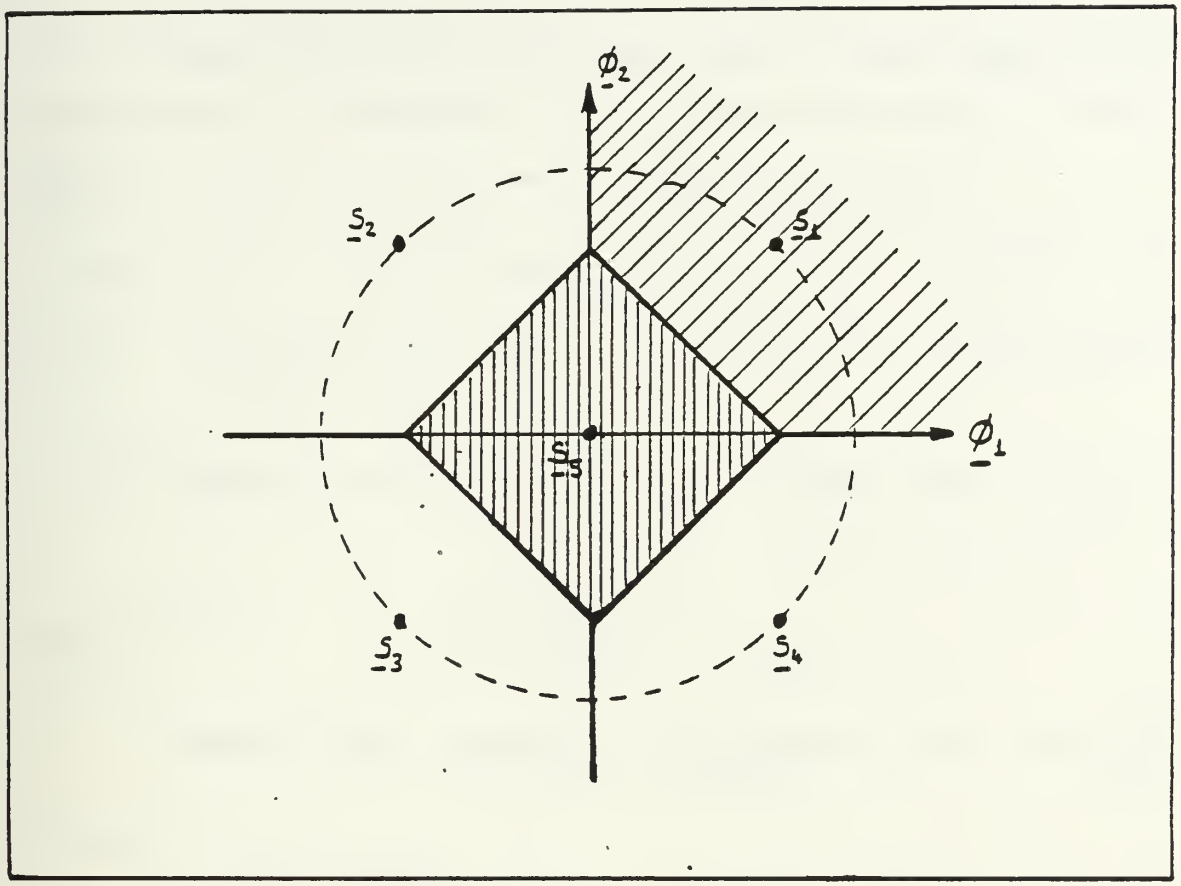

Figure 2.30. Signal-Space Diagram and Decision Regions for (4+1) PSK

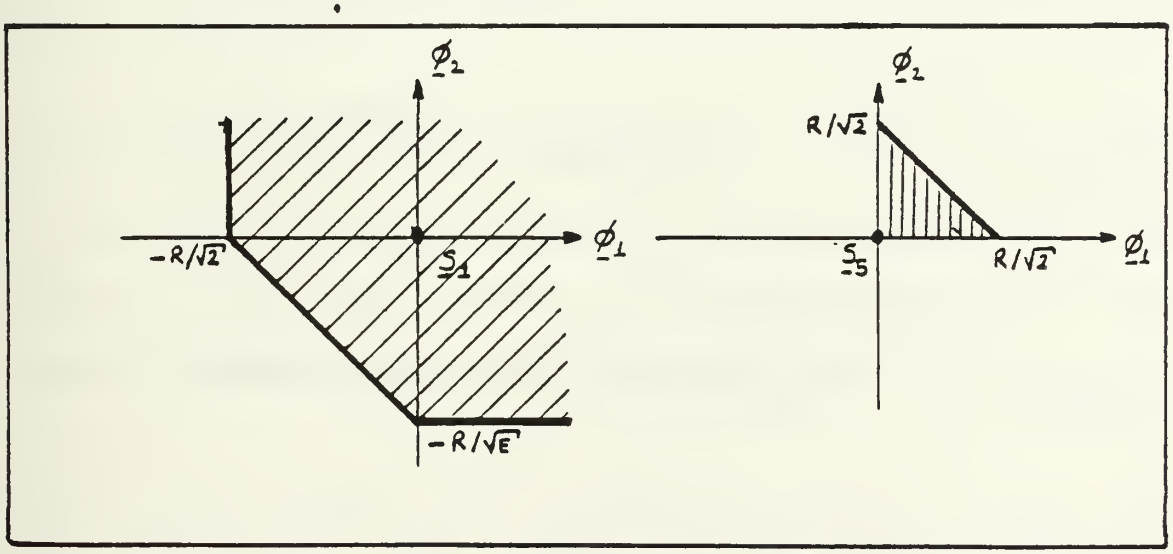

Figure 2.31. Transformed Decision Regions for (4+1) PSK

so that the radius R can be written in term of E as

$$R = (5E / 4)^{1/2} \qquad (2.88)$$

The decision region for the signal $\underline{s}_1$ is illustrated in Figure 2.31(a), so that

$$Pr\{c/s_1(t)\}=Pr\{-(R/(2)^{1/2}) \leqslant N_1 \leqslant 0 \ , \ N_2 \geqslant -(N_1+(R/(2)^{1/2}))\}$$

$$+ Pr\{ N_1 \geqslant 0 \ , \ - \frac{R}{(2)^{1/2}} \leqslant N_2\} \qquad (2.89)$$

The first joint probability in Equation 2.84 becomes

$$\left\{ \int_{-(R/(2)^{1/2})}^{0} \frac{1}{(2\pi N_0/2)^{1/2}} e^{-n_1^2/2(N_0/2)} \right.$$

$$\left. \int_{-(n_1+R/(2)^{1/2})}^{\infty} \frac{1}{(2\pi N_0/2)^{1/2}} e^{-n_2^2/2(N_0/2)} \right\} dn_2\, dn_1 =$$

$$= -(5Rd/8)^{1/2} \int_{}^{0} \frac{1}{(2\pi)^{1/2}} e^{-y^2/2}[1- erfc*(y+(5Rd/8)^{1/2})]dy$$

(2.90)

where the variable change $\frac{n_1}{(N_0/2)^{1/2}} \overset{\Delta}{=} y$ and $R=(5E/4)^{1/2}$

have been used to obtain Equation 2.90. The second joint probability in Equation 2.85 can be expressed by using a similar change of variables in the following form:

$$\left\{ \int_0^{\infty} \frac{1}{(2\pi N_0/2)^{1/2}} e^{-n_1^2/2(N_0/2)} \right.$$

$$\left. \int_{-R/(2)^{1/2}}^{\infty} \frac{1}{(2\pi N_0/2)^{1/2}} e^{-n_2^2/2(N_0/2)} \right\} dn_2\, dn_1 =$$

$$= -\frac{1}{2} - \text{erfc}^*(-(5Rd/8)^{1/2}). \qquad (2.91)$$

Finally,

$$\Pr\{c/s_i(t)\} = \int_{-(5Rd/8)^{1/2}}^{0} \frac{1}{(2\pi)^{1/2}} e^{-y^2/2} [1-\text{erfc}^*(y+(5Rd/8)^{1/2})]dy$$

$$+ -\frac{1}{2} - \text{erfc}^*(-(5Rd/8)^{1/2}). \qquad (2.92)$$

As can be seen in Figure 2.30, the decision region of signal $\underline{s}_5$ is the inside of the square shown. Due to the symmetry of the decision region we see that

$$\Pr\{c/s_5(t)\} = 4\,\Pr\{0 \leq N_1 \leq \frac{R}{(2)^{1/2}},\ 0 \leq N_2 \leq -N_1 + \frac{R}{(2)^{1/2}}\} =$$

$$= 4 \int_{0}^{(5Rd/8)^{1/2}} \frac{1}{(2\pi)^{1/2}} e^{-y^2/2} \left[-\frac{1}{2} - \text{erfc}^*(-y+(5RD/8)^{1/2}) \right] dy \qquad (2.93)$$

so that

$$\Pr\{\varepsilon\} = 1 - \frac{1}{5} \left[4\Pr\{c/s_1(t)\} + \Pr\{c/s_5(t)\} \right] \qquad (2.94)$$

or equivalently

$$\Pr\{\varepsilon\} = 1 - \frac{4}{5} \left\{ \int_{-d}^{0} \frac{1}{(2\pi)^{1/2}} e^{-y^2/2} \left[1 - \text{erfc}^*(y+d) \right] dy + \right.$$

$$\left. -\frac{1}{2} \text{erfc}^*(-d) + \int_{0}^{d} \frac{1}{(2\pi)^{1/2}} e^{-y^2/2} \left[-\frac{1}{2} - \text{erfc}^*(-y+d) \right] dy \right\} \qquad (2.95)$$

where $d \triangleq (5Rd/8)^{1/2}$.

The performance for the QPSK and the modified QPSK scheme is plotted in Figure 2.32. The $\Pr\{\varepsilon\}$ degradation associated with the modified scheme for a given SNR (Rd), or equivalently the increase in the SNR required in order to maintain a specified $\Pr\{\varepsilon\}$ is caused by the modified scheme having a smaller regions of correct decisions. This can be seen by comparison of the decision regions shown in Figures 2.29 and 2.31(a). We also note that the increase in SNR required to maintain a specified $\Pr\{\varepsilon\}$ becomes smaller for

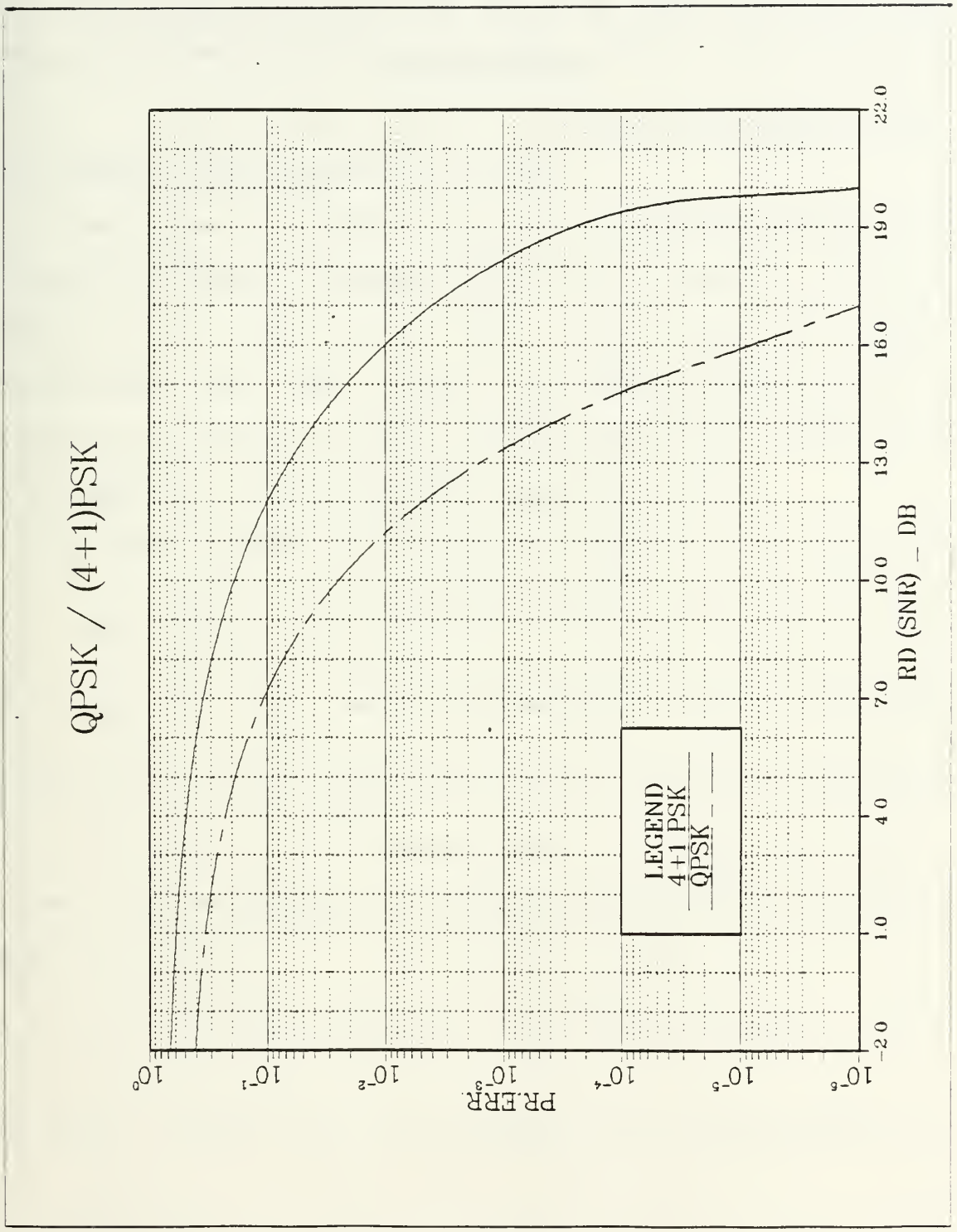

Figure 2.32. Comparison Pr(ε) Performance for QPSK and (4+1) PSK

$Pr\{\varepsilon\} < 10^{-4}$. The modified signaling scheme requires approximately 5.25 dB more SNR than the QPSK in order to achieve $Pr\{\varepsilon\} = 10^{-4}$, while only 3 dB more SNR is required to maintain $Pr\{\varepsilon\} = 10^{-6}$.

III. PERFORMANCE ANALYSIS OF QADRATURE AMPLITUDE MODULATED (QAM) SYSTEMS

A. RECEIVER PERFORMANCE FOR 16-QAM

The signal constellation of the Quadrature Amplitude Modulated signaling scheme involving 16 signals is shown in Figure 3.1 along with the optimum decision regions associated with each signal provided once again that the signals are equally likely to be transmitted and that they are received in additive white Gausssian noise.

As can be seen in Figure 3.1, signals $\underline{s}_1$, $\underline{s}_3$, $\underline{s}_{11}$, and $\underline{s}_9$, each have energy $(3A)^2 + (3A)^2 = 18A^2$, while signals $\underline{s}_6$, $\underline{s}_8$, $\underline{s}_{16}$, $\underline{s}_{14}$, each have energy $A^2 + A^2 = 2A^2$. Finally signals $\underline{s}_2$, $\underline{s}_4$, $\underline{s}_7$, $\underline{s}_{15}$, $\underline{s}_{12}$, $\underline{s}_{10}$, $\underline{s}_{13}$, $\underline{s}_5$ each have energy $(3A)^2 + A^2 = 10A^2$. Assuming that all signals are equally likely to be transmitted, the average energy of the signal set is

$$E = 1/16 \left[4(18A^2) + 4(2A^2) + 8(10A^2) \right] = 10A^2 \qquad (3.1)$$

so that in terms of E, the parameter A can be expressed as

$$A = (E / 10)^{1/2} \qquad (3.2)$$

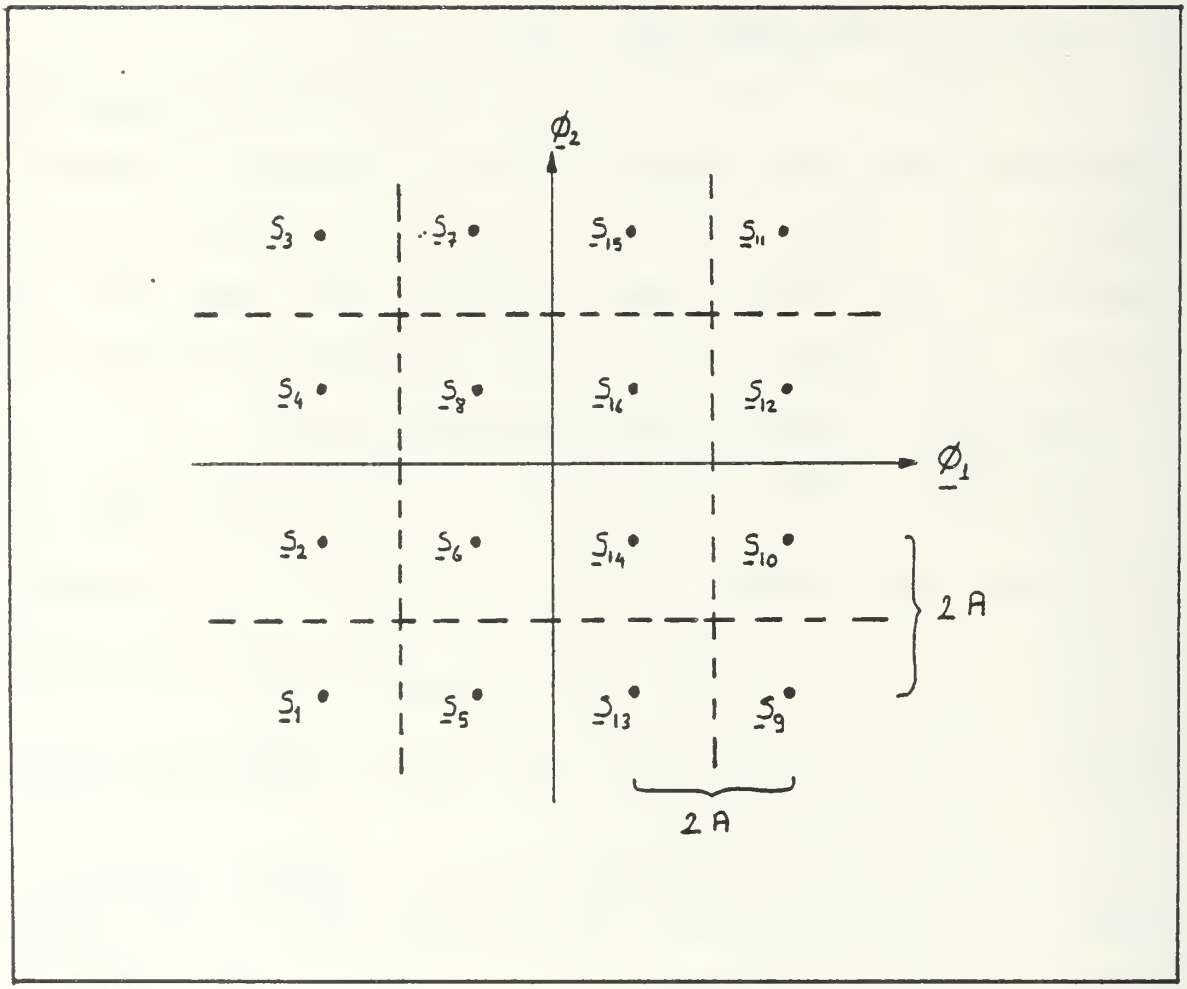

Figure 3.1. Signal Constellation and Decision Regions for 16-QAM

The decision region associated with the determination of the probability of correct decision given that signals $\underline{s}_1$, $\underline{s}_3$, $\underline{s}_9$ or $\underline{s}_{11}$ were transmitted is illustrated in Figure 3.2(a). From Figure 3.2(a) $Pr\{c/\ s_{11}(t)\}$ can be calculated

$$Pr\{C\ /\ s(t)\} = Pr\{-A \leqslant N_1\ ,\ -A < N_2\}$$

$$= \left[\int_{-A}^{\infty} \frac{1}{(2\pi\ N_0/2)^{1/2}} \exp\{-n_1^2\ /2(N_0/2)\}\ dn_1 \right]^2$$

$$= \left[\text{erfc}^*\left(- \frac{A}{(N_0/2)^{1/2}} \right) \right]^2 . \qquad (3.3)$$

Equation 3.3 has been simplified to its final form due to the fact that N_1 and N_2 are statistically independent, zero mean, $N_0/2$ variance Gaussian random variables.

Figure 3.2(b) shows the decision region associated with the determination of the probability of correct decision given that the signals $\underline{s}_6$, $\underline{s}_8$, $\underline{s}_{16}$ and $\underline{s}_{14}$ were transmitted. It can be seen that

$$Pr\{c/s_{16}(t)\} = Pr\{-A \leqslant N_1 \leqslant A\ ,\ -A \leqslant N_2 \leqslant A\}$$

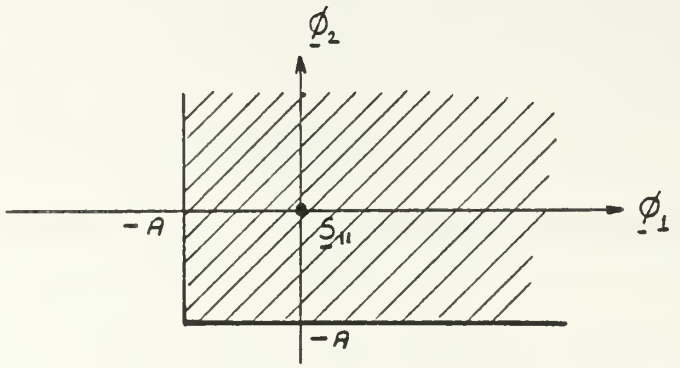

(a) Type I

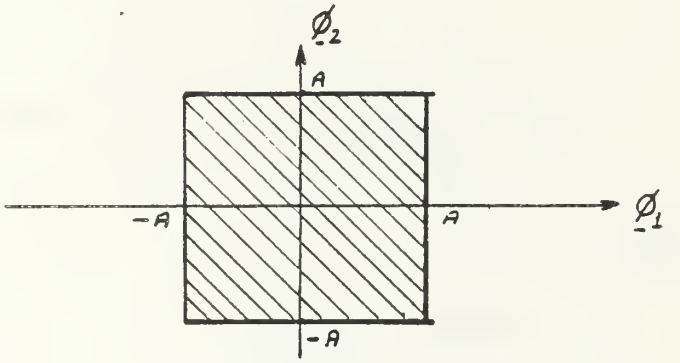

(b) Type II

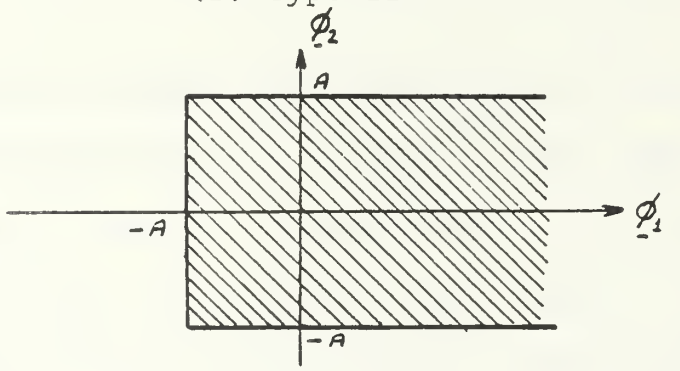

(c) Type III

Figure 3.2. Transformed Decision Regions for 16-QAM

$$= 4 \Pr\{-A \leq N_1 \leq A \ , \ -A \leq N_2 \leq A \}$$

$$= 4 \left[\int_0^A \frac{1}{(2\pi N_0/2)^{1/2}} e^{-n_1^2/2N_0/2} \, dn_1 \right]^2$$

$$= 4 \left[\frac{1}{2} - \text{erfc}^*(A/(N_0/2)^{1/2}) \right]^2 . \qquad (3.4)$$

Finally $\Pr\{c/s_{i2}(t)\}$ can be easily evaluated from Figure 3.2(c), namely

$$\Pr\{ c/s_{i2}(t) \} = \Pr\{ -A \leq N_1 \ , \ -A \leq N_2 \leq A \}$$

$$= \left\{ \int_{-A}^{\infty} \frac{1}{(2\pi N_0/2)^{1/2}} e^{-n_1^2/2(N_0/2)} \right.$$

$$\left. \int_{-A}^{A} \frac{1}{(2\pi N_0/2)^{1/2}} e^{-n_2^2/2(N_0/2)} \right\} dn_2 \, dn_1$$

$$= \text{erfc}^*\left(-\frac{A}{(N_0/2)^{1/2}}\right)\left[1-2\text{erfc}^*\left(-\frac{A}{(N_0/2)^{1/2}}\right)\right].$$

(3.5)

Thus the average probability of correct decision is given by,

$$Pr\{c\} = \frac{1}{16}\left[4Pr\{c/s_{i1}(t)\} + 4Pr\{c/s_{i6}(t)\} + 8Pr\{c/s_{i2}(t)\}\right] \tag{3.6}$$

so that

$$Pr\{\varepsilon\} \stackrel{\Delta}{=} 1 - Pr\{c\}$$

$$= 1 - \left\{ \left[\frac{1}{2} - erfc^*((Rd/10)^{1/2}) \right]^2 + \right.$$

$$erfc^*[-(Rd/10)^{1/2}) \left[\frac{1}{2} - erfc^*((Rd/10)^{1/2}) \right] +$$

$$\left. \frac{1}{4}\left[erfc^*(-(Rd/10)^{1/2}) \right]^2 \right\} \tag{3.7}$$

where Equation 3.2 has been used in order to express $Pr\{\varepsilon\}$ in terms of Rd, the signal to noise ratio, defined as

$$Rd \stackrel{\Delta}{=} \frac{2E}{N_0}$$

The performance of the 16-QAM receiver is compared with that of a 16-PSK receiver by plotting $Pr\{\varepsilon\}$ given by

Equation 2.31 with M = 16 together with $Pr\{\varepsilon\}$ given by Equation 3.7 and presenting the results together in Figure 3.3.

From this figure, we note that if $Pr\{\varepsilon\} = 10^{-4}$ is desired, then the required SNR that yields this level of performance is 22 dB for 16-QAM and 26 dB for the 16-PSK. In order to understand the superiority of 16-QAM over 16-PSK consider an M-ary PSK signal set with equally spaced points on a circle of radius R in which the distance between adjacent points is 2A, where the parameter A corresponds to that used in the signal constellation diagram of the 16-QAM signal set shown in Figure 3.1 [Ref. 3] (see Figure 3.4 also). The angular distance between adjacent points for MPSK is $2\pi/M$. It is required that

$$R = \frac{1}{\sin(\pi/M)} \approx \frac{M}{\pi} \quad \text{(for large M)}$$

in order to obtain the 2A separation between two adjacent points as shown in Figure 3.4. Therefore the average energy for M-ary PSK must increase as $(M/\pi)^2$ in order to maintain the same $Pr\{\varepsilon\}$ performance as M increases. When the average energy of the signal set is fixed so as to be able to compare system performances, the distance between adjacent signals become smaller in M-ary PSK than that encountered in the QAM case. Thus $Pr\{\varepsilon\}$ increases for M-ary PSK in comparison to that for QAM.

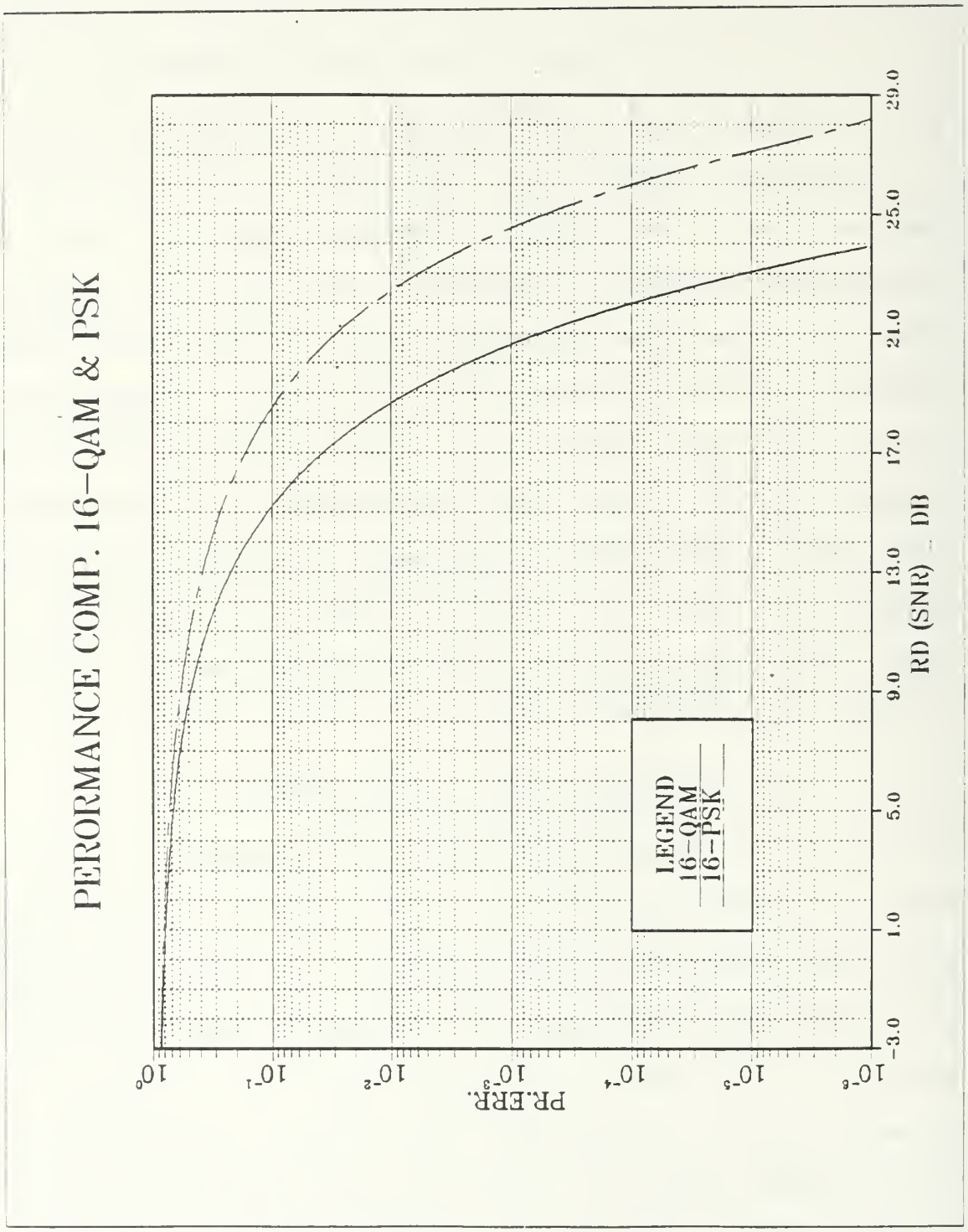

Figure 3.3. Pr{ε} Performance for 16-QAM and PSK

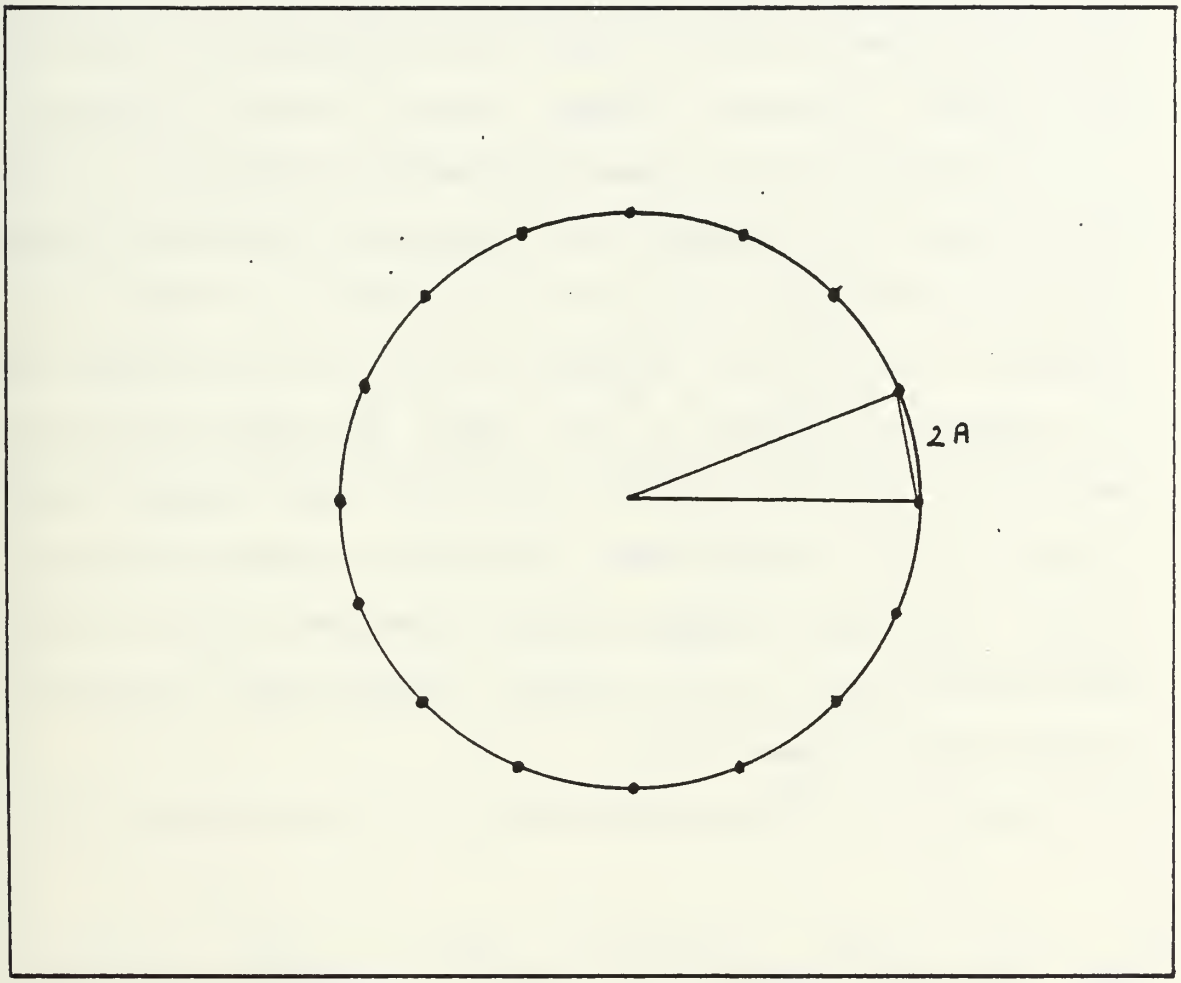

Figure 3.4. Signal Constellation for 16-PSK

B. RECEIVER PERFORMANCE FOR 64-QAM AND 256-QAM

The concepts of Section A are now extended to form a signal constellation of shape similar to 16-QAM except that now four times as many signals are used, thus forming a signaling scheme called 64-QAM, as diagrammed in Figure 3.5. The 64-QAM signaling scheme can be further extended in a form similar to that used to generate 64-QAM from 16-QAM. This results in 256-QAM, and its analysis as will be seen, is no more difficult than that for 16-QAM or 64-QAM. This is because in 64-QAM and 256-QAM we have three different types of decision regions of the form previously analyzed in Section A of this chapter. All signals are assumed equally likely to be transmitted and their energies are given in Table 3.1 for 64-QAM. Signal energies can be easily determined from the signal constellation diagram as illustrated in Figure 3.5.

From Table 3.1 the average energy can be calculated to be

$$E = \frac{1}{64}\left[\, 4(2A^2) + 8(10A^2) + 4(18A^2) + 8(26A^2) + 8(34A^2)\right.$$

$$\left. + 12(50A^2) + 8(58A^2) + 8(74A^2) + 4(98A^2) \,\right] = 42\, A^2 . \qquad (3.8)$$

Thus we can express

$$A = (E / 42)^{1/2} \qquad (3.9)$$

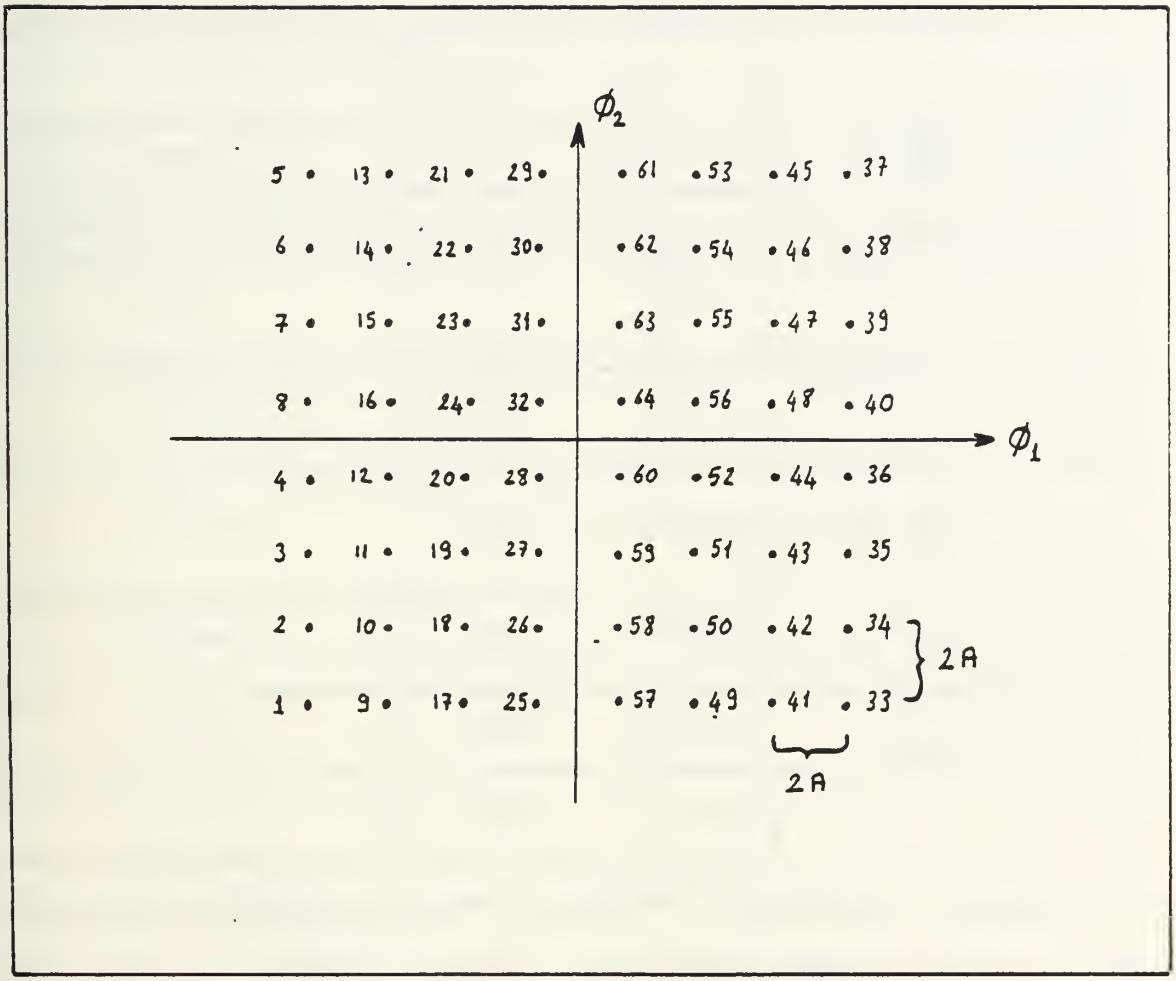

Figure 3.5. Signal Constellation for 64-QAM

TABLE 3.1

ENERGY OF THE SIGNALS IN 64-QAM

Signal Points i	Components Φ_1	Φ_2	Energy
28, 32, 64, 60	A^2	A^2	A^2
20, 24, 31, 63 56, 52, 59, 27	$9A^2$	A^2	$10\ A^2$
19, 23, 55, 51	$9A^2$	$9A^2$	$18\ A^2$
26, 12, 16, 30 62, 48, 44, 58	$25A^2$	A^2	$26\ A^2$
18, 11, 15, 22 54, 47, 43, 50	$25A^2$	$9A^2$	$34\ A^2$
25, 10, 4, 8 14, 29, 61, 46 40, 36, 42, 57	$49A^2$	A^2	$50\ A^2$
17, 7, 3, 21 53, 39, 35, 49	$49A^2$	$9A^2$	$58\ A^2$
9, 2, 6, 13 45, 38, 34, 41	$49A^2$	$25A^2$	$74\ A^2$
1, 5, 37, 33	$49A^2$	$49A^2$	$98\ A^2$

Signal vectors in Figure 3.5 can be grouped according to the type of decision region associated with each signal. If we label the decision regions shown in Figure 3.2 as Type I, Type II and Type III, there are 4 signals with decison region of Type I, 36 signals with decison region of Type II and 24 signals with decison region of Type III in 64-QAM. Therefore, there are three basic probability of correct decision expressions to be developed. These are denoted by

Pr{c/I}, Pr{c/II}, Pr{c/III} so that the probability of error is given by

$$Pr\{\varepsilon\} = 1 - \frac{1}{64}\left[\, 4Pr\{c/I\} + 36Pr\{c/II\} + 24Pr\{c/III\} \,\right] \tag{3.10}$$

Since Pr{c/I}, Pr{c/II} and Pr{c/III} are given by Equations 3.3, 3.4,. and 3.5 respectively, Equation 3.10 yields

$$Pr\{\varepsilon\} = 1 - \frac{1}{4}\left\{ \frac{1}{4}\left[\, erfc^*\left(-(Rd/42)^{1/2} \right) \,\right]^2 + 9\left[\, \frac{1}{2} erfc^*\left((Rd/42)^{1/2}\right)\right]^2 + 3\, erfc^*\left(-(Rd/42)^{1/2}\right)\left[\, \frac{1}{2} - erfc^*\left((Rd/42)^{1/2}\right)\right] \right\} \tag{3.11}$$

The same methodology used to obtain Equation 3.11 can now be applied to 256-QAM. First, the average energy of the signal set is given by

$$E = \frac{1359}{8} A^2 \tag{3.12}$$

so that the parameter A becomes

$$A = \left(\frac{8}{1359} E \right)^{1/2}. \qquad (3.13)$$

Equation 3.10 now becomes

$$Pr\{\xi\} = 1 - \frac{1}{256} [\, 4Pr\{c/I\} + 196Pr\{c/II\} + 56Pr\{c/III\} \,] \qquad (3.14)$$

which in terms of signal to noise ratio becomes

$$Pr\{\xi\} = 1 - \frac{7}{16} \left\{ \frac{1}{28} [erfc^*(-d)]^2 + 7 \left[\frac{1}{2} - erfc^*(d) \right]^2 + erfc^*(-d) \left[\frac{1}{2} - erfc^*(d) \right] \right\} \qquad (3.15)$$

where

$$d \triangleq \frac{A}{(N_0/2)^{1/2}} = \left(\frac{8}{1359} Rd \right)^{1/2}. \qquad (3.16)$$

The results of Equation 3.11 and 3.16 are graphically displayed in Figures 3.6 and 3.7 respectively. The probability of error performance of 64-PSK and 256-PSK are also presented in these figures in order to be able to compare the QAM schemes with the equivalent PSK schemes on the basis of similar SNR.

The difference between M-ary PSK and QAM signaling scheme becomes more significant as M increases. The required

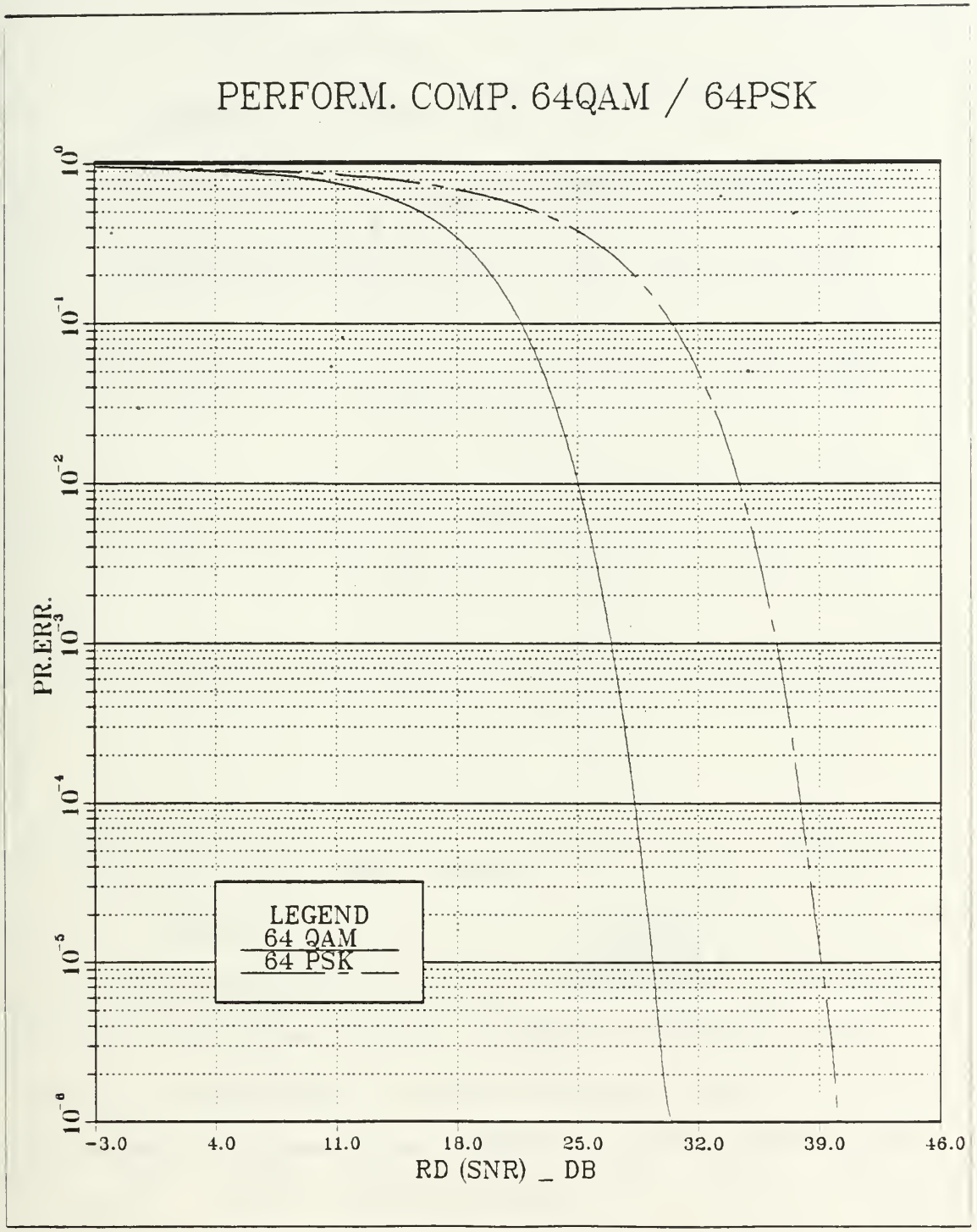

Figure 3.6. Pr{ε} Performance for 64-QAM and PSK

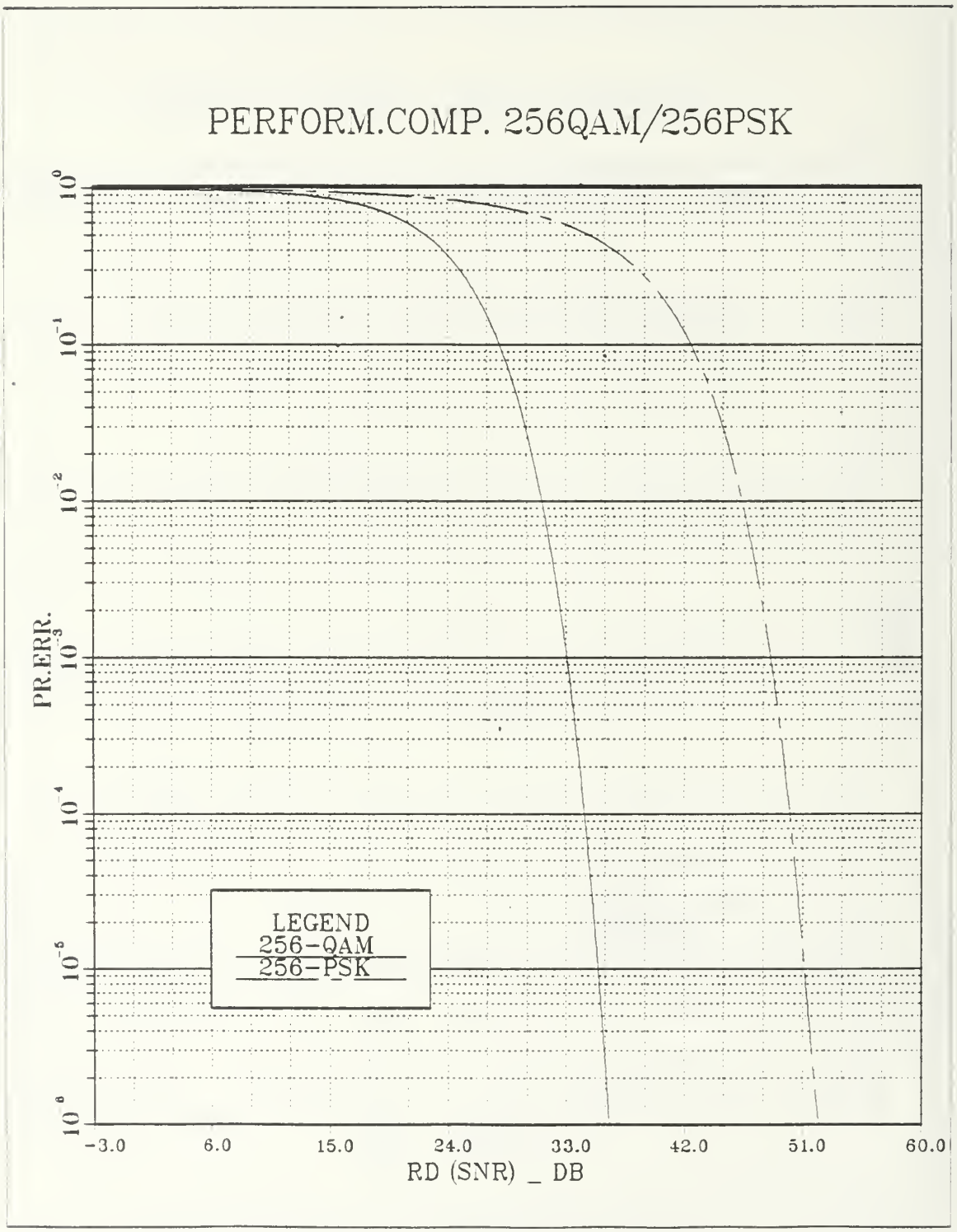

Figure 3.7. Pr(ε) Performance for 256-QAM and PSK

values of Rd are obtained from Figures 3.3, 3.5 and 3.6 for $Pr\{\varepsilon\} = 10^{-6}$, and displayed in Table 3.2 for M = 16, 64, and 256. For further purposes of comparison, the performance

TABLE 3.2

PERFORMANCE COMPARISON OF M-ARY QAM AND PSK FOR $Pr\{\varepsilon\} = 10^{-6}$.

M	Rd (dB)	
	QAM	PSK
16	24	28
64	30.5	40
256	36	52

of M-ary QAM and PSK schemes for M = 16, 64 and 256 are plotted together in Figure 3.8. We observe that for large values of M ($M > 4$), about 6 dB more SNR is required to maintain the same error probability for each doubling of signals. Furthermore, the SNR difference between QAM and PSK modulations for a fixed $Pr\{\varepsilon\}$ value, increases as M increases. Clearly, QAM is a relatively efficient signaling scheme composed to M-ary PSK.

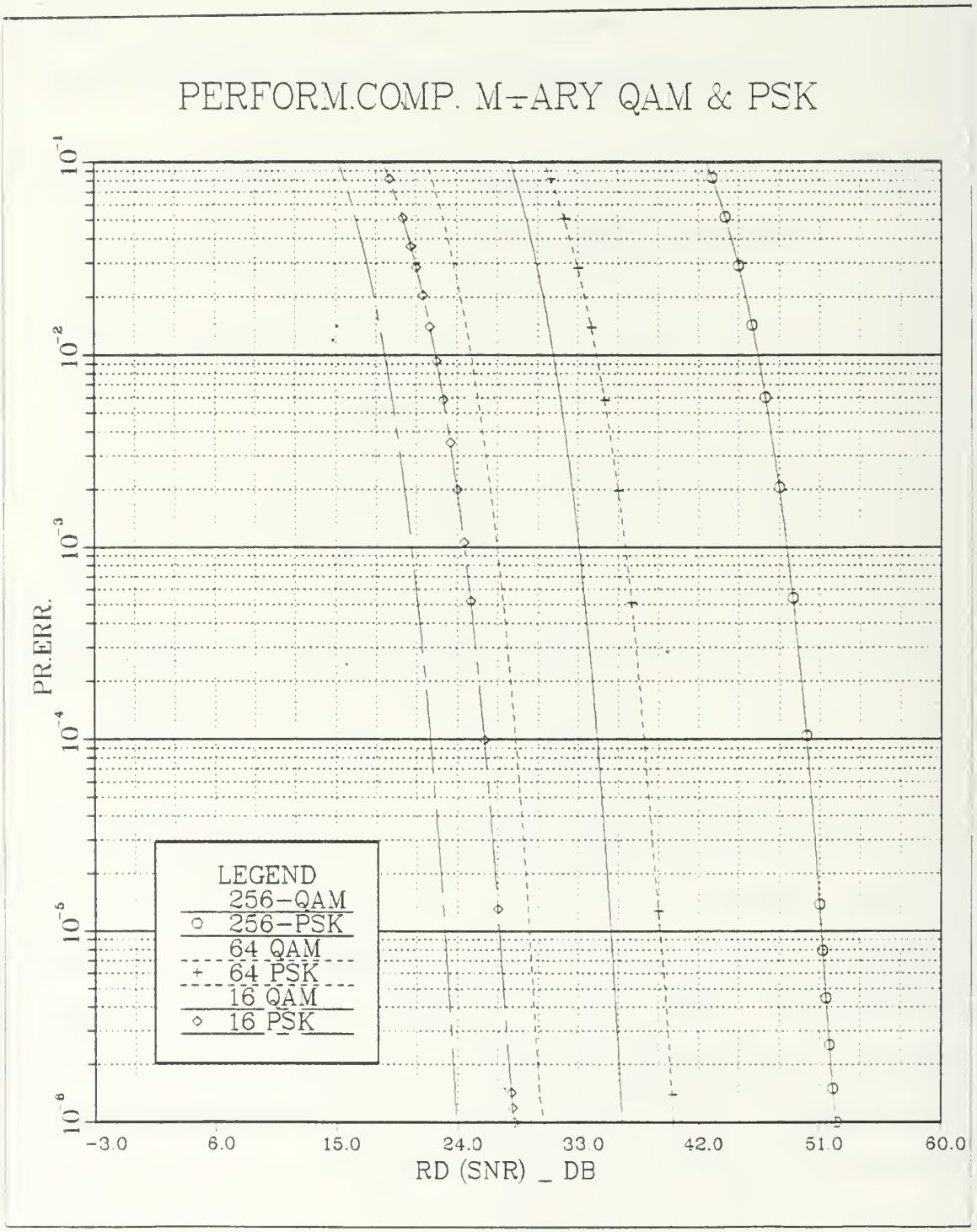

Figure 3.8. Comparison of Pr{ε} Performance for M-ary QAM and PSK

IV. PERFORMANCE OF A 16-QAM RECEIVER IN THE PRESENCE OF JAMMING

In this section, the vulnerability of the 16-QAM signaling scheme is analyzed by assuming that the optimum receiver built for the reception of the 16 QAM signals in additive WGN now encounters jamming in the form of an additive colored Gaussian noise process. Because of this, the vectorial signal representation and corresponding geometric approaches used previously are not directly applicable to the analysis of this problem so that mathematical signal and noise representations become necessary. Thus, the waveforms in the 16 QAM scheme can be expressed in the form

$$x_c(t) = A_1 m_1(t) \cos(2\pi f_0 t + \alpha) + A_2 m_2(t) \sin(2\pi f_0 t + \alpha) \tag{4.1}$$

where $A_1 = A_2 = a$, α is constant and $m_1(t)$ as well as $m_2(t)$ are digital signals of duration T second. Specifically

$$\left.\begin{aligned} m_1(t) &= \pm 1 \ , \ \pm 3 \\ m_2(t) &= \pm 1 \ , \ \pm 3 \end{aligned}\right\} \quad \text{over T sec.} \tag{4.2}$$

If we define

$$\phi_1(t) = \frac{\cos(2\pi f_0 t + \alpha)}{(T/2)^{1/2}} \quad , \quad \phi_2(t) = \frac{\sin(2\pi f_0 t + \alpha)}{(T/2)^{1/2}}$$

the 16 signals $s_i(t)$ $i = 1, 2, \ldots, 16$ can be expressed as

$$s_i(t) = A(T/2)^{1/2} \; m_1(t) \; \phi_1(t) + A(T/2)^{1/2} \; m_2(t) \; \phi_2(t). \tag{4.3}$$

Defining

$$A = a \; (T/2)^{1/2}$$

we obtain

$$s_i(t) = A \; m_1(t) \; \phi_1(t) + A \; m_2(t) \; \phi_2(t). \tag{4.4}$$

The signal constellation diagram associated with the 16-QAM scheme has been given in Figure 3.1. The probability of error of the 16 QAM signaling scheme assuming each signal is equally likely to be transmitted and is received in an additive white Gaussian noise interference environment is presented in Chapter III. The 16 QAM receiver structure shown in Figure 4.1 is optimum in the minimum probability of

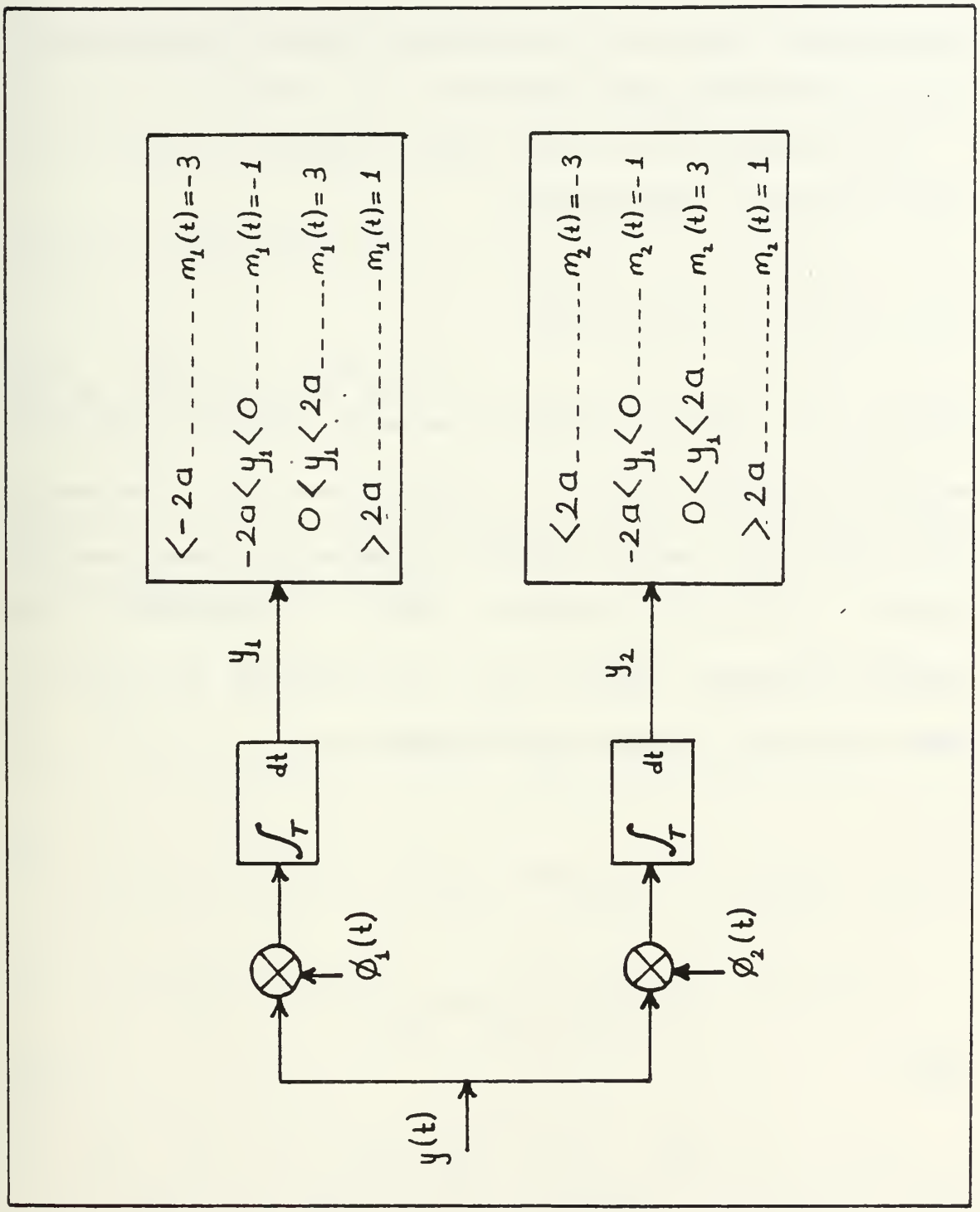

Figure 4.1. Optimum Receiver and Logic Processing for 16-QAM Signal Transmission

error sense when the transmitted signal is corrupted by additive white Gaussian noise only.

The vulnerability of the receiver shown in Figure 4.1 is now analyzed by assuming that

$$y(t) = s_i(t) + n_w(t) + n_c(t)$$

$$i = 1, 2, \ldots, 16 \qquad (4.5)$$

where $n_c(t)$ models colored Gaussian noise, having power spectral density $S_c(f)$. In Equation 4.5, $n_w(t)$ represents the zero mean white Gaussian noise having power spectral density level $N_0/2$ Watts/Hz. , which is independent of the colored Gaussian noise $n_c(t)$. The receiver of Figure 4.1 makes decisions based on the computations

$$y_1 = \int_T [s_{i1}\phi_1(t) + s_{i2}\phi_2(t) + n_w(t) + n_c(t)]\,\phi_1(t)dt =$$

$$= s_{i1} + n_{w1} + n_{c1}$$

and (4.6)

$$y_2 = \int_T [s_{i1}\phi_1(t) + s_{i2}\phi_2(t) + n_w(t) + n_c(t)]\,\phi_2(t)dt =$$

$$= s_{i2} + n_{w2} + n_{c2}$$

where Equation 4.6 has been written under the assumption that the ith signal $s_i(t)$ is transmitted. We define

$$n_{wj} = \int_T n_w(t)\,\phi_j(t)\,dt$$

$$j = 1, 2 \qquad (4.7)$$

$$n_{cj} = \int_T n_c(t)\,\phi_j(t)\,dt.$$

Observe that conditioned on $s_i(t)$ being transmitted, y_1 and y_2 are Gaussian r.v.'s with

$$E\{y_1\} \stackrel{\Delta}{=} m_{y1} = s_{i1} \quad , \quad E\{y_2\} \stackrel{\Delta}{=} m_{y2} = s_{i2} \qquad (4.8)$$

and

$$\text{Var}\{y_1\} \stackrel{\Delta}{=} \sigma_{y1}^2 = E\{(n_{w1} + n_{c1})^2\} = E\{n_{w1}^2\} + E\{n_{c1}^2\} \qquad (4.9)$$

$$\text{Var}\{y_2\} \stackrel{\Delta}{=} \sigma_{y2}^2 = E\{(n_{w2} + n_{c2})^2\} = E\{n_{w2}^2\} + E\{n_{c2}^2\}$$

where Equation 4.9 has been obtained in simplified form because n_w and n_c are statistically independent random variables. Furthermore

$$E\{[y_1 - E\{ y_1 \}][y_2 - E\{ y_2 \}]\} = E\{ n_{w1}\, n_{w2} \} + E\{ n_{c1}\, n_{c2} \}. \tag{4.10}$$

We first observe that,

$$E\{n_{wk}\, n_{w1}\} = E\{ \int_T n_w(t)\, \phi_k(t)\, dt \int_T n_w(\tau)\, \phi_1(\tau)\, d\tau \}$$

$$= \int_T \int E\{ n_w(t)\, n_w(\tau)\} \phi_k(t)\, \phi_1(\tau)\, dt\, d\tau$$

$$= \int_T \int N_0/2\, \delta(t - \tau)\, \phi_k(t)\, \phi_1(\tau)\, dt\, d\tau$$

$$= N_0/2 \int_T \phi_k(\tau)\, \phi_1(\tau)\, d\tau = \begin{cases} 0 & , \quad k = 1 \\ N_0/2 & , \quad k \neq 1 \end{cases} \tag{4.11}$$

so that

$$E\{ n_{w1}^2 \} = E\{ n_{w2}^2 \} = N_0/2. \tag{4.12}$$

and

$$E\{ n_{w1}\, n_{w2} \} = 0$$

Now

$$E\{n_{c1}\ n_{c2}\} = E\{ \int_T n_c(t)\ \phi_1(t)\ dt \int_T n_c(\tau)\ \phi_2(\tau)\ d\tau \}$$

$$= \int_T \int E\{ n_c(t)\ n_c(\tau)\}\ \phi_1(t)\ \phi_2(\tau)\ dt\ d\tau$$

$$= \int_T \int K_c(t - \tau)\ \phi_1(t)\ \phi_2(\tau)\ dt\ d\tau \qquad (4.13)$$

where $K_c(t)$ is the inverse Fourier Transform of $S_c(f)$, the colored noise PSD.

Let

$$\phi_j'(t) = \begin{cases} \phi_j(t) & , \quad 0 \leqslant t \leqslant T \quad , \quad j = 1, 2 \\ 0 & , \quad \text{otherwise} \end{cases}$$

so that

$$\Phi_j'(f) = F\{ \phi_j'(t)\} \quad , \quad j = 1, 2.$$

Expressing Equation 4.13 in terms of frequency demain functions, we obtain

$$E\{ n_{c1}\ n_{c2}\} = \int_{-\infty}^{\infty} \int K_c(t - \tau)\ \phi_1'(t)\ \phi_2'(\tau)\ dt\ d\tau$$

$$= \int_{-\infty}^{\infty}\int_{-\infty}^{\infty}\left[\int_{-\infty}^{\infty} S_C(f)e^{j2\pi f(t-\tau)}df\right]\phi_1(t)\,\phi_2(\tau)\,dt\,d\tau$$

$$= \int_{-\infty}^{\infty} S_C(f)\int_{-\infty}^{\infty}\phi_1(t)e^{j2\pi ft}dt\int_{-\infty}^{\infty}\phi_2(t)e^{-j2\pi f\tau}d\tau\,df$$

$$= \int_{-\infty}^{\infty} S_C(f)\,\Phi_1(-f)\,\Phi_2(f)\,df. \qquad (4.14)$$

In Appendix A, it is demonstrated that based on the result of Equation 4.14,

$$E\{n_{C_1}n_{C_2}\} = 0$$

so that the components of the colored noise along the dimensions $\phi_1(t)$ and $\phi_2(t)$ are uncorrelated. Due to the fact that n_{C1} and n_{C2} are jointly Gaussian r.v.'s, they are statistically independent. It can also be shown that

$$E\{n_{C1}^2\} = \int_{-\infty}^{\infty} S_C(f)\,\Phi_1(-f)\,\Phi_2(f)\,df$$

$$= \int_{-\infty}^{\infty} S_C(f)\,|\Phi_1(f)|^2\,df$$

$$\stackrel{\Delta}{=} \sigma_C^2. \qquad (4.15)$$

Because of the relationship between $\Phi_1'(f)$ and $\Phi_2'(f)$, it is clear that

$$\Phi_1'(-f)\,\Phi_1'(f) = \Phi_2'(-f)\,\Phi_2'(f) \tag{4.16}$$

so that

$$E\{n_{c1}^2\} = E\{n_{c2}^2\} \overset{\Delta}{=} \sigma_c^2. \tag{4.17}$$

Therefore

$$\begin{aligned} m_{y1} &= S_{i1} \\ m_{y2} &= S_{i2} \\ \sigma_{y1}^2 &= \sigma_{y2}^2 = N_0/2 + \sigma_c^2 \\ E\{[y_1 - m_{y1}][y_2 - m_{y2}]\} &= 0 . \end{aligned} \tag{4.18}$$

The last equality of Equation 4.18 shows that the r.v.'s y_1 and y_2 are uncorrelated, so that we can express the joint probability density function of y_1 and y_2 as

$$f_{y1\,y2}(Y_1 Y_2) = \frac{1}{2\pi\,\sigma_{y1}\,\sigma_{y2}}\, e^{-(Y_1 - m_{y1})^2/2\,\sigma_{y1}^2}\; e^{-(Y_2 - m_{y2})^2/2\,\sigma_{y2}^2}. \tag{4.19}$$

The probability of making a correct decision, given that $s_i(t)$ was transmitted, namely

$$Pr\{c/s_i(t)\} = Pr\{L_{i1} \leq y_1 \leq L_{iu} \ , \ L_{21} \leq y_2 \leq L_{2u}\} \qquad (4.20)$$

can now be determined by using the signal constellation diagram of Figure 3.1, in order to set the limits on the r.v.'s y_1 and y_2. From Equation 4.19 above, we obtain

$$Pr\{c/s_i(t)\} = \int_{L_{i1}}^{L_{iu}} \frac{1}{(2\pi((N_0/2)+\sigma_c^2))^{1/2}} e^{-(Y_1-S_{i1})^2/2((N_0/2)+\sigma_c^2)} dY_1$$

$$\int_{L_{21}}^{L_{2u}} \frac{1}{(2\pi((N_0/2)+\sigma_c^2))^{1/2}} e^{-(Y_2-S_{i2})^2/2((N_0/2)+\sigma_c^2)} dY_2 \qquad (4.21)$$

and letting

$$z \overset{\Delta}{=} \frac{Y_1 - S_{i1}}{((N_0/2)+\sigma_c^2)^{1/2}} \qquad (4.22)$$

as well as

$$w \overset{\Delta}{=} \frac{Y_2 - S_{i2}}{((N_0/2)+\sigma_c^2)^{1/2}} \tag{4.23}$$

Equation 4.21 becomes

$$\Pr\{c/s_i(t)\} = \int_{g_l}^{g_u} \frac{1}{(2\pi)^{1/2}} e^{-z^2/2}\, dz \int_{h_l}^{h_u} \frac{1}{(2\pi)^{1/2}} e^{-w^2/2}\, dw. \tag{4.24}$$

The limits of integration specified below, namely

$$h_l = \frac{L_{2l} - S_{i2}}{((N_0/2)+\sigma_c^2)^{1/2}} \tag{4.25}$$

$$h_u = \frac{L_{2u} - S_{i2}}{((N_0/2)+\sigma_c^2)^{1/2}} \tag{4.26}$$

$$g_l = \frac{L_{1l} - S_{i1}}{((N_0/2)+\sigma_c^2)^{1/2}} \tag{4.27}$$

$$g_u = \frac{L_{1u} - S_{i1}}{((N_0/2)+\sigma_c^2)^{1/2}} \tag{4.28}$$

depend on which signal $s_i(t)$ was transmitted. Since sixteen different signals must be considered, tables have been generated specifying the limits of the integrals for each of the signals. Tables 4.1, 4.2 and 4.3 list all necessary variables in order to calculate the limits of Equation 4.24, by using Equations 4.25 through 4.28. These tables show that again, three basic probability of correct decision expressions associated with three different types of decision regions must be considered.

TABLE 4.1

LIMITS FOR DECISION REGION TYPE I

M	S_{i1}	S_{i2}	L_{11}	L_{1u}	L_{21}	L_{2u}	h_1	h_u	g_1	g_u
1	-3A	-3A	$-\infty$	-2A	$-\infty$	-2A	$-\infty$	A/σ	$-\infty$	A/σ
3		3A			2A	∞	$-A/\sigma$	∞		
9	3A	-3A	2A	∞	$-\infty$	-2A	$-\infty$	A/σ	$-A/\sigma$	∞
11		3A			2A	∞	$-A/\sigma$	∞		

For any of the signals in Table 4.1 being transmitted,

$$Pr(c/I) = [erf*(\frac{A}{((N_0/2)+\sigma_C^2)^{1/2}})]^2 . \qquad (4.29)$$

TABLE 4.2

LIMITS FOR DECISION REGION TYPE II

M	S_{i1}	S_{i2}	L_{1l}	L_{1u}	L_{2l}	L_{2u}	h_l	h_u	g_l	g_u
2	$-3A$	$-A$	$-\infty$	$-2A$	$-2A$	0	$-A/\sigma$	A/σ	$-\infty$	A/σ
4		A			0	$2A$				
5	$-A$	$-3A$	$-2A$	0	$-\infty$	$-2A$	$-\infty$	A/σ	$-A/\sigma$	A/σ
7		$3A$			$2A$	∞	$-A/\sigma$	∞		
13	A	$-3A$	0	$2A$	$-\infty$	$-2A$	$-\infty$	A/σ	$-A/\sigma$	A/σ
15		$3A$			$2A$	∞	$-A/\sigma$	∞		
10	$3A$	$-A$	$2A$	∞	$-2A$	0	$-A/\sigma$	A/σ	$-A/\sigma$	∞
12		A			0	$2A$				

For any of the signals in Table 4.2 being transmitted,

$$Pr(c/II) = erf*\left(\frac{A}{((N_0/2)+\sigma_c^2)^{1/2}}\right)\left[1-2erfc*\left(\frac{A}{((N_0/2)+\sigma_c^2)^{1/2}}\right)\right]. \qquad (4.30)$$

TABLE 4.3

LIMITS FOR DECISION REGION TYPE III

M	S_{i1}	S_{i2}	L_{11}	L_{1u}	L_{21}	L_{2u}	h_l	h_u	g_l	g_u
6	-A	-A	-2A	0	-2A	0	$-A/\sigma$	A/σ	$-A/\sigma$	A/σ
8		A			0	2A				
14	A	-A	0	2A	-2A	0	$-A/\sigma$	A/σ	$-A/\sigma$	A/σ
16		A			0	2A				

For any of the signals in Table 4.3 being transmitted,

$$Pr\{c/III\} = [1 - 2erfc^*(\frac{A}{((N_0/2)+\sigma_c^2)^{1/2}})]^2. \qquad (4.31)$$

From Equation 3.2, we have $A = (E/10)^{1/2}$

so that

$$d \triangleq \frac{A}{((N_0/2)+\sigma_c^2)^{1/2}} = [\frac{E}{10\ (N_0/2)\ (1+(2\sigma_c^2/N_0))}]^{1/2}$$

$$= \left[\frac{Rd}{10\ (1 + Rd\ Rj)}\right]^{1/2} \qquad (4.32)$$

where

$$Rd \overset{\Delta}{=} \frac{2E}{N_o} \text{ ; Signal to Noise Ratio (SNR)}$$

and

$$Rj \overset{\Delta}{=} \frac{\sigma_c^2}{E} \text{ ; Jamming to Signal Ratio (JSR).}$$

Thus, since each signal is assumed equally likely to be transmitted, we obtain

$$Pr\{c\} = 1/16\ [4\ Pr\{c/I\} + 8\ Pr\{c/II\} + Pr\{c/III\}] \qquad (4.33)$$

so that

$$Pr\{\varepsilon\} \overset{\Delta}{=} 1 - Pr\{c\}$$

$$= 1 - (1/4)\ \{\ [erf*(d)]^2 + 2\ erf*(d)\ [1 - 2erfc*(d)]$$

$$+ [1 - 2erfc*(d)]^2\ \}. \qquad (4.34)$$

Observe that if jamming is not present (Rj = 0), then from Equation 4.32, $d = (Rd/10)^{1/2}$ so that Equation 4.34

becomes identical to the expression for the performance of the 16-QAM receiver operating in the presence of additive WGN only (Equation 3.7). Furthermore, as $R_j \to \infty$, for fixed values of R_d, then $d \to 0$ and we have

$$Pr\{c\} = \frac{1}{4}\left[(1/2)^2 + 0 + 0\right] = \frac{1}{16}$$

which is the minimum value for a set of sixteen equiprobable signals.

From the point of view of the jammer, it is desirable to maximize $Pr\{\varepsilon\}$ with minimum or at least constrained use of jammer power. Such optimization will now be considered by first investigating the dependence of $Pr\{\varepsilon\}$ on the parameter d.

Observe that

$$\frac{\partial Pr\{\varepsilon\}}{\partial d} = -\frac{1}{4}\left\{ 2\,erf^*(d)\,\frac{\partial}{\partial d}\,erf^*(d) + \right.$$

$$2\,erf^*(d)\,\frac{\partial}{\partial d}(-2\,erfc^*(d)) + (1-2\,erfc^*(d))\frac{\partial}{\partial d}(erf^*(d) +$$

$$\left. 2(1-2\,erfc^*(d))\frac{\partial}{\partial d}(-2\,erfc^*(d)) \right\}. \quad (4.35)$$

Taking the derivatives by using Leibnitz's rule, we have

$$\frac{\partial Pr\{\varepsilon\}}{\partial d} = -\frac{3}{2\,(2\pi)^{1/2}}\; e^{-d^2/2}\; [-1 + 3\,\mathrm{erf}^*(d)] \qquad (4.36)$$

From the above expression observe that the term in the bracket is always positive since d is a positive quantity and erf*(d) takes the values between 1/2 for d = 0, and 1 for $d \to \infty$. This proves that

$$-\frac{\partial}{\partial d}\, Pr\{\varepsilon\} \leqslant 0$$

which means that $Pr\{\varepsilon\}$ is a monotonically decreasing function. Therfore in order to maximize $Pr\{\varepsilon\}$ "d" must be made as small as possible. Making Rj as large as possible or equivalently, σ_c^2 as large as possible results in the smallest "d" and the greatest error probability.

Recalling that

$$\sigma_c^2 = \int_{-\infty}^{\infty} S_c(f)\; |\Phi_1'(f)|^2\, df$$

in order to maximize σ_c^2 as a function of $S_c(f)$, by the Cauchy-Schwarz inequality, we have

$$\sigma_c^2 = \int_{-\infty}^{\infty} S_c(f)\; |\Phi_1'(f)|^2 df \leqslant \left[\int_{-\infty}^{\infty} S_c^2(f) df \int_{-\infty}^{\infty} \Phi_1'(f)\, df\right]^{1/2} \qquad (4.37)$$

with equality if and only if

$$S_c(f) = \alpha \left| \Phi_1'(f) \right|^2 . \qquad (4.38)$$

We must select α such that the power constraint is satisfied. A constraint that would always have to be obeyed is

$$P_c = \int_{-\infty}^{\infty} S_c(f)\, df < \infty \qquad (4.39)$$

which holds provided $\int_{-\infty}^{\infty} \left| \Phi_1'(f) \right|^2 df < \infty$.

Equation 4.34 provides a mathematical result on the performance of the 16-QAM receiver in presence of WGN and colored Gaussian noise jamming. Graphical results on the performance of a 16-QAM receiver in the presence of jamming are presented in Figure 4.2. Plots of Pr{ε} were computed as a function of SNR (Rd) for various values of JSR (Rj). The JSR=0 case is included in order to provide a basis for comparisons of the jammer effect on the receiver performance as it relates to additive WGN only interference. From Figure 4.2, it can be noted that 18.5 dB SNR is required in order to obtain $Pr\{\varepsilon\} = 10^{-2}$ at a JSR value of zero. In comparison, it takes approximately 24 dB of SNR to obtain same Pr{ε} for a JSR=-20 dB. When the JSR is greater than -10 dB, Pr{ε} cannot be reduced below the value of 0.3 even for SNR=48 dB.

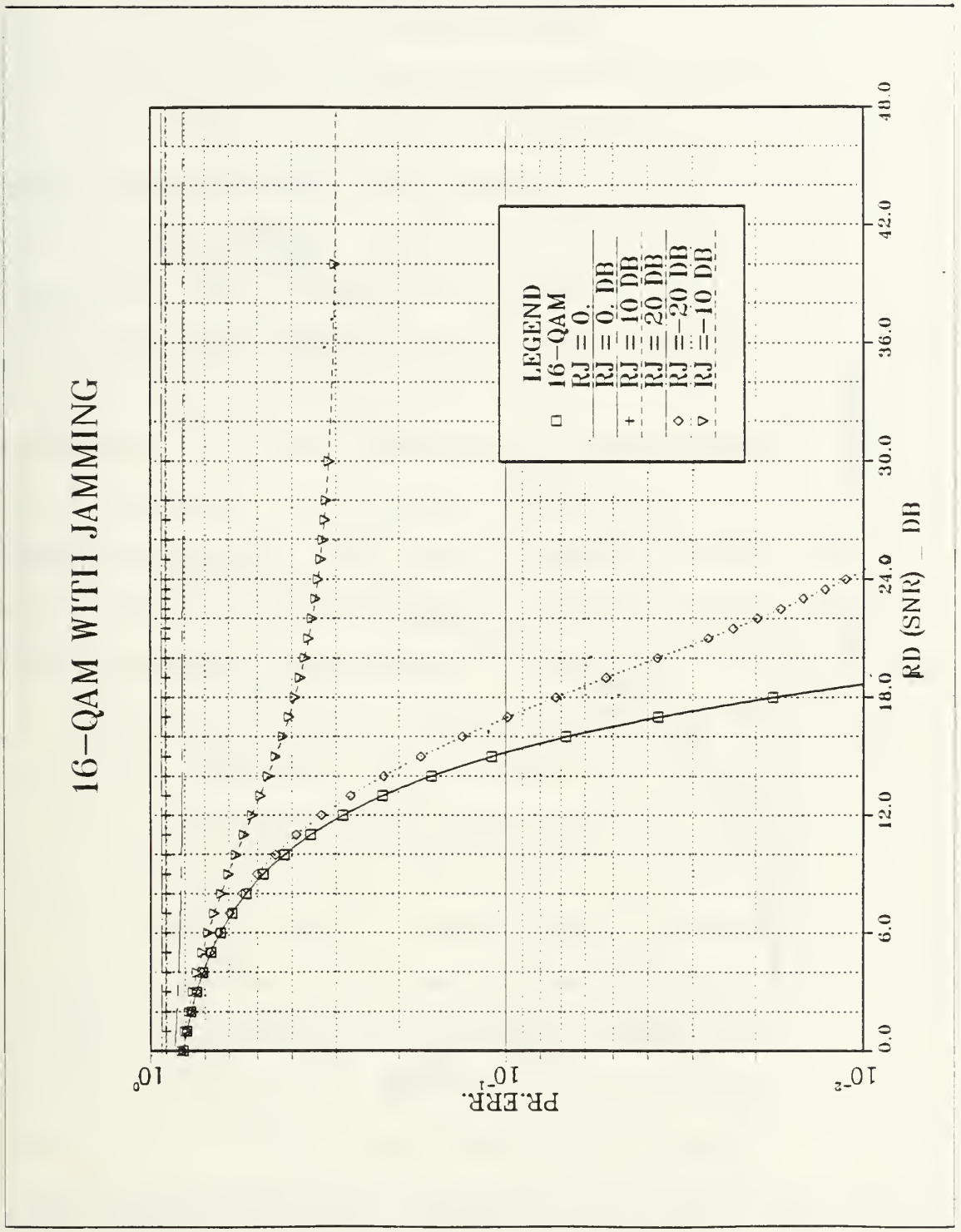

Figure 4.2. Pr{ε} Performance of the 16-QAM Receiver for Various Values of JSR

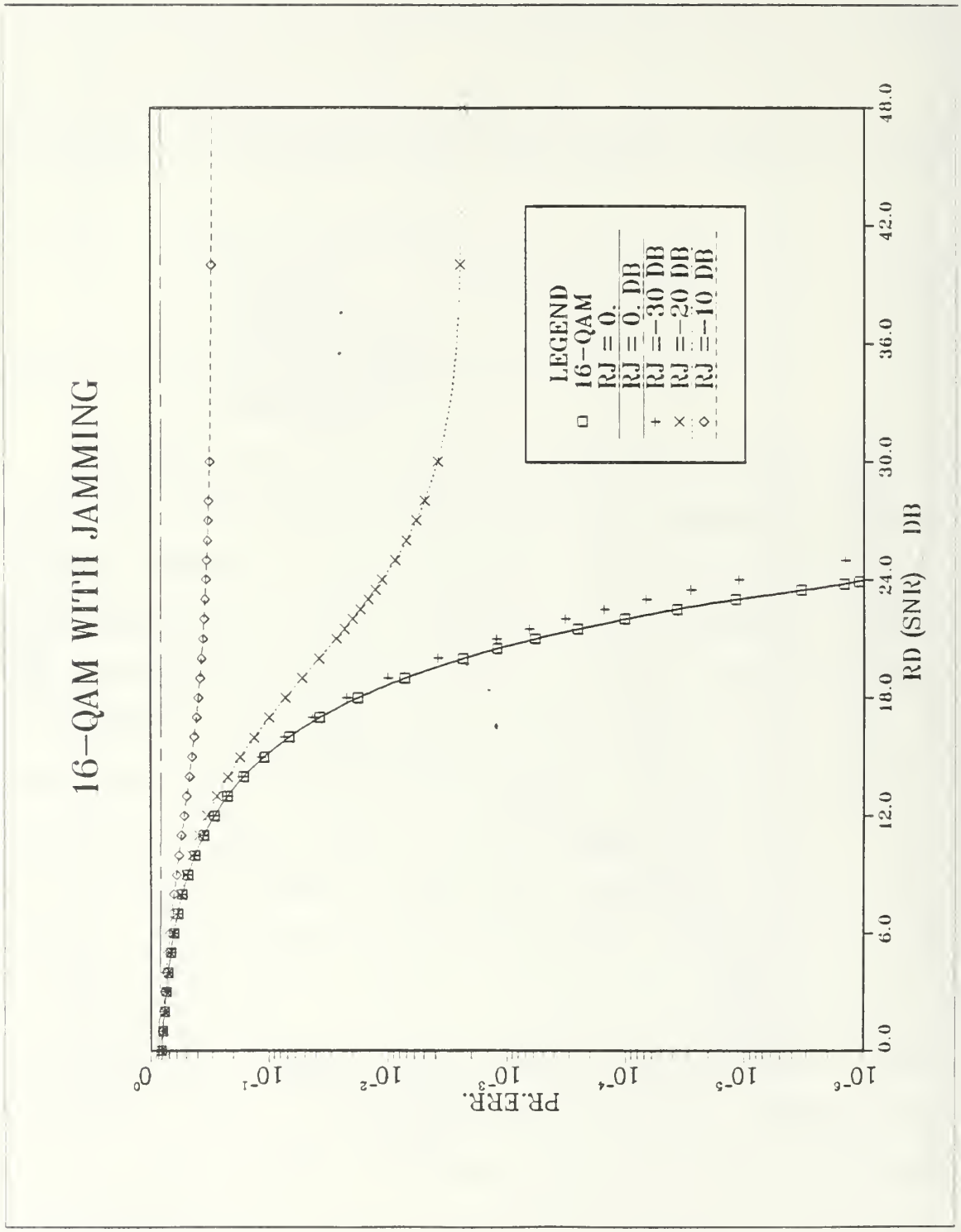

Figure 4.3. Pr{ε} Performance of the 16-QAM Receiver for Various Values of JSR

V. CONCLUSIONS

The first part of this thesis presents a review of signal-space methods of statistical communication theory which lead to the design of optimum (in MAP sense) receivers. The results were applied to the design of the well-known MPSK receiver and its performance in terms of the receiver average probability of error was obtained under the assumption of signal reception in the presence of additive white Gaussian noise. Some modifications to this signaling scheme (for M=8) were then examined. First a signaling scheme which has been labeled as the "rectangular" signaling scheme because of the shape of its signal space diagram was considered. Next, a 7+1 signaling scheme in which 7 signals are phase modulated and 1 signal is identically zero was analyzed as still another modification of the 8 PSK scheme. The results for probability of error on the basis of equal average signal energy showed that the modified signaling schemes tend to perform better than the 8-PSK scheme. From Figure 2.8, the 8-PSK signaling scheme can be seen to require 0.8 dB more SNR than the rectangular signaling scheme and 1.8 dB more SNR than the 7+1 signaling scheme in order to achieve an error probability of 10^{-6}. However, this

performance improvement is obtained at the expense of more complicated decision logic that the receiver must implement.

Further modifications to 8-PSK modulation that involved combined signal amplitude and phase modulation were considered . One such modification shown in Figure 2.9 was analyzed for various values of the parameter ε which quantified the difference between two signal amplitudes. When ε' ($= \frac{\varepsilon}{(2E)^{1/2}}$) is zero, all signal amplitudes are identical resulting in the conventional 8 PSK modulation scheme. The derived error probability result for arbitrary values of ε' (see Equaion 2.73) yields the result of Equation 2.30 when $\varepsilon' = 0$. For ε' equals to 0.2391, the signal constellation diagram takes on the shape of that of the rectangular signaling scheme, and it is demonstrated that for this case Equation 2.73 becomes identical to Equation 2.41. The modified scheme that includes both signal amplitude and phase modulation tends to yield system performance, i.e., lower $Pr\{\varepsilon\}$ in comparison to that of 8 PSK for values of ε' up to approximately 0.4. Performance curves are presented in Figures 2.14 and 2.15 for different values of ε'. They demonstrate that as ε' continues to increase, the overall system performance degrades severely. This is caused by the fact that as ε' continues to increase, four out of the 8 transmitted signals become "bunched"

together in the signal space diagram making their discrimination increasingly difficult. A further disadvantage of this scheme (even for $\varepsilon' < 0.4$) is the extremely complicated shapes of the optimum decision regions. In practice, it would be very difficult to implement the decision logic necessary to discriminate among the transmitted signals. This motivated a reevaluation of this signaling scheme in which simpler (however suboptimum) regions were assigned to each signal in such a way that implementational difficulties could be overcome. Two such modifications were considered. The first modification assumed that all signals could be recovered by simple phase measurement without regard to their energy. This lead to the decision regions shown in Figure 2.16. The second modification established rectangular decision regions similar to those used for the "rectangular" signaling scheme. A parameter Δ was introduced in order to be able to control the size of the rectangular decision regions. The presence of this parameter Δ makes it possible to optimize (in principle) the (suboptimum) decision regions. Figures 2.21 thru 2.27 present performance curves for both modified schemes as well as the optimum scheme for different values of ε' and Δ so that performance comparisons can be carried out. For $\varepsilon' = 0$, simple phase measurement decision regions as shown in Figure 2.16 are optimum and the performance of

the modified receiver is equal to that of the 8-PSK receiver. However, it can be observed that the performance degrades as ε' increases. This is not surprising because of the fact that the suboptimum decision regions are not modified as ε' changes. Furthermore, four out eight signals cluster around the origin as ε' approaches 1. Figure 2.18 demonstrates if 22.5 dB SNR is available, $Pr\{\varepsilon\}$ equal to 10^{-6} could be achieved by the conventional 8-PSK scheme, while the suboptimum receiver could achieve only $Pr\{\varepsilon\}=10^{-5}$ for $\varepsilon'=0.2$, $Pr\{\varepsilon\}\approx 10^{-2}$ for $\varepsilon'=0.6$, and $Pr\{\varepsilon\}=10^{-1}$ for $\varepsilon'=0.8$.

The suboptimum receiver with rectangular decision regions as shown in Figure 2.19 (for $\Delta=0.5$, $\varepsilon'=0.0$) gives us a chance to compare performances of the 8-PSK schemes utilizing rectangular decision regions as shown in Figure 2.19 with that of the conventional 8-PSK scheme. From Figure 2.21, the modified scheme requires about 22.8 dB SNR in order to achieve an error probability of 10^{-6} while the 8-PSK scheme requires 22.3 dB SNR in order to maintain the same error probability. When Δ takes on the value of 0.5 the error probability of the suboptimum receiver is almost identical to that of the optimum receiver for values of ε' that are greater than zero as can be seen from Figures 2.22, 2.24, 2.25, 2.26, 2.27. The $\varepsilon'=.2391$ case results in a

performance similar to that encountered for the "rectangular" signal set shown in Figure 2.23. When the decision regions are shifted to both directions by changing the value of Δ, significant performance degradation is observed up to the value of $\varepsilon'=0.7$. When ε' takes on the values of 0.7 and 0.8 the suboptimum receiver tends to perform very close to the level of an optimum receiver when $\Delta=0.5$, 0.3 and 0.7. We also notice that the suboptimum receiver utilizing phase measurment decision regions shown in Figure 2.16 yields the same error probability as the suboptimum receiver with rectangular decision regions for $\Delta \neq 0.5$ at a saving in SNR. When $\varepsilon' = .2$, Figure 2.22 illustrates that the saving in SNR is 2.5 dB for $\Delta=0.3$ and 0.7 while achieving an error probability of 10^{-3}. However as ε' increases, the saving in SNR approaches 0 dB. In Figure 2.25 (for $\varepsilon'=0.4$) the error probability of both suboptimum receivers become identical when $\Delta=0.3$ and 0.7. If ε' continues to increase above 0.4 the performance of the suboptimum receiver utilizing phase measurement decision regions as shown in Figure 2.16 exhibits degraded performance in comparison to that of the other suboptimum receiver for $\Delta=0.3$ and 0.7.

Chapter II. concludes with a performance comparison between conventional QPSK modulation and a modified scheme in which one extra signal is included in addition to the

four phase modulated signals. On the basis of same average energy per signal set, the latter has superior performance. For example, for an error probability of 10^{-6} this scheme requires 20 dB SNR while conventional QPSK requres 17 dB SNR.

In Chapter III, well-known results on the performance of M-ary QAM are presented, as well as performance comparisons between this scheme and MPSK modulation. M-ary QAM exhibits superior performance in comparison to that of MPSK. Figure 3.7 shows that the performance difference between M-ary QAM and MPSK becomes more significant as M increases. MPSK receivers require 4 dB more SNR to achieve $Pr\{\xi\} = 10^{-6}$ for M = 16, about 10 dB more for M = 64 and 16 dB more for M = 256.

Finally in Chapter IV, the performance of the 16-QAM receiver has been derived under the assumption that the interference consists of both additive WGN and jamming which has been modeled as additive colored Gaussian noise. The error probability of the receiver was evaluated for different values of SNR (Rd) and JSR (Rj). The results demonstrate (see Figure 4.2) that significant increases in receiver error probability can be achieved by this form of jamming even at relatively low JSR values. Furthermore, it was demonstrated that if a constraint is placed on total jamming power, it is possible to optimize the Power

Spectral Density of the colored noise jamming so as to produce a maximum receiver error probability while satisfaying the maximum power constraint. Figure 4.2 demonstrates that we can not achieve an error probability of less than 10^{-2} for JSR greater than -10dB.

APPENDIX

DETAILED INVESTIGATION OF THE PRODUCT OF $\Phi_1(-f)$ AND $\Phi_2(f)$

Let $\phi_1(t)$ and $\phi_2(t)$ be given by

$$\phi_1(t) = \frac{\cos(2\pi f_0 t + \alpha)}{(T/2)^{1/2}} \quad , \quad \phi_2(t) = \frac{\sin(2\pi f_0 t + \alpha)}{(T/2)^{1/2}}$$

and define

$$\phi_l'(t) \overset{\Delta}{=} \begin{cases} \phi_l(t) & , \ 0 \leq t \leq T \ , \ l = 1,2 \\ 0 & , \ \text{otherwise} \end{cases} \qquad (A.1)$$

Thus, $\phi_l'(t)$ for $l = 1, 2$ can be expressed as

$$\phi_1'(t) = p(t) \cos 2\pi f_0 t \qquad (A.2)$$

$$\phi_2'(t) = p(t) \sin 2\pi f_0 t$$

where α has been set to zero for mathematical simplicity and

$$p(t) = \begin{cases} 1/(T/2)^{1/2} & , \quad 0 \leq t \leq T \\ 0 & , \quad \text{otherwise} \end{cases} \qquad (A.3)$$

The Fourier transform of p(t), namely P(f) is given by

$$P(f) = (T/2)^{1/2} \frac{\sin \pi f T}{\pi f T} e^{-j\pi fT} = (T/2)^{1/2} \text{sinc}(fT) \qquad (A.4)$$

so that

$$\Phi_1'(f) = -\frac{1}{2} [\, P(f-f_0) + P(f+f_0) \,]$$

$$= -\frac{1}{2} (T/2)^{1/2} [\, e^{-j\pi(f-f_0)T} \text{sinc}(f-f_0)T +$$

$$e^{-j\pi(f+f_0)T} \text{sinc}(f+f_0)T \,] \qquad (A.5)$$

and

$$\Phi_2'(f) = -\frac{1}{2j} [\, P(f-f_0) + P(f+f_0) \,]$$

$$= \frac{1}{2j} (T/2)^{1/2} [\, e^{-j\pi(f-f_0)T} \text{sinc}(f-f_0)T +$$

$$e^{-j\pi(f+f_0)T} \text{sinc}(f+f_0)T \,] \qquad (A.6)$$

carrying out the product, we obtain

$$\Phi_1'(-f)\ \Phi_2'(f) = -\frac{T}{8j}\left[\, e^{j2\pi f_0 T} S_+S_- + S_-^2 - S_+^2 - e^{-j2\pi f_0 T} S_-S_+\right] \tag{A.7}$$

where

$$S_+ \overset{\Delta}{=} \text{sinc}(f+f_0)T \quad \text{and} \quad S_- \overset{\Delta}{=} \text{sinc}(f-f_0)T \tag{A.8}$$

Through factoring, we can show that

$$\Phi_1'(-f)\ \Phi_2'(f) = -\frac{T}{8j}\left[\, S_- e^{j\pi f_0 T} - S_+ e^{-j\pi f_0 T}\right]$$

$$\left[\, S_+ e^{j\pi f_0 T} + S_- e^{-j\pi f_0 T}\right] \tag{A.9}$$

and expanding each term in brackets results in

$$G(f) \overset{\Delta}{=} \Phi_1'(-f)\ \Phi_2'(f) = -\frac{T}{8}\left\{ j\left[\text{sinc}^2(f+f_0)T - \text{sinc}^2(f-f_0)T\right] + \right.$$

$$\left. \text{sinc}(f+f_0)T\ \text{sinc}(f-f_0)T\ \sin(2\pi f_0 T)\right\} \tag{A.10}$$

and similarly

$$G(-f) \overset{\Delta}{=} \Phi_1'(f)\ \Phi_2'(-f) = -\frac{T}{8}\left\{-j\ [\mathrm{sinc}^2(f+f_0)T - \mathrm{sinc}^2(f-f_0)T]\right.$$

$$\left. + \mathrm{sinc}(f-f_0)T\ \mathrm{sinc}(f+f_0)T\ \sin 2\pi f_0 T \right\} \qquad (A.11)$$

observe that

$$\mathrm{Im}\{G(f)\} \text{ is odd function}$$

$$\mathrm{Re}\{G(f)\} \text{ is even function}$$

Therefore

$$\int_{-\infty}^{\infty} S_c(f)\ G(f)\ df = \int_{-\infty}^{\infty} S_c(f)[\mathrm{Re}\{G(f)\} + j\ \mathrm{Im}\{G(f)\}]\ df$$

$$= \int_{-\infty}^{\infty} S_c(f)\ \mathrm{Re}\{G(f)\}\ df$$

$$\approx 0 \qquad (A.12)$$

since

$$\mathrm{sinc}(f-f_0)T\ \ \mathrm{sinc}(f+f_0)T\ \approx 0$$

LIST OF REFERENCES

1. Wozencraft, J. and Jacobs, I. M., Principles of Communication Engineering, pp. 211-273, John Wiley & Sons, Inc., 1965.

2. Ziemer, R.E. and Peterson, R. L., Digital Communication and Spread Spectrum Systems, pp. 184-213, Mcmillan Publishing Company, 1985.

3. Proakis, John G., Digital Communications, pp. 183-193, Mc Graw-Hill, Inc., 1983.

4. Feher, K., Digital Communications, pp. 46-68 and pp. 115-138, Prentice-Hall, Inc., 1981.

INITIAL DISTRIBUTION LIST

		No. Copies
1.	Defence Technical Information Center Cameron Station Alexandria, Virginia 22304-6145	2
2.	Library, Code 0142 Naval Postgraduate School Monterey, California 93943-5000	2
3.	Department Chairman Code 62 Department of Electrical and Computer Engineering Naval Postgraduate School Monterey, California 93943-5000	1
4.	Prof. D. Bukofzer, Code 62Bh Naval Postgraduate School Monterey, California 93943-5000	5
5.	Prof. J. B. Knorr, Code 62Ko Naval Postgraduate School Monterey, California 93943-5000	1
6.	LTCDR. Mario C. Neiva Brasilian Naval Commission 4706 Wisconsin Avn. NW Washington, DC 20016	1
7.	LT.JG. Fikret Gunes Tuccarbasi Kozyatagi Cad. 56 Evler Selale Sok. No:12/2 Erenkoy, Istanbul TURKEY	3
8.	Deniz Kuvvetleri Komutanligi Kutuphanesi Bakanliklar, Ankara TURKEY	5
9.	Deniz Harb Okulu Kutuphanesi ve Elektrik Bolumu Kutuphanesi Tuzla, Istanbul TURKEY	2

10. Istanbul Teknik Universitesi 1
Elektrik Fakultesi Dekanligi
Istanbul, TURKEY

11. Orta Dogu Teknik Universitesi 1
Elektrik Fakultesi Dekanligi
Ankara, TURKEY

12. Bogazici Universitesi 1
Elektrik Fakultesi Dekanligi
Istanbul, TURKEY

13. Dokuz Eylul Universitesi 1
Elektrik Fakultesi Dekanligi
Izmir, TURKEY

17898 2

DUDLEY KNOX LIBRARY
NAVAL POSTGRADUATE SCHOOL
MONTEREY, CALIFORNIA 93943-5002

ID:32768000671976
G864475
Performance analysis
\Gunes, Fikret
due:9/21/1997,23:59

219253

Thesis
G864475 Gunes
c.1

Perfromance analysis of modified M-ARY PSK and QAM signaling schemes in the presence of noise and jamming.

thesG864475
Performance analysis of modified M-ARY P
3 2768 000 67197 8
DUDLEY KNOX LIBRARY